NASA CR-144854

FINAL REPORT
"LASER APPLICATION TO MEASURE VERTICAL SEA TEMPERATURE AND TURBIDITY"
DESIGN PHASE

by

J.G. Hirschberg, A.W. Wouters, K.M. Simon

J.D. Byrne, and C.E. Deverdun

prepared for

NATIONAL AERONAUTICS AND SPACE ADMINISTRATION

NASA CONTRACT NAS10–8795

Laboratory for Optics and Astrophysics

of the

Department of Physics

University of Miami

Coral Gables, Florida

January, 1976

STANDARD TITLE PAGE

1. Report No.	2. Government Accession No.	3. Recipient's Catalog No.
CR-144854		

4. Title and Subtitle	5. Report Date
Laser Application to Measure Vertical Sea Temperature and Turbidity -- Design Phase	March 1976
	6. Performing Organization Code
7. Author(s) J.G. Hirschberg, et al.	8. Performing Organization Report No.
9. Performing Organization Name and Address Laboratory for Optics & Astrophysics Department of Physics University of Miami Coral Gables, Florida 33124	10. Work Unit No.
	11. Contract or Grant No. NAS10-8795
12. Sponsoring Agency Name and Address National Aeronautics and Space Administration John F. Kennedy Space Center Kennedy Space Center, Florida	13. Type of Report and Period Covered Detailed Technical Report
	14. Sponsoring Agency Code

15. Supplementary Notes

16. Abstract

The important oceanographic parameters temperature, salinity, turbidity, and sound velocity have, in the past, been obtainable as a function of depth only by relatively time-consuming methods. We have designed an experiment to test a new method, using backscattered radiation from a laser beam to measure these quantities in a fraction of a second. Tyndall, Rayleigh, Brillouin, and Raman scattering all are utilized to evaluate the parameters. A beam from a continuous argon-ion laser will be used together with a Fabry-Perot interferometer and interference filters to gather the information. The results will be checked by direct measurements. Future shipboard and airborne experiments are described.

17. Key Words	18. Distribution Statement. Announced in STAR

19. Security Classif. (of this report)	20. Security Classif. (of this page)	21. No. of Pages	22. Price
Unclassified	Unclassified		

NASC FORM [illegible]

LASER APPLICATION TO MEASURE VERTICAL SEA TEMPERATURE AND TURBIDITY

-- DESIGN PHASE --

CONTRACT NASA NAS10-8795

DETAILED TECHNICAL REPORT

by

J.G. Hirschberg, A.W. Wouters, K.M. Simon,
J.D. Byrne and C.E. Deverdun

March 1976

Joseph G. Hirschberg
Principal Investigator

Laboratory for Optics and Astrophysics
of the Department of Physics
University of Miami
Coral Gables, Florida

TABLE OF CONTENTS

I. Introduction

A. The Problem and Its Importance

As knowledge of man's physical environment is improved, the relative lack of information about the seas around us becomes ever more important. We actually know far more about the moon's surface than we do about the waters beneath the surface of the ocean.

The knowledge, however, of the condition of the water around us is continually shown to be vital. Recreation, fisheries, transport, fresh water utilization; all these are threatened by various forms of pollution of the waters, as depicted in Fig. I.1. To cope with this situation, accurate measurements of various water parameters must be provided. Although gross indications of major ocean currents and water masses are known, there has been until very recently virtually no continuous source of information about even such elementary quantities as sound velocity, temperature, salinity and turbidity. Without a knowledge of these basic building blocks of any theory, we shall find it difficult to proceed in our conquest of the water surface of the earth, which comprises more than three fourths of its surface. Very recently, it has become possible through the methods of remote sensing to obtain some of the needed data. By measuring the infrared emission from the water, the surface temperature may be continuously determined. The water surface radiates infrared energy very nearly like a black body (a perfect absorber). The intensity of this radiation at a wavelength of 10 micrometers can be related to the sea surface temperature. However, infrared emission of this wavelength can only be used for temperature measurements of the upper few hundredths of a millimeter of the water, since water is extremely opaque to radiation of this frequency.

Often, the temperature of this upper skin is not really representative of the body temperature of a body of water. This is because the processes by which water loses its heat occur in the upper tenth of a millimeter or less immediately

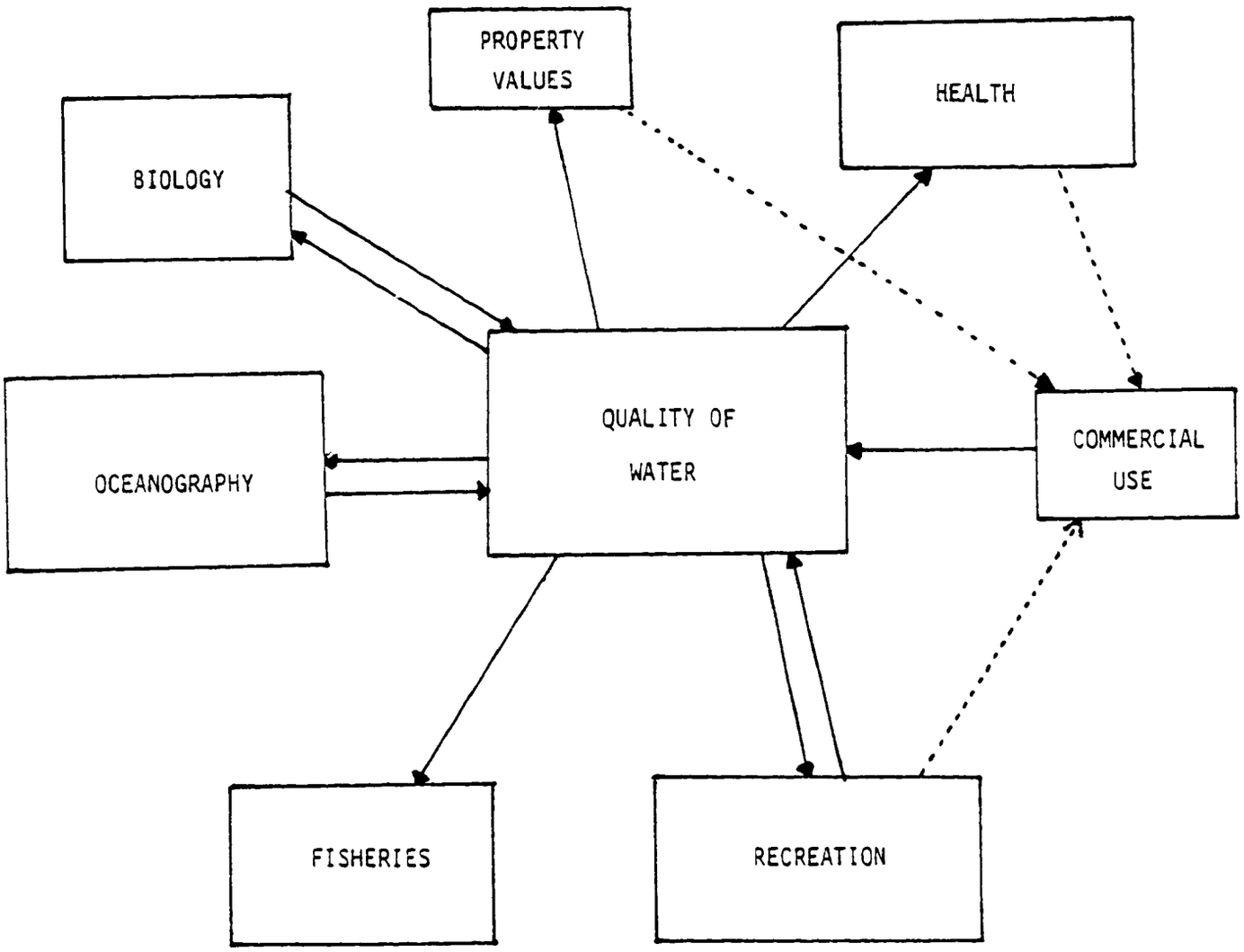
PROPERTY VALUES
HEALTH
BIOLOGY
QUALITY OF WATER
OCEANOGRAPHY
COMMERCIAL USE
FISHERIES
RECREATION

FIGURE I.1

below the surface. These processes include radiation, evaporation and conduction. The result is that, unless there is violent mixing induced by a strong wind, the upper skin of the sea may be a degree centigrade or even more cooler than the water just below.[1] It is this lower temperature that is measured by ordinary infrared remote sensing, so that a true picture is not obtained.

In addition many problems in oceanography require data not only from the surface but from deeper layers in the ocean. Typical of these problems is the question of survival of life in the neighborhood of a fossil or nuclear power plant cooling canal outfall. Here, for example, if the deeper waters remain tolerably cool, the damage is minimized, while if the water becomes too hot all the way to the bottom the result is catastrophic Another important piece of data is the existence of a region of rapid change in temperature beneath the surface. Such layers are common in the sea and cause problems in acoustic transmission, since they bend or reflect sound waves; their detection is often important, especially in military applications.

As present, the only way to measure the subsurface temperature at depth is to introduce thermometers directly into the water to the desired levels. Such methods are expensive, time-consuming, or do not provide the continuous picture that remote sensing could provide of the surface. It would be very valuable, therefore, to be able to provide remote sensing of the ocean parameters at various depths. The methods described here will provide continuous information on temperature, salinity, sound velocity and backscatter turbidity without directly introducing devices into the ocean. Ultimately remote sensing may be carried out from an aircraft. Initially, however, the measurements will be made from a platform such as a dock or a ship on the water surface. Other important oceanographic parameters to be measured

include salinity, turbidity and the velocity of sound. These parameters are depicted in Fig. I.2, with representative curves for the principal subjects of this report, temperature, turbidity, and salinity. Note that each parameter is determined as a function of the depth, h. In addition, information on total depth and the sea surface may be obtained.

These quantities are measured at present by relatively slow and tedious methods. The classical procedure involves the use of Nansen bottles, as shown schematically in Fig. I.3. A cable is lowered with a high capacity winch, and the Nansen bottles are attached by a technician standing on a grating suspended over the sea. Each bottle is equipped with a thermometer, a pressure-sensing device, and stoppers. When all the bottles are in position, a messenger weight is dropped down the wire. The weight strikes a trigger on the first (top) bottle which closes the bottle, activates the pressure sensor and the thermometer, and releases a second messenger weight which falls to the next bottle, and the process repeats until all the bottles are closed. The string of bottles is then raised by the winch and each bottle removed as it passes the grating. The temperature and pressure sensors are read and the bottle is emptied into a flask which is stored until analysis in the laboratory (for turbidity and salinity, for example) can be performed. This is a time-consuming process. For the measurement depicted (samples each 5 meters for a depth of 40 meters), approximately one hour would be required for the station. The ship must, of course, be held as motionless as possible during the operation.

A more modern and rapid method of obtaining the oceanographic data is by the use of temperature, pressure, salinity and turbidity sensors which measure these qualities electrically, transmitting the information to the surface continually via a suspension cable, which carries insulated electric wires in its core, see Fig. I.4. This method is far more rapid than the Nansen bottles for the same depth as before, perhaps only 15 minutes is necessary for each

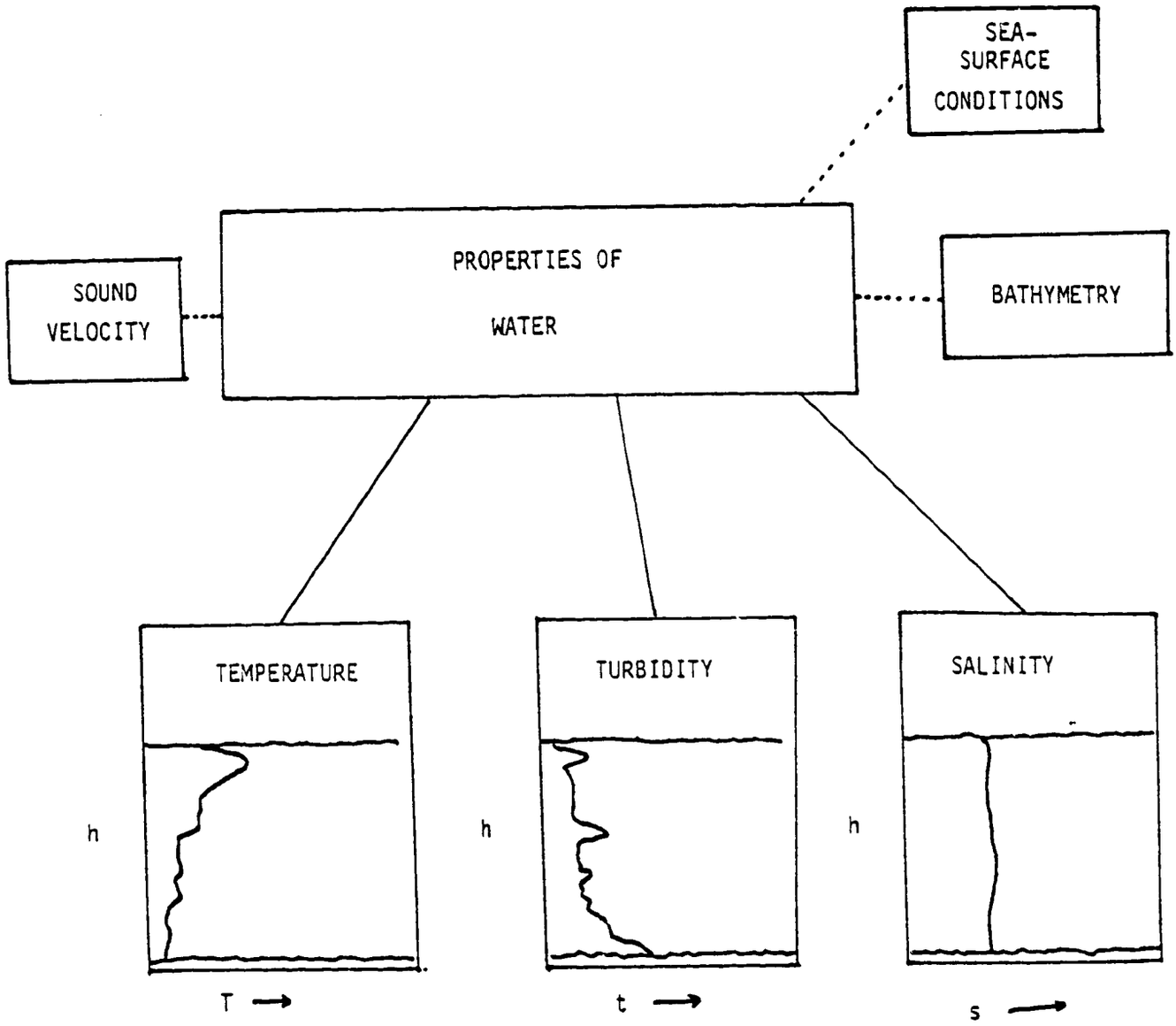
SEA-
SURFACE
CONDITIONS
PROPERTIES OF
WATER
SOUND
VELOCITY
BATHYMETRY
TEMPERATURE
TURBIDITY
SALINITY
h
h
h
T
t
s

FIGURE I.2

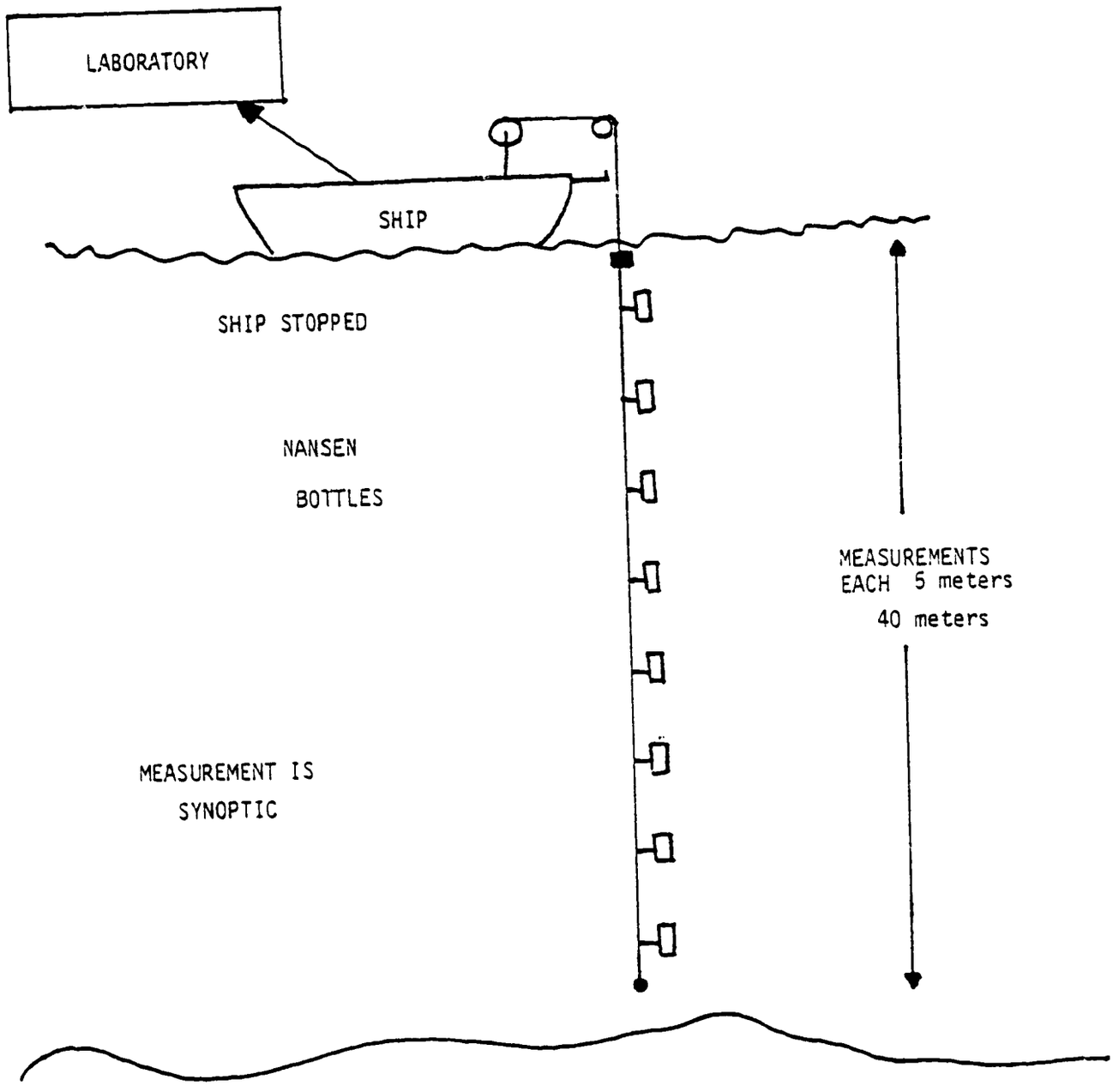

NANSEN BOTTLES

FIGURE I.3

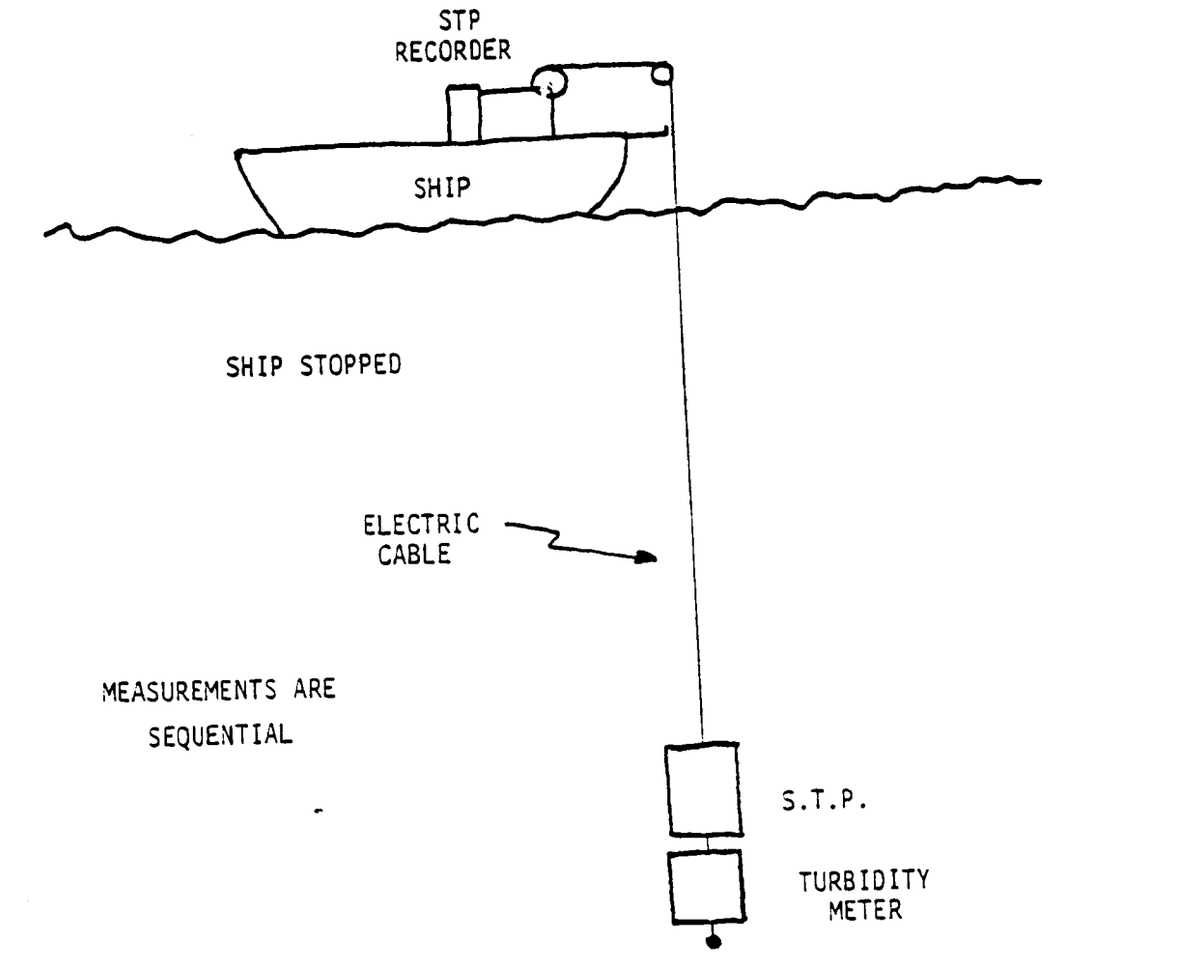

STP PLUS TURBIDITY METER

FIGURE I.4

station, not counting the time to stop the ship. The measurements, however, are not simultaneous, since the sensors must be mechanically raised or lowered between each depth. Again, however, the ship must be held strictly stationary during each series of measurements. The process of slowing and stopping a ship is very time-consuming, in many cases taking almost as much time as the actual making of observations.

B. Advantages of Our Proposed System.

Our method, first described in detail at the Symposium: "Remote Sensing Applied to Energy-Related Problems", Miami, Florida, December 1974 and reproduced in the Proceedings, is far more rapid. It utilizes a laser beam to probe the sea, and the measurement is essentially carried out at the velocity of light in water, 0.75 c. As is shown in Figure I.5, in this method a laser beam is projected downward into the water. Return light is received, and the information contained is computer-processed to obtain the speed of sound, temperature, turbidity, and salinity, all as a function of depth. The ship need not stop at all, even during measurements. This makes the new method very much faster than any previously used procedure. In five minutes, for example, a ship steaming at a steady speed of 7 knots can make 150 measurements (one each 2 seconds), with a separation of about 7 meters between each observation. Such a series with the sensors would require at least 15 minutes per sounding, assuming 10 meter depth, or about 35 hours, and with bottles considerably more!

In addition, the proposed method, as we will show, can be adapted to making airborne measurements. In this case the saving in time is further extended so that rapid simultaneous surveys will be possible, which at present are far beyond the range of practicability.

As an example of the kind of problem that could be studied with a system of this kind would be the three-dimensional behavior of an estuary under conditions of tidal flow. Tides change each six hours in typical U.S.

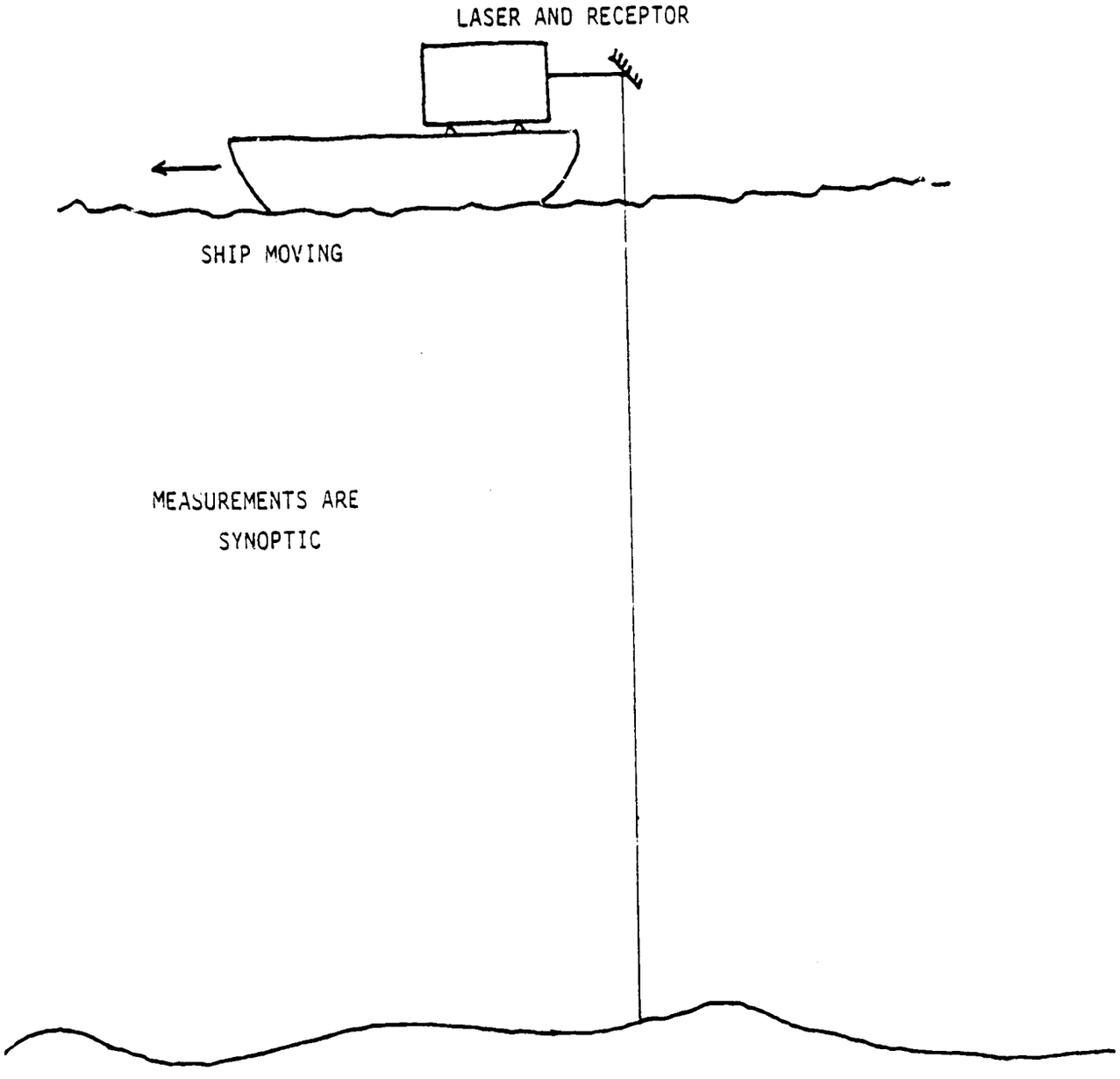

SHIPBORNE LASER PROBE

FIGURE I.5

East Coast estuaries, and maximum currents and slack conditions often last for a very short time[3] (a few minutes in many cases). A three-dimensional grid of aircraft observations of temperature salinity and turbidity can then be compared to three-dimensional theoretical models such as that developed in NASA Project NAS10-8740, "The Application of Remote Sensing to Detecting Thermal Pollution", University of Miami, Coral Gables, Florida, 1974 to date.

In this way our knowledge of oceanographic parameters in a given dynamic situation will be increased many-fold. It would, therefore, seem that a quantum jump in understanding of the dynamics of the sea could result from the application of this method.

C. Summary of Feasibility Study.

Any proposed method, no matter how attractive in theory, must be studied in detail before too much time and money is lavished upon it in order to see if it is feasible at all. Accordingly a Feasibility Study was made by our Laboratory, which was reported in the NASA CR-139184 document[2] dated January 1975 mentioned above.

This study examined whether there was enough intensity in the returned scattering from the sea to make measurements of the parameters, turbidity, salinity, and temperature. Using information theory, this data was then expressed in terms of accuracy obtainable in a given time of observation.

To obtain information from layers beneath the surface, it is necessary to use radiation for which the sea is transparent. The band of electromagnetic radiation which penetrates best into seawater lies between 0.48 and 0.55 micrometers, or between 4800 and 5500 Angstroms*. It is, therefore, proposed

*One Angstrom equals 10^{-10} meter.

to project a beam of light this wavelength into the sea and to use it to probe the deeper layers for information on oceanographic parameters, particularly temperature, salinity and turbidity. Either of two methods can be used. A light source constant in time can be projected downward while a collimated detector system some distance away is used to vary the position in depth of the scattering received. This is the bistatic system which, being the simplest, will be the first investigated experimentally. An alternate system employs colinear source and receiver beams; here the depth information is obtained by means of the time delay between projected and received signals, analogous to radar and lidar. For this purpose, rapid modulation of a continuous light or short pulses of light (of the order of a few nanoseconds) are necessary in order to provide meaningful depth information. A moderately powerful light source is also required so that measurements may be made to as great a depth as possible. Finally, the temperature and salinity information is contained in small changes in wavelength of the light returned from the sea, so that the light source used must have a narrow wavelength spread. All these requirements can be satisfied by the use of a laser. The laser will be mounted on a ship or aircraft and will project its light downward into the sea. Returning light scattered in a backward direction by the sea will be detected and analyzed with respect to time, intensity, polarization and wavelength. This information will in turn be recorded and processed to yield the desired parameters as a function of depth. The system is shown schematically in Fig.I.6.

In order to measure the parameters the evaluation of light scattered by a number of processes is necessary.

1. Scattered light from a laser beam:

a) Tyndall and Mie scattering: Here the wavelength of the incident light is unchanged. The intensity is, in general, proportional to the density of

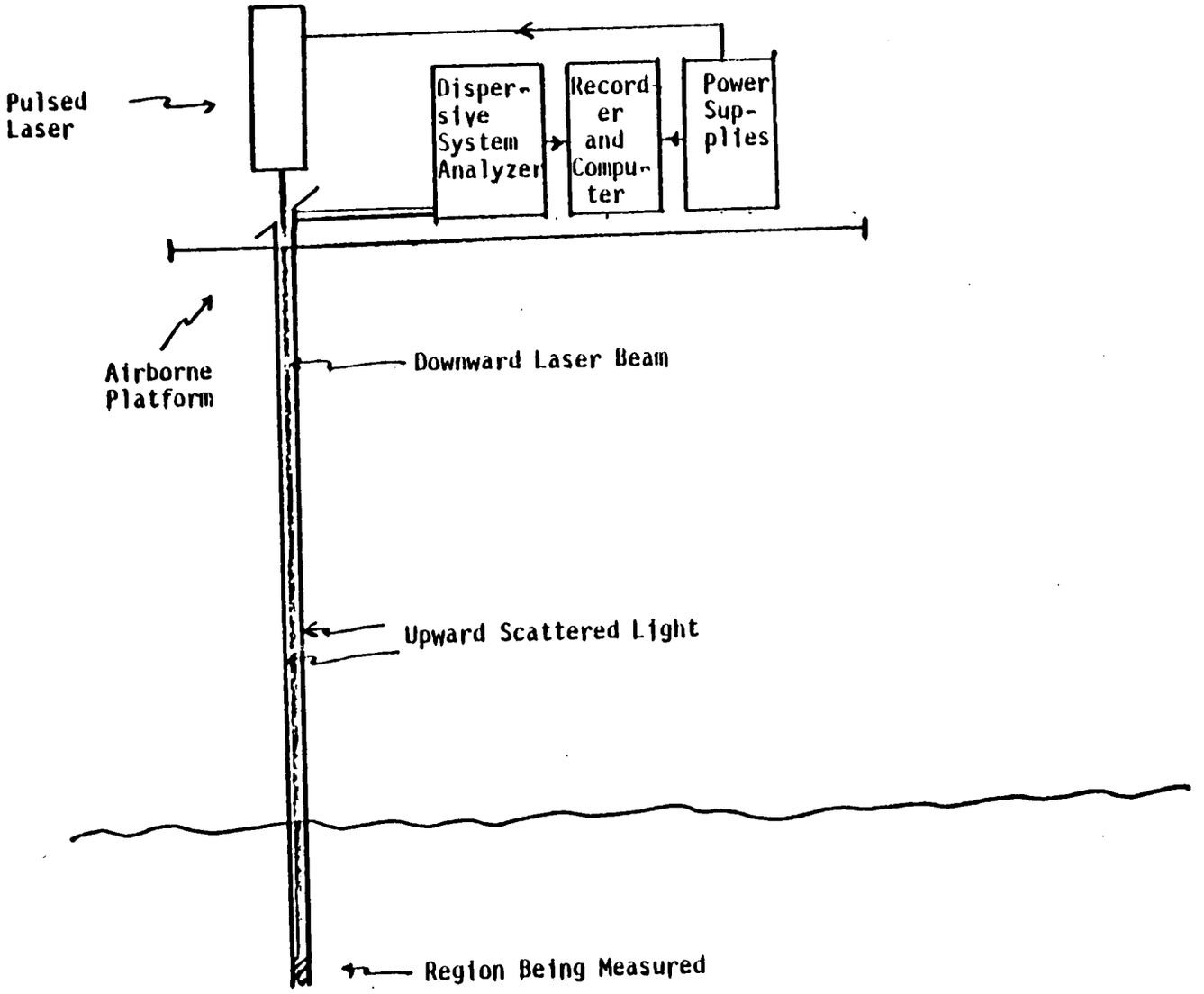
Pulsed Laser
Dispersive System Analyzer
Recorder and Computer
Power Supplies
Airborne Platform
Downward Laser Beam
Upward Scattered Light
Region Being Measured

FIGURE 1.6

particles suspended in the water. These forms of scattering give rise to cloudiness or turbidity which is the phenomenon that interferes with the clarity of the water. The amount of scattering depends on angle, but for most situations of interest a single measurement at a particular angle can be used. Here we propose a normalization function to correlate measurements made at different angles.

b) Rayleigh scattering: This occurs in clear water and is analogous to the molecular scattering in the atmosphere that gives rise to the blue color of the sky. The intensity of Rayleigh scattering is usually much less than Tyndall scattering, and its intensity is a known function of temperature and can be predicted. In general, Rayleigh scattering will be of no direct use to us, but because it can be predicted and is very faint, it will not interfere with our measurements.

c) Brillouin scattering: Photons in the incident light react with phonons in the liquid to produce wavelength-shifted light, where the shift is proportional to the velocity of sound in the liquid. The shifted wavelength[4] is given by:

$$\lambda = \lambda_0 \left(1 \pm 2n \frac{v_s}{c} \sin \frac{\theta}{2}\right)$$

where λ_0 is the incident wavelength, n is the index of refraction of the water, v_s is the sound velocity, c is the velocity of light, and θ is the scattering angle. This means that there are two shifted spectral lines with scattering proportional to v_s, the sound velocity. For backscattering, the angle between incident and scattered radiation is π. The resulting wavelength shifts are about 0.08 A, which can be measured using a Fabry-Perot interferometer. This measurement yields the sound velocity in the sea, v_s.

The Fabry-Perot is a spectroscopic instrument with extremely high resolving power and sensitivity. In addition it can be prepared[5] to have several

channels operating simultaneously. Thus the measurement of the Brillouin peaks can be carried out rapidly enough to preserve the depth information provided by the time delay, which amounts to 6 nanoseconds per meter.

d) Raman scattering: The Raman scattering differs from the components considered so far in that the wavelength of the scattered light differs much more from that of the incident. For this reason, the spectroscopic problem is much simpler, and interference filters can be used for its measurement. Salinity information can be obtained either from depolarization of water Raman lines, or the intensity of certain ion lines, principally the sulphate ion.

In the Feasibility Report it was shown that a moderately powerful laser operating in the blue region of the spectrum (440 to 490 nanometers wavelength) can, for a relatively clear sea, be used to provide data on the parameters mentioned above as a function of depth. Brillouin, Raman, and Tyndall scattering from the laser beam are all to be utilized, as summarized below. The process for each parameter is described in turn.

2. Sound Velocity

The sound velocity, v_s, in the sea is well known, having been of military as well as scientific interest for many years. It depends on salinity, depth and especially temperature. It turns out that the sound velocity in liquids can be measured using a beam of light as a probe, and that light from a laser is particularly well suited to the purpose. If such light is passed through water, it is found that two additional wavelengths appear in the scattered light. These additional wavelengths carry the information on the speed of sound; their spacing is proportional to v_s, the sound velocity. For backscattering, the wavelength shifts are about 0.08 A, which can be measured using a Fabry-Perot or a Mach-Zehnder interferometer. This measurement yields the sound velocity in the sea, v_s.

3. Salinity and Temperature

Measurements of the salinity are to be carried out by using the Raman effect. In the Raman effect, unlike the Brillouin effect, the wavelength of the backscattered light is considerably altered by the interaction of the light with energy levels of the salt and water molecules. Since the population of these levels is temperature dependent, the characteristics of the Raman spectrum depend on the water temperature and the salinity. It turns out that both the wavelength and the polarization of the Raman light are temperature and salinity dependent. A recent study[6] by Chang and Young has shown that if the laser light is circularly polarized, the Raman scattered light will show depolarization which is dependent on salinity and temperature. This dependence is different from that of the Brillouin effect mentioned above. A combination of the two observations yields the temperature and salinity separately.

A more direct method involves the SO_4 ion. Due to its internal structure this ion gives rise to a vibration-rotation Raman effect which is favorable in wavelength to transmission by the sea. Except in very unusual circumstances, the SO_4 concentration and those of the principal constituents of the salinity of the sea, Na and Cl, are strictly proportional. This means that a measure of the SO_4 ion will suffice to measure the salinity. There seems no reason why this cannot be done with sufficient accuracy to reduce our temperature measurements. An experimental study of this approach in seawater is planned. The salinity measurements are then combined with those of sound velocity to obtain the temperature.

4. Turbidity

In the literature there are at least ten definitions of turbidity. We

choose it to be the lack of clarity of water resulting from suspended particles which causes light to be scattered at random. A laser beam is particularly well suited to make this kind of measurement, since the quantity of backscattered light from a laser beam is a direct measure of turbidity. This component of scattered light exhibits no change in wavelength from the incident light and is called Tyndall scattering. The ratio of the intensity of Tyndall scattering to incident light intensity gives the turbidity. In previously used methods a difficulty has always been the incident light intensity measurement. The intensity of the Brillouin scattering corresponding to a given incident intensity is a known function of the water parameters and will give a direct measure of the intensity of the laser light at a particular layer of the sea. This is then compared to the Tyndall component, and the turbidity of the various depths can be directly deduced from their ratio. Thus, the measurement of turbidity can now be made much more accurately than before, since a ratio is used where both quantities come from the same water sample.

D. Feasibility Criteria

1) Seaborne Operation.

The acid test of any measurement is the accuracy obtainable in a given time of observation. The mechanisms of Tyndall, Rayleigh, Brillouin and Raman scattering are sufficiently well known that a calculation can be performed on the beam of scattered light from the sea when the optical parameters (size of lenses, for example) are known, and the intensity of the incident laser light is given.

We have assumed the use of a relatively modest laser (0.1 joule), an average optical system, and determined the accuracy of each measurement by means of a computer simulation. First the intensity of scattering was determined.

This calculation was checked against a Brillouin spectrum in the Laboratory, as shown in Fig. III.2 (p. 32). Then using information theory and the characteristics of typical interferometers of the type to be used, the information content of signals from the sea was evaluated. Fig. III.4 (p. 34) shows a computer simulation with a separation of the Brillouin peaks of 0.28 cm^{-1} and a turbidity of 0.285.

The main configuration considered was a three channel Fabry-Perot interferometer, shown in Fig. VI.6 (p.68). A laser sends its light by a right-angle mirror into the sea. It is backscattered and collected by the collecting lens. Rendered parallel by a negative lens the light passes through a Fabry-Perot interferometer and a focussing lens and falls on a Pafnir image divider. The three channels are separated here and are directed to separate photomultipliers as shown.

The parameters chosen were:

a) LASER

Power	100 mJ/pulse
Wavelength λ_o	variable 5,300 Å - 4,000 Å
Line Width	0.05 cm^{-1}
Pulse Length	4 nsec

b) GEOMETRY

Height Above Surface	0 (Shipborne)
Sea Surface Factor	1
Area of Collecting Lens	300 cm^2
Efficiency of Instrument	0.1

A typical result is shown in Fig. VII.1 (p.82). Here the accuracy of temperature measurements is shown at various depths in clear seawater as a function of wavelength. It is seen that the most favorable wavelength lies in the neighborhood of 450 nanometers and at 50 meters an accuracy of about 0.2 degrees C is forecast.

One of the most important questions pertaining to an optical system of this sort is the effect of turbidity in the water on the depth which can be reached. This can be answered by the computer model and a typical result is shown in Fig. VII.3 (p. 84). Here two Fabry-Perot interferometers, one with high finesse F and one lower are compared. Accuracy in degrees centigrade obtainable at 20 meters is plotted against turbidity. We note that the effect of turbidity is relatively small, indicating that clarity of the water is not as vital as we had thought, an encouraging result.

2) Airborne Operation

For the airborne experiment, the height above the surface (see Parameters, part b, above) may be given a value, for example, of 200 meters. Here the effects of sea-surface also enter. However, the airplane bathymetry experiments of the Wallops Island group in the Key West area have indicated that, except for very strong wind conditions, the sea surface does not appreciably interfere with the bathymetry accuracy. Our own calculations indicate the same thing. The feasibility of airplane measurements is certainly indicated.

3) Bistatic Experiment

The airborne measurements require a coaxial laser and scattering beam, so that the effect of the non-flat sea surface is eliminated. This, in turn, means that depth information is to be obtained from time-of-flight data. Such measurements require fast pulses from the laser as well as very short gated receiving systems. These lasers are expensive to buy and probably cannot be obtained surplus.

It happens, however, that for a seaborne experiment another far less expensive method can be used for depth information. This is to use two positions, one for sending and one for receiving, and to vary the angle between them for depth measurement. This is the principle of the ordinary

rangefinder. Such a configuration is shown in Fig. VIII.1 (p. 88). The depth of the shaded area from which the measurement comes can be deduced from the angles of the two beams by trigonometry. Our first experiments in actual outdoor salt water will be made using this configuration. This is because due to a restricted budget, we are relying mostly on equipment either on hand in the Laboratory or borrowed (like the laser). Since this method measures the Brillouin, Raman and Tyndall Scattering as a function of depth just as the final system will do, it provides an extremely valuable check on our calculations, and so is a logical first step in our Experimental Program. When we have actual Brillouin spectrum results from a natural body of water outside the Laboratory, our level of confidence will be greatly increased.

II. Delineation of the Quantities

A. Temperature

The object of our measurement here is the thermodynamical bulk temperature of the water, the quantity normally measured when a thermometer is introduced into the water. This temperature is required in considerations of water circulation and biota distribution and can be used as a labelling parameter of water masses in certain circulation studies.

In our measurements, the temperature is inferred from the speed of sound, and, assuming sufficient knowledge of the other parameters pressure and salinity, this inference is very precise. An expression we have used for the speed of sound is exact to better than 0.5 m/s[8], and with the linear temperature variation of about 3 m/s per °C, the precision is already better than 0.2 °C. Using suitable calibration, we do not expect any observable error in this inference; the temperature will be computed with the precision with which the speed of sound, salinity and pressure are known.

The Brillouin spectrum is a very direct method of measuring the speed of sound: the wavelength of the laser pulse is shifted in the scattering volume by an amount directly proportional to the speed of sound at this location; this modified light is then observed without any possibility of further change, since a second scattering would reduce the intensity to nothing. For comparison, the only presently employed method of temperature remote sensing by thermal infrared intensity measurement is sensitive only to the observed skin temperature. There are indications[1,9] that this skin temperature may be lower than the bulk temperature by 1°C and even more, depending on relative humidity and wind conditions. In addition, the infrared measurements have to be corrected for the absorption in the atmosphere, which varies with path length and humidity.

The measurement of temperature using the Brillouin spectrum, on the other hand, is only limited by the power of the laser and the ability to measure salinity.

B. Turbidity

Until very recently, the quality of our waters in lakes, streams and near the coast at sea has been deteriorating steadily. Dredging operations, discharge of industrial and municipal wastes, and agricultural usage all have contributed to a decrease in quality of those very neighboring waters most useful to us for recreation and for fisheries. Since the general realization a few years ago that we must preserve our water heritage and limit our despoilation of this important natural resource, there seems to have been a dramatic turn of events. In some cases the rate of deterioration has apparently been slowed, and even reversed. Controls on activities which may adversely affect water quality have multiplied, and considerable expenditures have been made or projected to improve water quality. Fisherman have reported improvements in the Great Lakes, and coastal waters such as Biscayne Bay seem somewhat clearer than a few years ago. But how is water quality to be measured? How are we to know whether we are winning the battle; whether the expenditures are fully effective.

Of the measurements of water quality, that of turbidity or lack of clarity is probably the most useful. This is not only because measurements can be made optically, and therefore quickly without complicated chemical analysis, but also because it is exactly the lack of transparency which turbidity implies that is perhaps the most direct and obvious measure of water deterioration.

The literature discloses[10] at least nine distinct definitions of turbidity or lack of clarity. Here we shall consider that turbidity causes

the cloudiness in water which obscures objects on the bottom. We shall not be concerned with absorption, which limits the transparency of water but does not reduce the definition or contrast of what we see. The cloudiness that we wish to measure is caused by suspended small particles in the water. When light encounters these particles, it is scattered in all directions. The result is a decrease in the clarity and contrast of an image.

Consider a beam of monochromatic light incident on a sample of water. It is assumed to have wavelength λ and irradiance I_o. In an infinitesimal volume dxdydz, a certain amount of light, dI, is scattered in a solid angle $d\Omega$. This amount is proportional to the incident intensity I_o, to the solid angle $d\Omega$, and to the volume dxdydz, and is a function of angle and wavelength:

$$dI = \sigma(\vartheta,\lambda)\ I_o\ d\Omega\ dxdydz$$

Here $\sigma(\vartheta,\lambda)$ is the scattering coefficient which is to be measured. In those cases where the particles doing the scattering are small, of diameter d, the same order or smaller that the wavelength λ of the light, the angular dependence is very complicated. In most of the turbidity which affects water quality, however, the particles are considerably larger than wavelength, $d >> \lambda$, and the variations with angle are simple while the wavelength dependence is negligible.

Measurements of turbidity are thus equivalent to the measurement of scattering, which is dependent on angle. A type of scattering meter, the nephelometer, is adapted to measurements at 90°. Other methods include the taking of water samples, the Secchi disk, and measurement of the intensity of a light beam after passage through a definite length of water compared to its original intensity. They may be classified as follows:

1) transmissometer

measure either diffuse or true extinction coefficients

either in situ or in vitro.

2) scatterometer (nephelometer)

measure the scattering properties of the sample, usually

but not always at 90° in vitro.

3) combination of the preceding two methods

a) contrast meter:
- Jackson candle turbidimeter
- Secchi disk
- rotating black and white disk

b) ratio of transmitted beam and scattered beam.

In order to be able to make even the most approximate comparison of measurements by these methods, some kind of standard angle dependence must be assumed. We found that instead of making each of the comparisons with ad hoc assumptions, it is much simpler and more consistent to refer all these measurements to a new unit based on the definition of turbidity:

> "Turbidity corresponds to the amount of suspended matter in a sample of water, as ascertained by optical observations. The units are required to be proportional to dilution, viz: dilution by half of a sample will reduce its turbidity by half."

We define then a sample of turbidity 1 as having a scattering coefficient $\sigma(\theta,\lambda)$ equal to the turbidity normalization function $\beta(\theta)$ shown in Fig. II.1 This function was obtained as the simplest closed analytical form that approximates the scattering angular dependence of most bodies of water. Its intensity corresponds roughly to the transition between clean and dirty water. Some technical data of this normalization function are

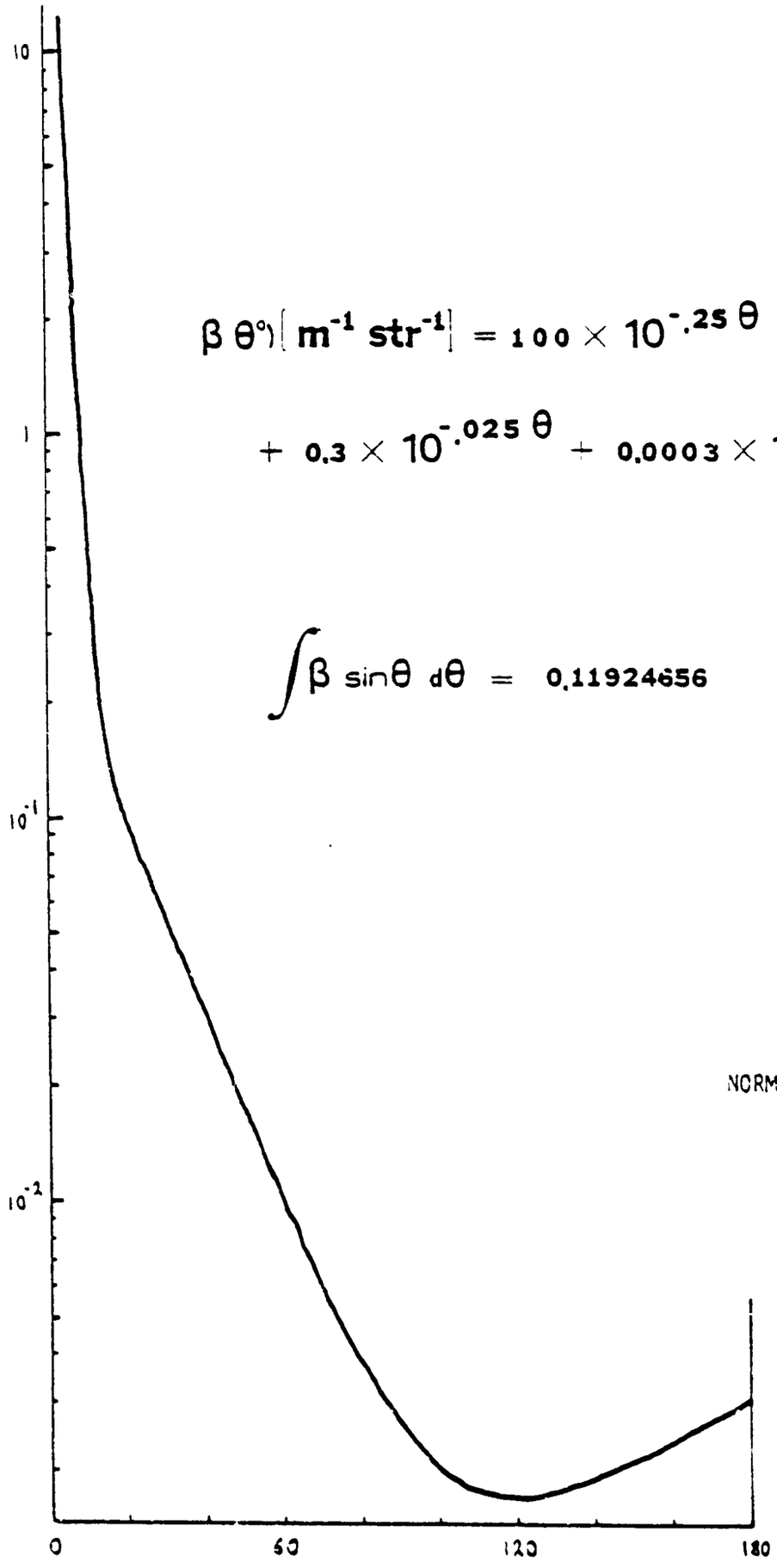

$$\beta(\theta^\circ)\left[\mathrm{m^{-1}\ str^{-1}}\right] = 100 \times 10^{-.25\,\theta} + 0.3 \times 10^{-.025\,\theta} + 0.0003 \times 10^{\theta/180}$$

$$\int \beta \sin\theta \, d\theta = 0.11924656$$

TURBIDITY
NORMALIZATION FUNCTION
FIG. II.1

are given below, and all the turbidities discussed in this and the following reports will be given in this unit.

The normalization turbidity function $\beta(\theta)$:

1) defines a sample of turbidity 1 and has an angular dependence chosen to approximate the scattering of most bodies of water (for instance,

$$10^2 \frac{\beta(45°)}{4\pi\ \sigma} = 3$$

while this quantity varies from 2.5 to 3.5 in oceans and lakes.)

2) when multiplied by 16.77197 gives an angular function in turbidity normalized to 4π.

3) can be understood as corresponding approximately[12] to about 1.2×10^6 particle liter, of index 1.6 , with diameters above 2 μm distributed in Junge distribution slope 1 (assuming density of 2.5, this gives about .6mg/liter).

In the ocean, the actual particulate matter giving this scattering would probably be closer[13] to 5×10^{10} particles/liter, of index (1.4 + 0.01i), distributed between the diameter of 0.08 and 10μm by a Junge distribution of slope 3. This results in an absorption coefficient $\alpha = 5.2 \times 10^{-2}$ that we use as the normalized absorption coefficient of a sample of turbidity 1.

4) the total scattering coefficients of a sample of turbidity t is $t \times 0.59623$; with the normalized absorption α of the particles, this corresponds to a half intensity propagation length HIL = $\frac{625}{t}$ cm.

C. Salinity

The presence of salt in sea water results in appreciable changes in the physical properties of the water. The simplest expressions for the speed of sound, the index of refraction, and the density must have at least one salinity parameter. Fortunately, since most of the variations of salinity are due to rain or evaporation, the ratio of the different salt constituents stays about constant, and only one salinity parameter is quite sufficient for most uses: most physical properties of sea water can be written in a T p S system, i.e. as a function of only temperature, pressure and salinity.

The salinity parameter can be expressed in many ways, but parts per thousand of salt has been a fairly standard one for a long time. It has the advantage that it can be understood as gram of salt per kilogram of sea water in thermodynamical computations. These are the units we use in this report. A normal value for salinity in the ocean is 35 gm/kgm and is distributed as[14]:

19.353	Chlorine
10.76	Sodium
1.292	Magnesium
2.712	Sulfate
0.412	Calcium
0.399	Potassium

The rest is Bicarbonate and some trace elements.

D. Speed of Sound

The Brillouin spectrum corresponds to two peaks shifted in wavenumber by an amount equal to

$$\frac{2n\,v_s}{c}\,\nu_0 \sin\frac{1}{2}\theta$$

where n is the index of refraction
v_s is the speed of sound
ν_0 is the laser wavenumber and
θ^0 is the scattering angle.

Since the wavelength of a laser is well fixed and the $\sin \frac{1}{2} \theta$ variation is negligible in backscattering ($\theta = 180$), the separation of the peaks gives a very precise measure of $n\, v_s$, or more exactly the index of refraction at the laser wavelength multiplied by the speed of sound at that frequency: $2n\, v_s\, v_o \sin \frac{1}{2} \theta$. This is a very well defined physical quantity, which is a local bulk property of the water at the scattering point. Although this water characteristic can be referred to the T p S system, its measure is very direct and, since it is never influenced by the surroundings, it may be advantageous to consider it independently in certain studies. We expect these kind of measurements to be very useful in studies of stratification of water bodies, to obtain a fast three dimensional picture of the plume from a river or cooling water outlet, and as a labelling parameter in circulation studies.

III. Turbidity

A. Theory

A computer model of the Brillouin Spectrum of water based on the theory reviewed in Chapter V of this report was developed during this phase of the contract. A brief review of the Tyndall or particle scattering information used is presented in this section and is shown to be a means of measuring turbidity when coupled with the intensity of the Brillouin spectrum.

Tyndall scattering was mentioned[2] as typically the brightest of the detected returning radiation. Its central wavelength and spectral width are essentially the same as those of the laser. The angular dependence of the scattered intensity has been studied by others in many bodies of water. The combining of results of several of these experiments has led to the turbidity normalization function shown in Fig. II.1 (p. 24) which matches the data over a wide range of variation.

The separation of the Brillouin peaks contains information about the water sample temperature and is independent of the absolute intensity of the laser. Since the temperature of the water is calculated, it follows that the intensity of the Brillouin effect carries the information needed to determine the intensity of the probing laser light that interacts with the volume of water being studied. Using the turbidity normalization function mentioned above, the normalized Tyndall peak intensity can be directly compared to the Brillouin effect intensity and an accurate and repeatable measure of turbidity obtained.

This method of measuring turbidity has a significant advantage over previous methods because the standard for comparison (Brillouin) originates in the same volume of water as the effect under study (Tyndall). Both the Brillouin and Tyndall scattered light reaches the receiver after transversing the same optical path so no assumptions need be made about the medium between the receiver and the volume under study.

B. Experimental

During the feasibility study of this project the Brillouin spectrum was observed using a helium-neon laser and a Fabry-Perot interferometer. In this phase of the project the computer model was used to simulate the laboratory conditions as reported earlier. The purpose was to obtain "a posteriori" the turbidity of our water samples by matching the laboratory data with the computer simulation.

1. Laboratory Work

The light source used was a SPECTRA-PHYSICS Model 124 helium-neon laser (6328 A) with an output power of 10 mW. The water samples were contained in a spherical glass flask and the purity of the sample was varied. The non-specific description of purity was then replaced by our definition of turbidity so in essence, scans of the Brillouin spectrum were made on samples having different values of turbidity. Most of the scans were performed at a scattering angle of 90°. A lens system relayed the scattered light to a Fabry-Perot interferometer as shown in Fig. III.1.

The Fabry-Perot interferometer was in a pressurized housing with a 1 cm spacer giving a free spectral range of 0.5 cm^{-1} (0.20A at 6328 A). With this spacer the Brillouin scattered light fell approximately 0.3 free spectral range from the Tyndall central peak. Freon 12 ($C_2Cl_2F_2$) was used to scan the Fabry-Perot with a change in pressure of about 0.3 lbs/in^2 corresponding to a complete free spectral range of the interferometer.

A lens imaged the fringe pattern on a plate with a centered small aperture followed by a photomultiplier. When the laser light was put through the optical system, the finesse of the whole system was measured and found to be about 6.

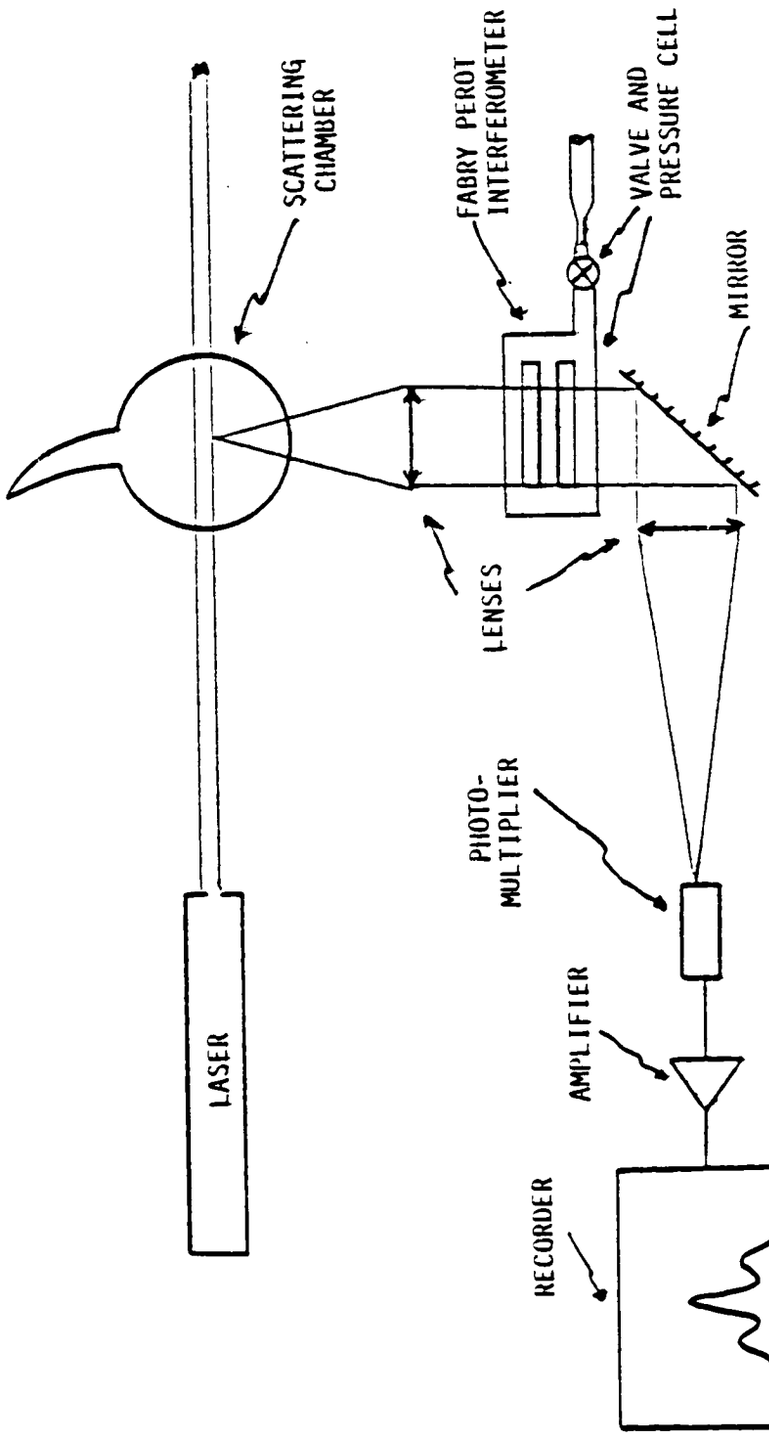
SCATTERING CHAMBER
FABRY PEROT INTERFEROMETER
VALVE AND PRESSURE CELL
MIRROR
LENSES
PHOTO-MULTIPLIER
AMPLIFIER
RECORDER
LASER

FIGURE III.1

A typical output from this system including the Brillouin spectrum is shown in Fig. III.2. The scattering angle was 90° and the water was considered to be relatively clean. The limitation of available finesse (using off-the-shelf components only) did not permit better isolation of the central peak. It is moreover not necessary to clearly isolate the Brillouin peaks to obtain an accurate measure of turbidity. A signal-to-noise calculation in chapter VII of this report demonstrates this effect in detail. Typical results indicate that the method easily gives turbidities with a precision of a few per cent, which is much better than any previous method.

2. Computer Simulation

The computer model of the Brillouin spectrum was developed using the theory presented in Chapter V of this report. The temperature, salinity, and pressure of the water are input data. From these specified quantities other properties of the sample are derived. These are density, index of refraction, speed of sound, partial derivatives of the index of refraction (with respect to temperature, pressure, and salinity), volume expansion coefficient, and isothermal compressibility.

Additional information is then added, giving the angle of scatter of the receiver and the wavelength of the laser. The scattering coefficients, spectral widths, and spectral shifts for each type of scattering are then calculated (isobaric, salinity, Brillouin, and anisotropic). A Tyndall scattering coefficient can then be assumed and the complete simulated spectrum displayed.

The simulated spectrum can be put through a theoretical Fabry-Perot interferometer. This can be done after a finesse and free spectral range is specified. Figs. III.3, III.4, and III.5, show a sequence of modelings as the scattering coefficient τ_p is varied. The pressure, temperature, and salinity were assumed to be 1.0 atm, 20°C, and 0.0 parts/thousand respectively.

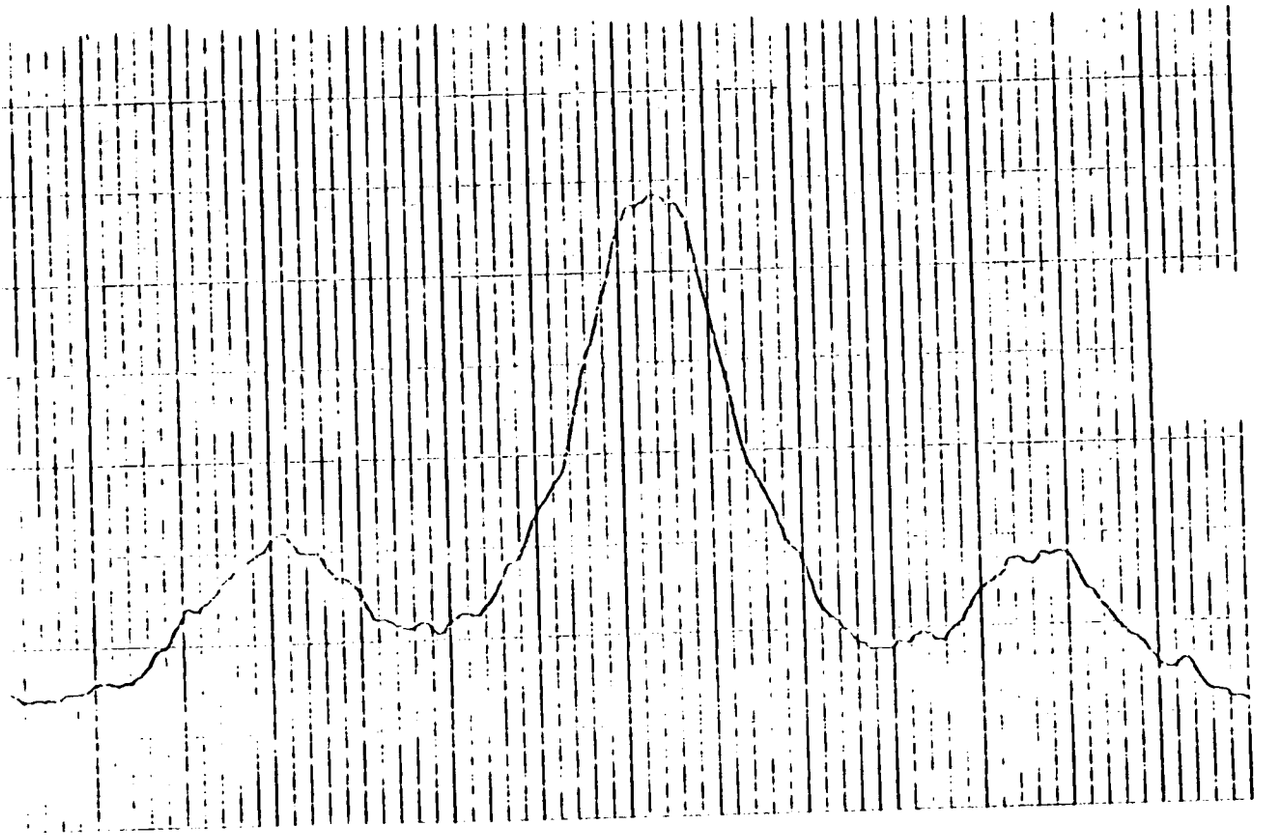

Experimental Brillouin Spectrum at 90°.

FIGURE III.2

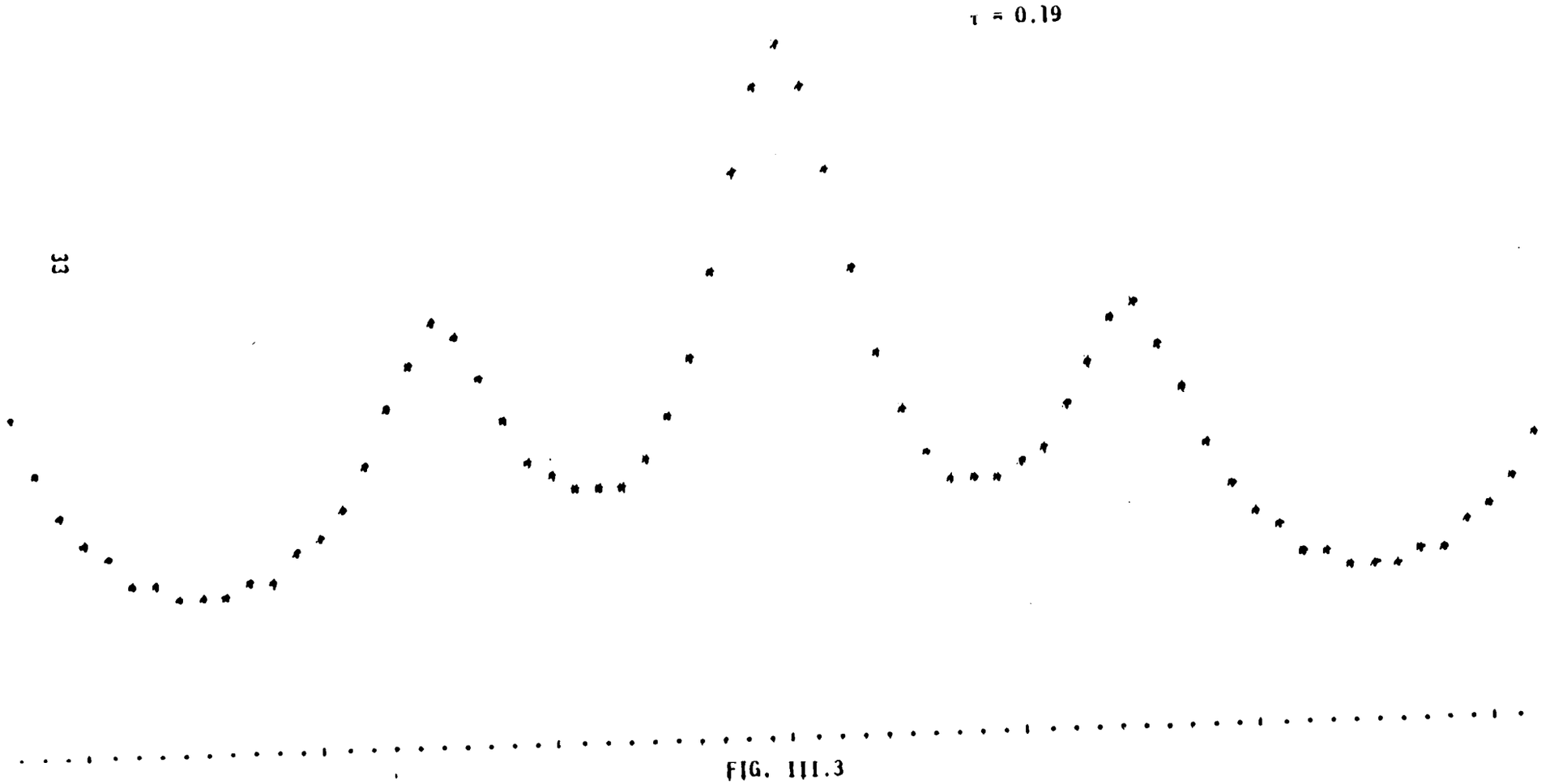

FIG. III.3

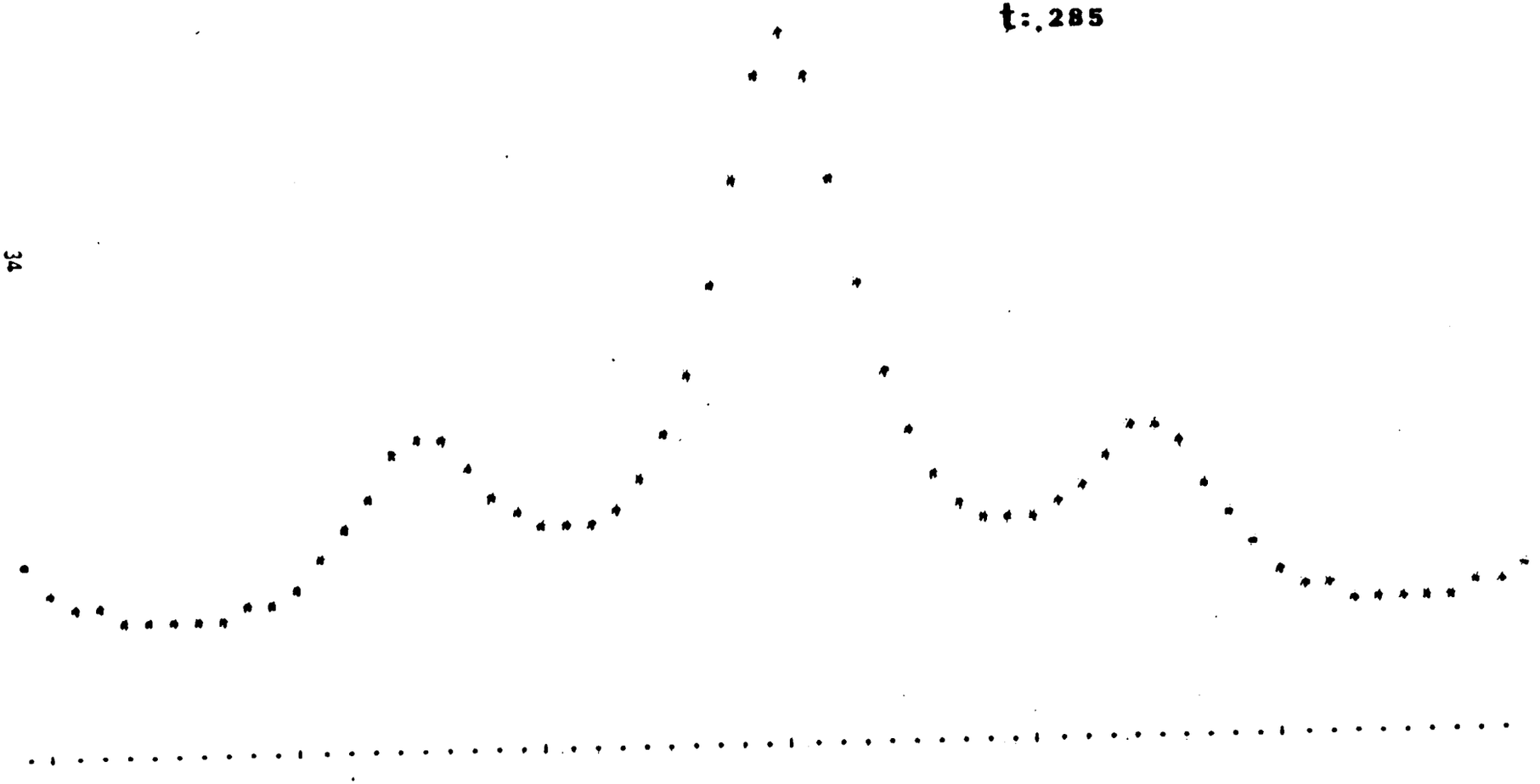

FIGURE III.4

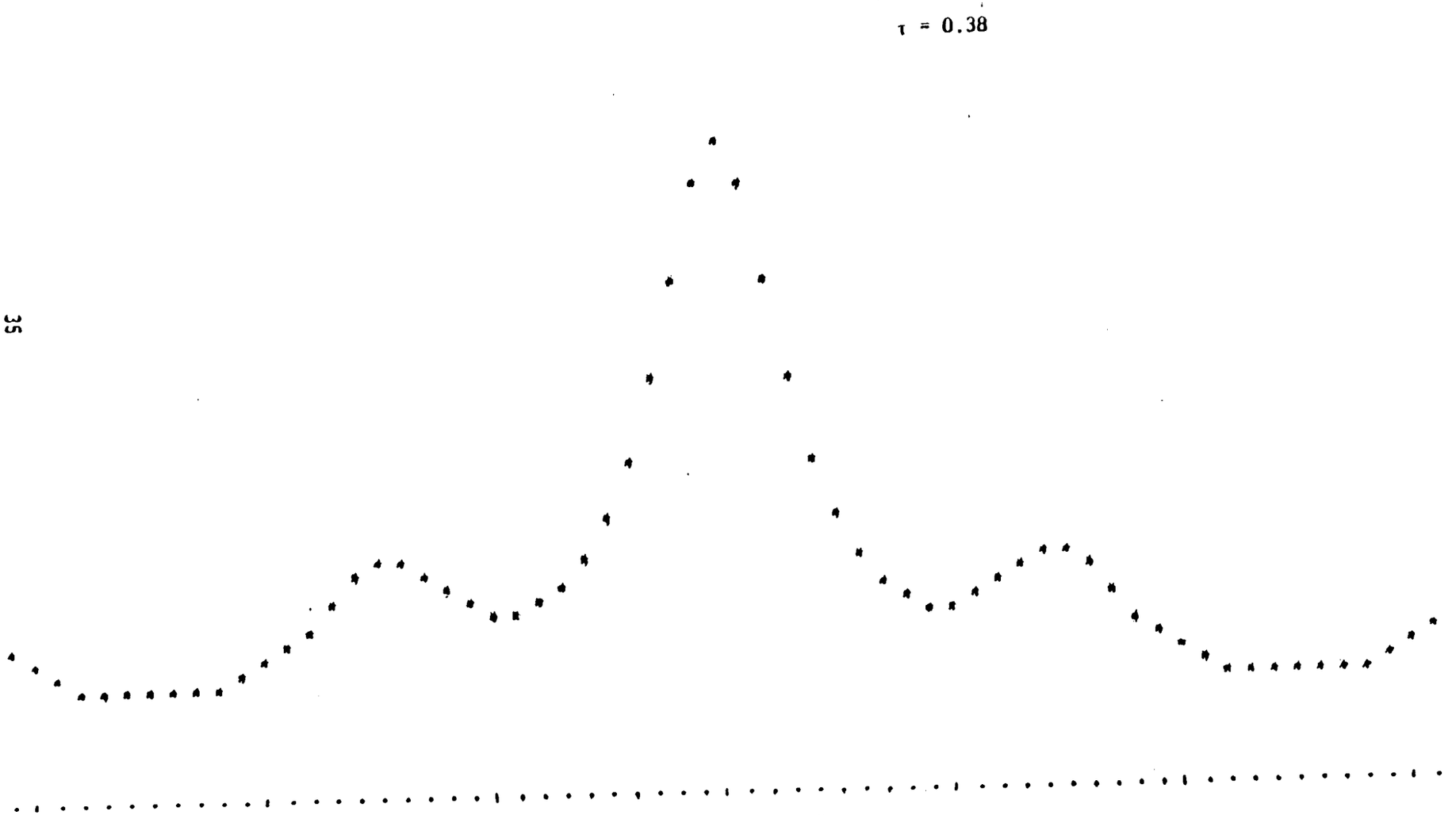

FIGURE III.5

The scattering angle was 90° and the laser wavelength was 6328 A. The Fabry-Perot was assigned a free spectral range of 0.5 cm^{-1} and a finesse of 8. The closest match (relative height and half-width) is Fig. III.4 with a turbidity of 0.285.

IV. The Problem of Determination of Salinity

A. The Need for the Measurement

Brillouin spectroscopy can provide a measurement of the speed of sound in the sea. This is discussed in more detail in other sections of this report.

The speed of sound is given as a function of temperature, salinity, and pressure (depth) by many authors. The depth for each value of the speed of sound can be found by measuring the time delay in the arrival of the back-scattered light from the sea following the arrival of a reflection from the surface; or in a bistatic system one can provide depth information by the use of trigonometry.

The temperature and salinity information cannot be separated by the speed of sound measurement alone, and so an independent method for measuring one or both quantities must be achieved, except in special cases described below, where simplifying assumptions can be made.

1. In fresh water the salinity may be assumed to be zero. The speed of sound and depth measurements are then sufficient to provide a measurement of water temperature.

2. In the ocean the salinity near the surface changes gradually over distances of hundreds of kilometers. Figure IV.1 depicts the mean surface salinity of the world's oceans.[14] The surface layers are often well mixed and therefore the salinity may be assumed to be constant. A mean value for salinity may be chosen with which to calculate temperature from speed of sound measurements, allowing for some uncertainty of results.

3. Some water bodies of interest may not fit these special cases. For example, brackish water in estuaries generally exhibits large vertical and horizontal gradients of both temperature and salinity, as does the sea in regions of high precipitation or evaporation. In these cases an

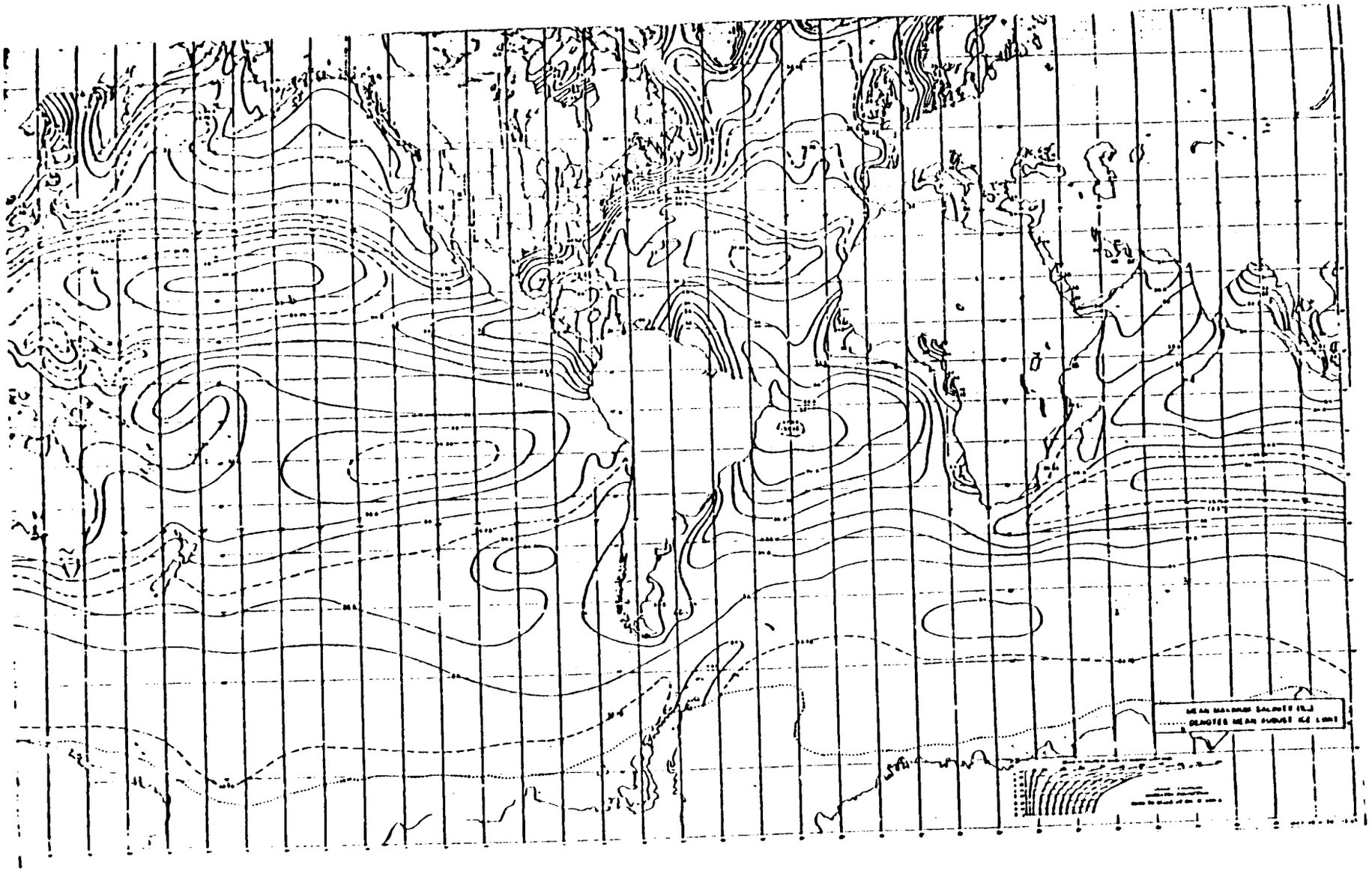

FIG. IV.1

MEAN SURFACE SALINITY OF THE OCEAN

independent salinity measurement should be obtained to allow accurate calculation of temperature in conjunction with the Brillouin speed of sound measurement.

B. Methods of Measuring Salinity

1. Microwave Method (surface only).

When microwaves are reflected from an object, the electrical properties of that object strongly influence the reflectivity. Microwave sensors have been proposed for use in SEASAT and were used in Skylab for oceanographic purposes. Measurements of the electrical conductivity of the surface layers of the sea would allow the calculation of the sea surface salinity. Such systems have been flown in aircraft and give values accurate to one part in 1000.[15] We are, however, more interested in determining salinity in depth.

2. Raman Scattering

The Raman spectrum of a molecule can be understood as scattering involving a quantum jump between two energy levels of the molecule. Since the energy of the scattered photon is equal to the energy of the incident photon minus the energy difference between the final and initial states of the molecule, the wavenumber shift J is obtained directly by

$$J = E_i - E_f$$

with all energy levels in cm^{-1}.

Raman Scattering produces spectral bands of lower and higher energy referred to respectively as Stokes and anti-Stokes bands. The Stokes band is the most intense and is the form of Raman scattering in which we are chiefly interested. The Raman effect arising from the vibration of water molecules is depicted in Fig. IV.2.

a. Raman Depolarization of H_2O

It turns out that both the wavelength and the polarization of the water Raman spectrum are temperature and salinity dependent. A recent study by

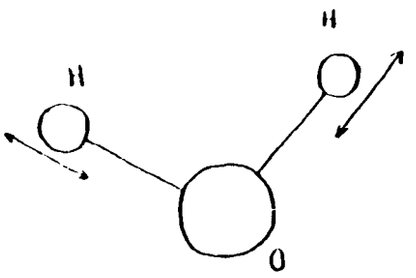

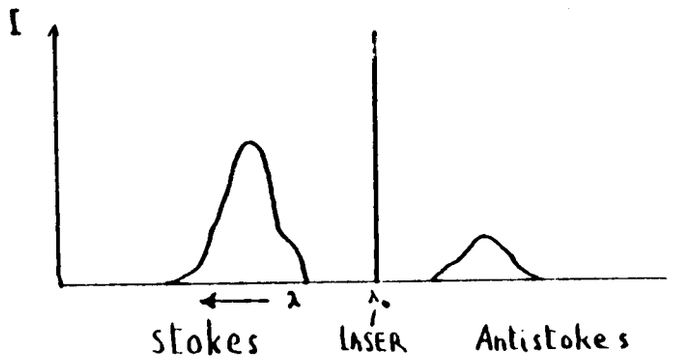

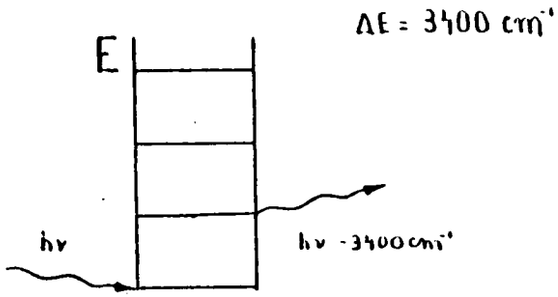

Raman Effect

FIGURE IV.2

Chang and Young[6] has shown that because seawater may absorb certain colors in unpredictable quantities, the wavelength shifts of Raman spectra are not useful in measuring temperature and salinity. However, the study further shows that, if the exciting light is circularly polarized, the Raman scattered light will show depolarization which is dependent on salinity and temperature. The circular depolarization, ρ_c, cannot yield the salinity or the temperature separately. Chang and Young proposed to treat the ocean as a body of constant salinity and thereby obtain the temperature profile from one measurement. If this method is instead combined with the Brillouin method, we will have two independent equations available from which the two unknown variables, temperature and salinity, may be simultaneously calculated. The discussion of this system of simultaneous equations can be found in our previous report.[2]

One possible instrumentation system to utilize the Chang and Young results consists of a blue green laser to obtain maximum penetration of the sea. The laser light is circularly polarized by a Brewster window and a quarter wave plate.

The Raman backscattered light from the sea is passed through an interference filter to limit background radiation noise. The light is then passed through another quarter wave plate, a beam splitter and two linear polarization filters so that the right and left hand polarization states may be simultaneously observed. A photomultiplier and amplifier must be provided for each channel. The schematic for the system is given in Fig. IV.3.

b) Determination of Salinity from Raman Spectroscopy of Sulfate Ions in the Sea.

A measurement of the concentration of sulfate ions in seawater allows the direct calculation of the salinity.[16,17] The concentration of the

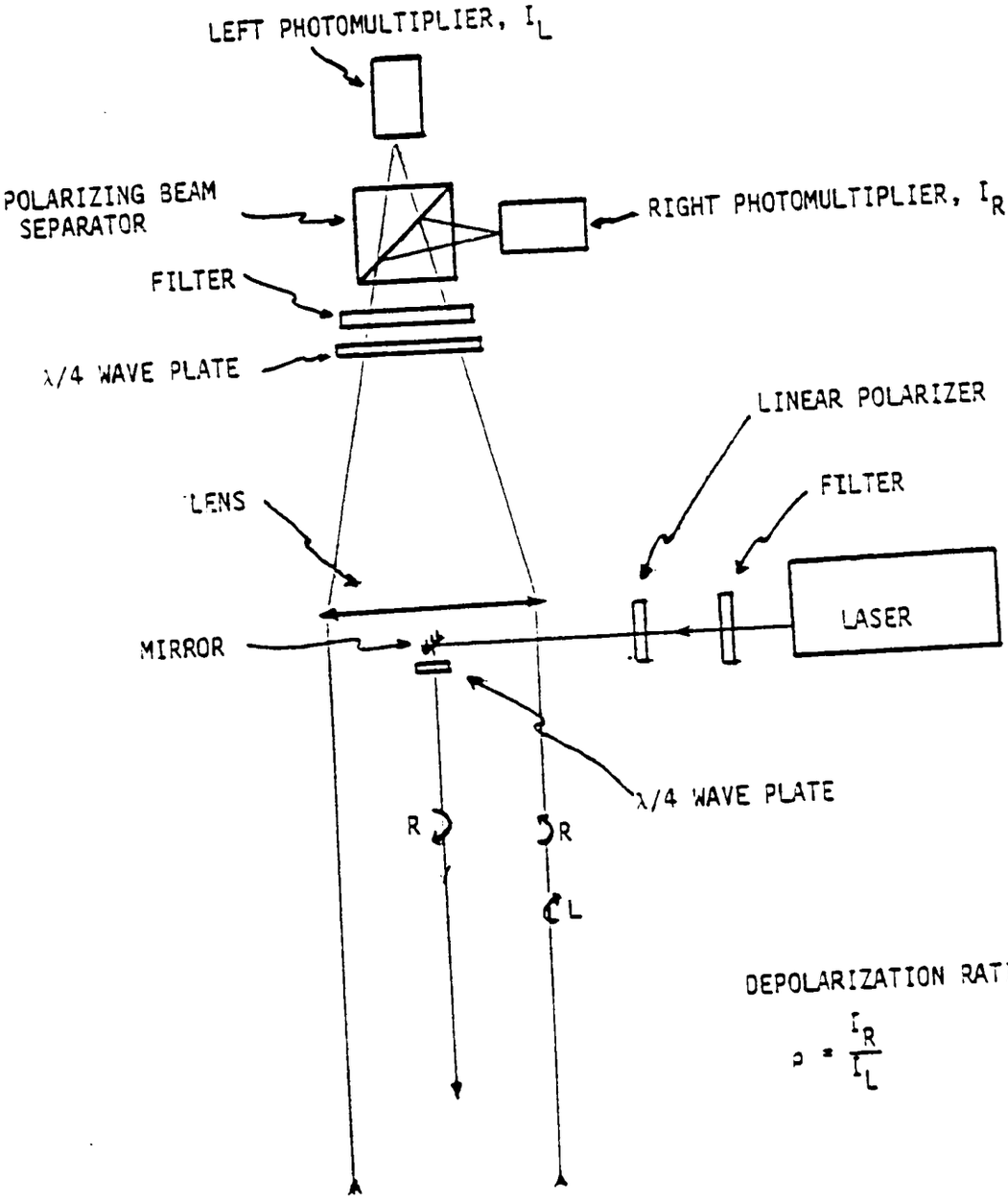

DEPOLARIZATION RATIO :

$$\rho = \frac{I_R}{I_L}$$

SCHEMATIC OPTICAL SYSTEM FOR RAMAN TRANSMITTER AND RECEIVER

FIGURE IV.3

ions may be measured by observing the ratio in amplitude between the Raman scattered light and the light incident in the sample volume.

The instrumentation required to measure the sulfate Raman effect are an appropriate interference filter, a photomultiplier, and an amplifier. Information on the intensity of light incident on a sample volume may be obtained from the Brillouin measurements.

Other investigators have studied the Raman spectrum of sulfate in the sea, and careful attention will be paid to their results[18,19]. The combination of the salinity thus obtained with the independently measured speed of sound and depth information would allow the calculation of the temperature of the sea with depth.

c) Discussion.

The Argon Ion laser on loan to the University of Miami Laboratory for Optics and Astrophysics from the Navy (via NASA) will be useful in examining the relative merits of the different Raman spectroscopic methods. Experiments will be performed to determine which method provides the best means of obtaining an independent measurement of salinity. H_2O Raman backscatter depolarization and $SO_4^=$ Raman backscatter intensity will be measured for solutions of salts and typical seawater in the laboratory.

These experiments will serve to verify the results of other researchers and provide experience in the techniques for future application in a combined Brillouin-Raman instrument.

V. Brillouin Scattering

One of the reasons we are so confident of the practicality of the Brillouin spectrum method of temperature sensing is that the theoretical basis of the phenomenon is well established and that computation of the effect is possible. Brillouin spectroscopy is one of the rare fields of physics where theoretical work and computations normally agree with the experiment to within the experimental error. This agreement can be shown for the intensity of the Brillouin peaks as a function of the thermodynamical quantities, width of the peaks due to sound absorption, etc., and Fig. V.1, taken from the work of C.L. O'Connor and J.P. Schluff,[20] shows the agreement for the measurement we plan, the speed of sound in water. In this figure, the speeds of sound computed from laboratory observations of the Brillouin spectrum are plotted as open circles as a function of temperature and compared to the standard ultrasonic sound speed, indicated by the black curve.

We use the Brillouin theory extensively in our computer simulations because it allows us to compute a large range of problems. Since it is the fitness of theory which is at the basis of our confidence in the workability of the design, we thought it worthwhile to study the derivation of the equations, to determine the assumptions used, and thus reveal any limits of the validity of the models chosen. The flow diagram of the derivation, seen in Fig. V.2, is a proof that the starting equations are basic. These equations, Maxwell's equations (V.2-7) and the differential fluid equations (V.8-10), are applied to the solution of a specific problem: the electromagnetic waves driven by the polarization induced by the electric field of a strong laser beam (V.1) in an isotropic medium whose index of refraction is written in a T p s system. We employ various mathematical methods: Green's function (V.11), Fourier transform (V.12) and Wiener spectrum (V.13) with a rather delicate substitution

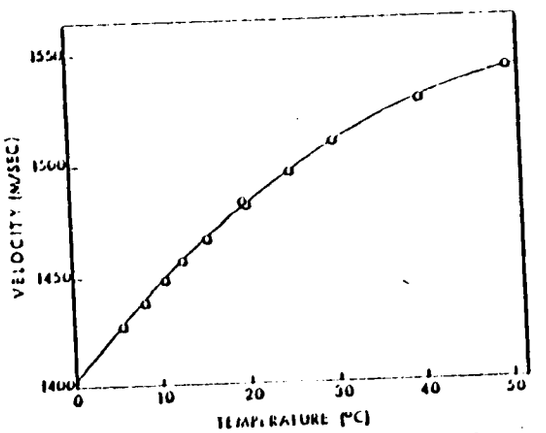

FIG. 8. Plot of experimental values of sound velocity in water at 4.5 Gc/sec as a function of temperature. Solid line is experimental data from ultrasonic measurements.

from C.L. O'Connor and J.P. Schlupf
J. Chem. Phys. 47, 31 (1967).

FIGURE V.1

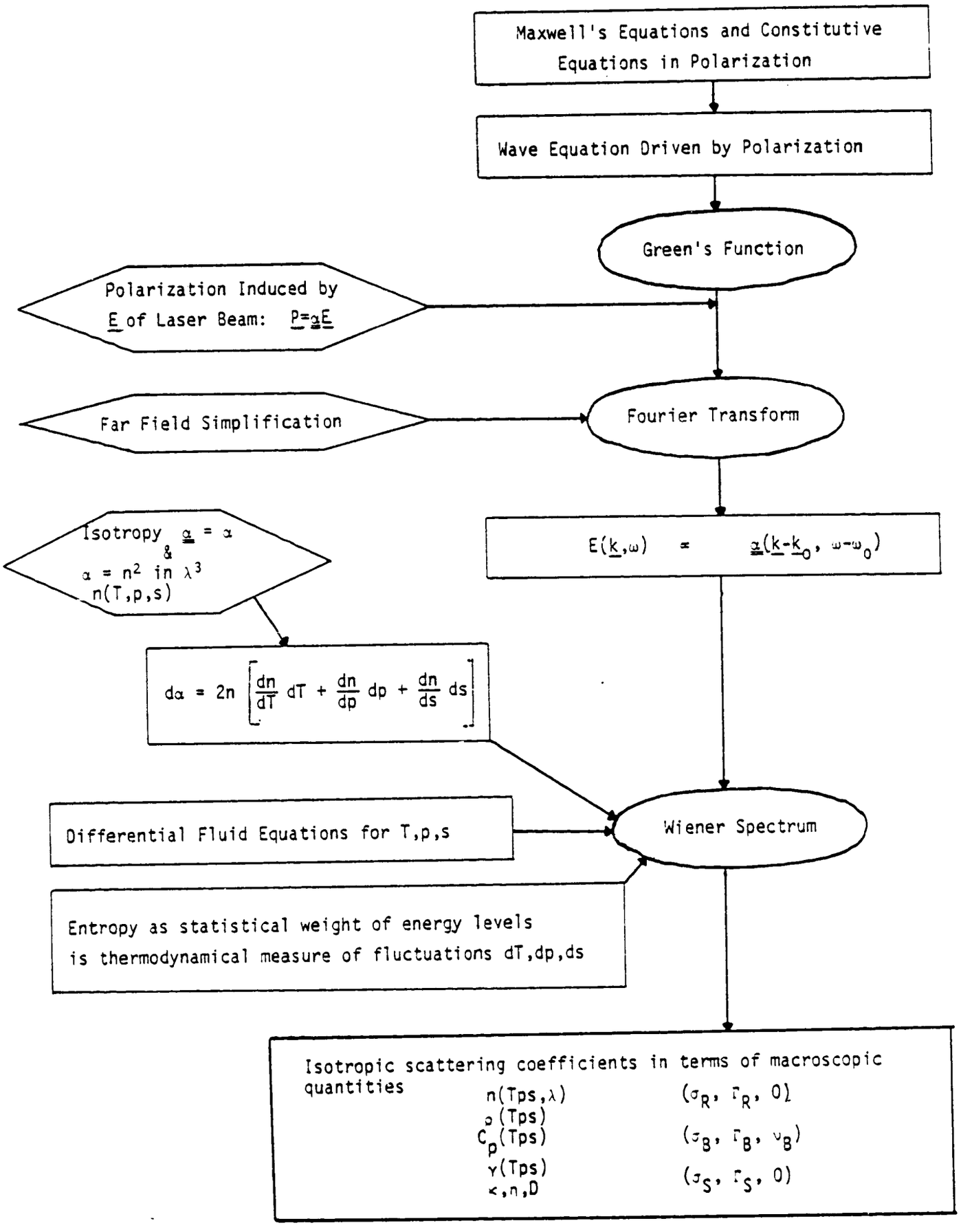
Maxwell's Equations and Constitutive Equations in Polarization
Wave Equation Driven by Polarization
Green's Function
Polarization Induced by E of Laser Beam: P=αE
Far Field Simplification
Fourier Transform
Isotropy α = α
& α = n² in λ³
n(T,p,s)
E(k,ω) = α(k-k₀, ω-ω₀)
dα = 2n [dn/dT dT + dn/dp dp + dn/ds ds]
Differential Fluid Equations for T,p,s
Wiener Spectrum
Entropy as statistical weight of energy levels
is thermodynamical measure of fluctuations dT,dp,ds
Isotropic scattering coefficients in terms of macroscopic quantities
n(Tps,λ) (σR, ΓR, 0)
ρ(Tps)
Cp(Tps) (σB, ΓB, νB)
γ(Tps)
κ,η,D (σS, ΓS, 0)

FIGURE V.2

$$\frac{c}{4\pi}(\underline{E}\,\underline{H}) = \frac{c}{8\pi}E_o^2 = \text{Flux in ergs/cm}^2\text{sec} \qquad \text{V.1}$$

POYNTING'S THEOREM IN GAUSSIAN UNITS

$$\nabla \cdot \underline{D} = 4\pi\rho \qquad \text{V.2}$$

$$\nabla \cdot \underline{B} = 0 \qquad \text{V.3}$$

$$\nabla \times \underline{E} = -\frac{1}{c}\frac{\delta \underline{B}}{\delta t} \qquad \text{V.4}$$

$$\nabla \times \underline{H} = \frac{4\pi \underline{J}}{c} + \frac{1}{c}\frac{\delta \underline{D}}{\delta t} \qquad \text{V.5}$$

$$\underline{D} = \underline{E} + 4\pi \underline{P} \qquad \text{V.6}$$

$$\underline{B} = \mu \underline{H} \qquad \text{V.7}$$

MAXWELL'S EQUATIONS AND

CONSTITUTIVE EQUATION

$$\nabla^2 p - \frac{1}{v^2} \frac{\delta^2 p}{\delta t^2} = - \frac{\eta}{\rho_0 v^2} \frac{\delta}{\delta t} (\nabla^2 p) \qquad \text{V.8}$$

$$\rho \, c_v \frac{\delta T}{\delta t} = -k \, \nabla^2 \, T \qquad \text{V.9}$$

$$\frac{\delta s}{\delta t} = - D \, \nabla^2 \, s \qquad \text{V.10}$$

DIFFERENTIAL FLUID EQUATIONS

$$L\,\phi(x) = S(x)$$

Define Green's Function $G(x,x')$ so that

$$L\,G(x,x') = \delta(x-x') \ .$$

And

$$\phi(x) = \int_{-\infty}^{+\infty} S(x')\,G(x,x')\,dx'$$

When

$$L = \nabla^2 - \frac{1}{c^2}\frac{\partial}{\partial t^2}$$

$$G(\underline{r},t,\underline{r}',t') = \frac{\delta\left[\frac{|\underline{r}-\underline{r}'|}{c} + (t-t')\right]}{4\pi\,|r-r'|}$$

GREEN"S FUNCTIUN FOR WAVE EQUATION

V.11

$$f(k,\omega) = \int_{-\infty}^{+\infty} d\underline{r}\, dt\, e^{-i(k\cdot r + \omega t)}\, f(r,t)$$

$$f(r,t) = \frac{1}{(2\pi)^+} \int_{-\infty}^{+\infty} d\underline{k}\, d\omega\, e^{i(k\cdot r + \omega t)}\, f(k,\omega)$$

FOURIER TRANSFORM

V.12

Random function $f(x)$

of Fourier Transform $F(\omega)$

has a Wiener Spectrum defined by

$$W(\omega) = \frac{1}{4\pi^2} \lim_{A \to \infty} \frac{1}{A} \iint_{A(\omega,-\omega)} F^*(-\nu)\, F(\eta)\, d\nu\, d\eta \,.$$

The Wiener Spectrum is sometimes called Power Spectrum and is used to obtain the average effect of random fluctuations.

WIENER SPECTRUM

V.13

of thermodynamical for statistical quantities. These lengthy computations yield the characteristics of the isotopic scattering by the equations of Table IV.1. For each kind of isotopic scattering, Rayleigh, Brillouin and salinity, the characteristics appear as these quantities: σ scattering coefficient, Γ width and ν shift. These are computed in terms of the macroscopic quantities in the water:

$n(T,p,s,\lambda)$	= index of refraction
$\rho(T,p,s)$	= density
C_p	= specific heat at constant pressure
γ	= activity coefficient of the salt
$<$	= thermal conductivity
η	= viscosity
D	= diffusion coefficient of the salt

The computation requires some first partial derivatives of the index of refraction and density. To this exactly computed isotropic scattering, we add in constant proportion the anisotropic scattering and the assumed turbidity t with the help of the turbidity normalization function. Thus, for each T,p,s,t we can compute the intensity scattered from the $\sigma_i(\theta)$, Γ_i, ν_i (15 quantities, 10 non-zero) as shown in Table V.2.

As explained in our January 1975 Final Report, CR-139184, neither the salinity nor the anisotropic scattering are of appreciable intensity and, therefore, can be neglected.

An example of the modeling of the spectrum of the scattered light return from a laser beam is shown for 20 and 40 C in Figs. V.3 and V.4. The separations are, respectively, of .3036 and .3114 cm^{-1}. The Brillouin peaks have a finite width, but it is much smaller than the separation so that it should not interfere with the measurement.

Angular dependence

$$p_1^{\,o}(\vartheta) = \frac{3}{4}\left(1 + \cos^2\vartheta\right)$$

$$p_2^{\,o}(\vartheta) = 0$$

Rayleigh

$$\sigma_R = \frac{32}{3}\pi^3 k \frac{n^2T^2}{c_p\rho\lambda_o^4}(n_T)^2$$

$$\Gamma_R = \frac{K}{\pi c\rho c_p}\left[\frac{4\pi n}{\lambda_o}\sin\frac{\vartheta}{2}\right]^2$$

Brillouin

$$\nu_R = 0$$

$$\sigma_B = \frac{32}{3}\pi^3 k \frac{\rho n^2 T}{\lambda_o^4} \frac{\left[n_p - n_T \rho_T \frac{T}{\rho^2 c_p}\right]^2}{\left[\rho_p - \rho_T \rho_T \frac{T}{\rho^2 c_p}\right]}$$

$$\Gamma_B = \frac{1}{2\pi\rho c}\left[\frac{4}{3}\eta + \frac{K}{c_p}\left[\frac{\rho_T^{\,2}T}{\rho^2\pi_p c_p - \rho_T^{\,2}T}\right]\right]\left[\frac{4\pi n}{\lambda_o}\sin\frac{\vartheta}{2}\right]^2$$

$$\nu_B = \frac{2nv_s}{c\lambda_o}\sin\frac{\vartheta}{2}$$

Salinity

$$\sigma_s = \frac{32{,}000\,\pi^3}{3\,N_A}\frac{n^2\,s\,u}{\lambda_o^4}n_s^{\,2}F(\gamma)$$

$$\Gamma_s = \frac{D}{\pi c}\left[\frac{4\pi n}{\lambda_o}\sin\frac{\vartheta}{2}\right]^2$$

$$\nu_s = 0$$

Table V.1 ISOTROPIC SCATTERING

To the isotropic scattering $[\sigma_R\ p^o(\theta),\ \Gamma_R(\theta),\ 0]$

$[\sigma_B\ p^o(\theta),\ \Gamma_B(\theta),\ \nu_B(\theta)]$

$[\sigma_S\ p^o(\theta),\ \Gamma_S(\theta),\ 0]$

We add the anisotropic scattering (unimportant since $\Gamma_a >>$) $[\sigma_a\ p^a(\theta),\ 5,\ 0]$

and assume turbidity t $[t\ \beta(\theta),\ 0,\ 0]$

Thus for each (T,p,s,t) of the water

and λ_o of laser with pulse intensity $I_o(\nu)$

we define Shape Function

$$S(\nu,\theta) = \frac{1}{2} \sum_{i,\pm} \frac{\sigma_i\ \Gamma_i\ (\theta)}{\Gamma_i^2(\theta) + 4(\nu \pm \nu_i(\theta))^2}\ p^i(\theta)$$

and obtain the intensity scattered by a length ℓ of water in a solid angle Ω as

$$I(\nu) = I_o(\nu) \quad * \quad S(\nu,\theta)\ \frac{\Omega}{2\pi^2}\ \ell \quad .$$

TABLE V.2

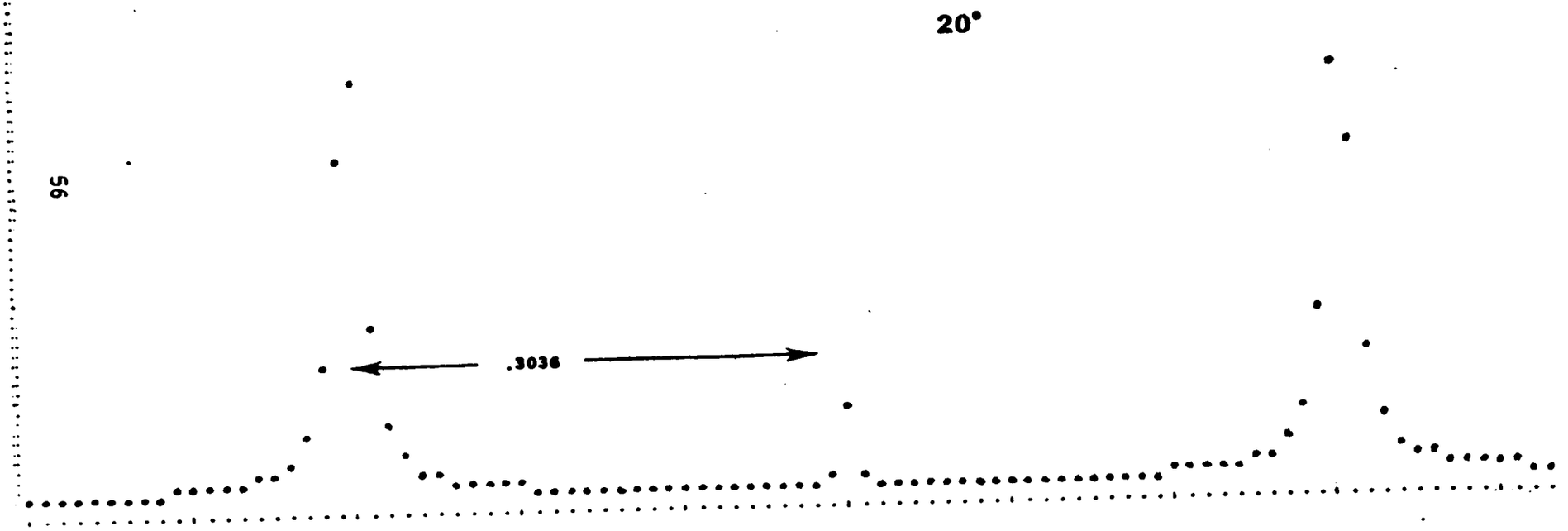

FIGURE V.3

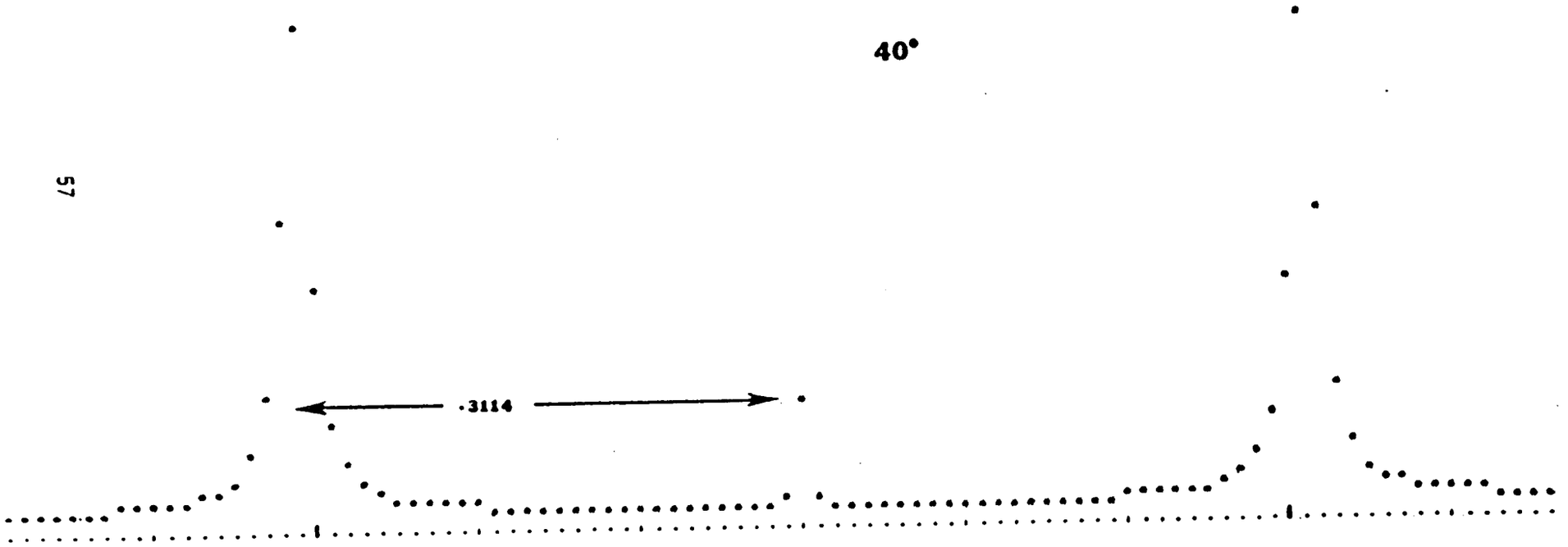

FIGURE V.4

VI. System Design

Once we have a reliable method of predicting the scattering of the laser beam, it is possible to model the features of any design. During the period of the contract covered by this report, a large portion of the work has been the analysis of a number of possible subcomponents, rejecting the ones that were for some reason unsuitable, and finding simple and correct expressions to model the remaining ones. The end result of these studies can be found in this chapter, which represents the basis from which the designs can be composed and contains the algorithms for their evaluations. The system to measure the Brillouin and Tyndall scattering consists of a laser, an optical system, a dispersive element, optical detection and data processing. Each of these subcomponents will be analyzed in turn.

A. Laser Parameter

Naively, the most important parameters of the laser should be its intensity and wavelength. However, the situation is a little more complex because of the difficulty of comparing the intensities of continuous, pulsed and modulated lasers, and also because the length of the pulse influences the scattering length observed and thus the intensity, while the spectral width may widen the Brillouin peaks. The simplest modeling is normalized with respect to pulsed lasers characterized by four parameters as shown in Table VI.1

A modulated or continuous laser is just considered as a succession of pulses. The measurement of a succession of pulses is usually equivalent to the measurement of one pulse of the same total power. For instance, the measurement of a 1 watt continuous laser for 1 second is equivalent to that of a pulsed laser of 1 joule.

Although the continuous progress in the laser field will probably result in new possible laser choices for the future, we have determined that at least 3 now existing laser systems could be used for Brillouin temperature remote sensing.

LASER PARAMETERS

Power	100 mJ/pulse
Wavelength λ_o	variable 5300 A - 4000 A
Line Width	0.05 cm^{-1}
Pulse Length	4 nsec

Table VI.1

1) Yag-Nd^{++} pulsed laser frequency doubled to 5300 A:

This laser appeared at the start of the design phase to be the most interesting system: There are no limitations in power, pulse width or line width with suitable accessories, and powerful lasers of this kind have been routinely flown in airplanes. However, it turns out that the laser wavelength 5300 A is not the best for maximum penetration in the sea, and that the accessories for reducing the pulse length and spectral width are expensive in funds and energy. Its use would then be reserved for a possible expensive large system.

2) Dye Laser, excited by N_2 Laser:

Dye lasers have many advantages, such as complete tunability in the wavelength region of interest, a natural pulse length of about 5 nanosec, and the additional availability of the powerful UV N_2 laser pulse itself for Raman salinity measurements. They however require a double Fabry-Perot in the laser cavity for spectral width reduction and are at present limited in power by dye destruction.. Since they have efficient energy conversion, they may be used for the airborne system, if the technology of more powerful large bore lasers with narrow spectral width continues to make progress.

3) Argon Ion Laser

These provide easily sufficient continuous power in a series of very narrow spectral lines in the region of interest 5000 - 4500 A with a well proven technology. However, the need for modulation in the monostatic systems will tend to slow down the measurements and reduce the power available. This laser system clearly appears to be the least expensive and the easiest to use for the first phase of the experimental program.

B. Optical System

The optical system, as shown in Fig. VI.1, may be kept rather simple: A method to bring the laser beam to the water to be analyzed, and a large lens

$$I(\nu) = \left| I_o(\nu) \circledast S(\nu,\theta) \frac{\Omega}{2\pi^2} L \right| \left[k\, e^{-2h(\lambda)Y} \right] \eta$$

$$\Omega = \frac{A}{(Y + nH)^2}$$

$$L = \frac{c\,\Delta t_d}{2n}$$

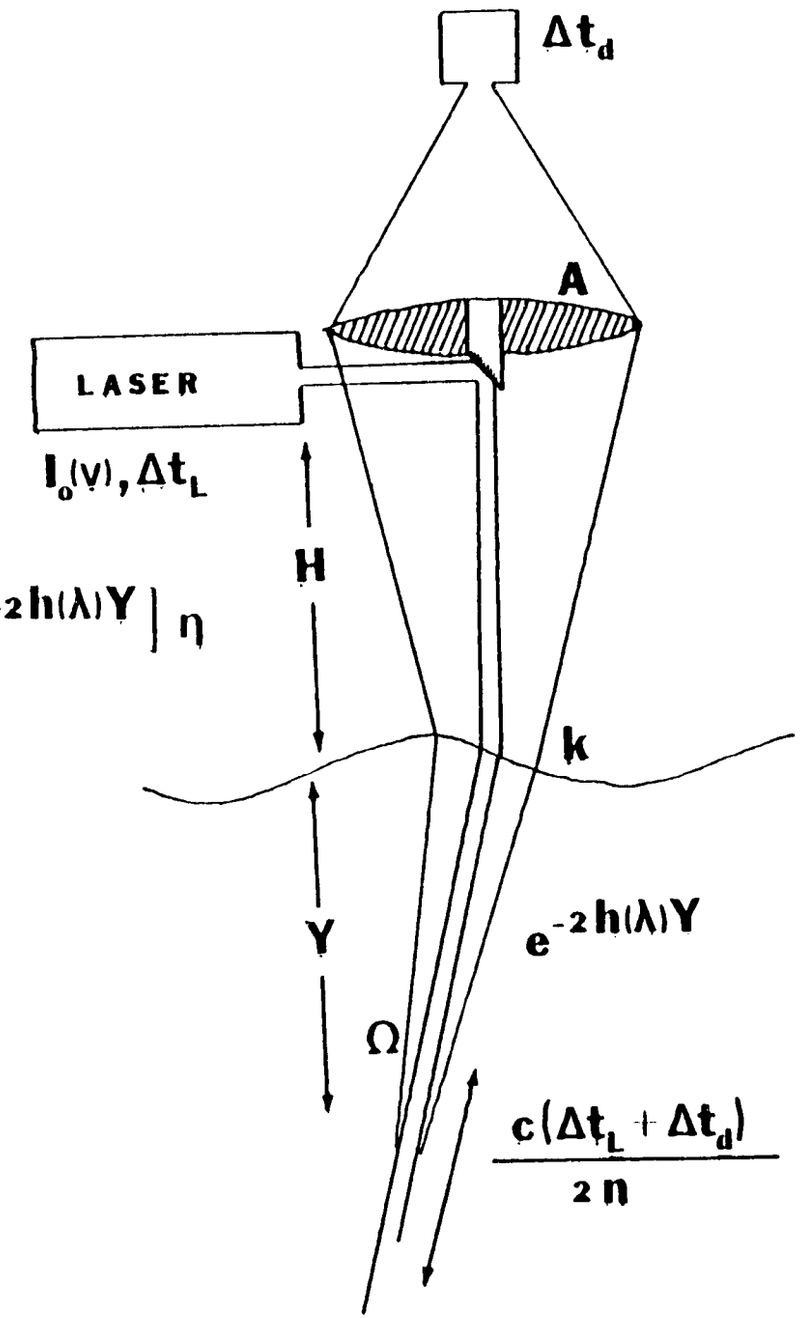

FIG. VI.1

for collecting the scattered light. Since all considerations indicate definite advantages of keeping the laser beam as small as possible, we have only to steer the beam by a mirror, and the only attenuation is due to the absorption $h(\lambda)$ of the underwater path Y (the small reflection at the surface should be negligible and will be included in the sea surface factor). The scattered light is then collected by the largest possible lens (of area A) at a height H above the water. Taking into account the refraction at the sea surface, the solid angle collected is $\frac{A}{(Y + nH)^2}$, where n is the index of refraction of the water. The power scattered in this solid angle is then the laser power multiplied by the scattering coefficient, the solid angle, and the length of the scattering medium observed. This length L is found from the geometry in a bistatic system and from the integration time of the detector Δt_d in the monostatic system $L = \frac{c \Delta t_d}{2n}$. This scattered intensity is attenuated by the absorption of the underwater path by a factor $e^{-h(\lambda)Y}$ and by losses at the sea surface described by a factor k, a function of the dimension of the re· . beam. In conclusion, the light intensity passing through the area A of the lens can be computed as a function of wave number:

$$I(\upsilon) = k\, e^{-2h(\lambda)Y} \{I_o(\upsilon) * \sigma(\upsilon,\theta)\} \frac{cA\, \Delta t_d}{2n(Y + nH)^2}$$

and the instrument has to make the best use of this observed light.

C. Dispersive System

This collected light has to be analyzed for the spectral information that will give the speed of sound and the turbidity. This is done by distributing the photons in several channels; to obtain two quantities (speed of sound and turbidity) by ratio of intensity in the channels requires three channels. After discarding several interesting schemes of dispersive systems,

we are now considering only two options: Fabry-Perot and Mach Zehnder interferometers. We will probably use the Fabry-Perot system in the first stage of the experimental work because a suitable Fabry-Perot interferometer is available at our laboratory and we have years of experience in its use, but because the Mach Zehnder system is not as sensitive to the effect of the sea surface and is more stable, we plan to use it for the airborne system.

Fig. VI.2 illustrates the principle of the Fabry-Perot: Each wavelength λ is transmitted in a ring of angle θ. A multimirror inclined at an angle α can then direct various wavelength ranges towards photomultipliers at angles 2α (Fig. VI.3). The quality of the Fabry-Perot is best expressed by the "finesse" F, defined as the inverse of the unavoidable spectral spreading compared to the free spectral range FSR. The effect of the Fabry-Perot can then be written as the convolution of the spectra with the spread function

$$S(\nu) = \sum_{-\infty}^{+\infty} \frac{\pi FSR^2}{FSR^2 + F^2(\nu + k\ FSR)^2} \quad ,$$

and the multimirror selects a suitable wavelength range in this convoluted spectra. The range of the three channels are shown in Fig. VI.4 and VI.5 compared to the convoluted Brillouin spectra at 20 and 40°C. The signals are given for a shipborne system looking at a depth of 20 meters with a 0.1 joule laser at 4500 Å in units of 10^7 photons. The schematic of the Fabry-Perot system is given in Fig. VI.6.

The Mach Zehnder system is based on another interferometer shown in Fig. VI.7. This instrument is often thought as an unfolded Michelson interferometer yielding the same channeled spectrum, but in reality the unfolding allows the transmission of two complementary channeled spectra. The advantage of a Mach Zehnder is a consequence of the fact that no photons are rejected: This not only results in a great sensitivity, but it also frees the design of the necessity of insuring uniform illumination of the channels.

FABRY-PEROT in TRANSMISSION

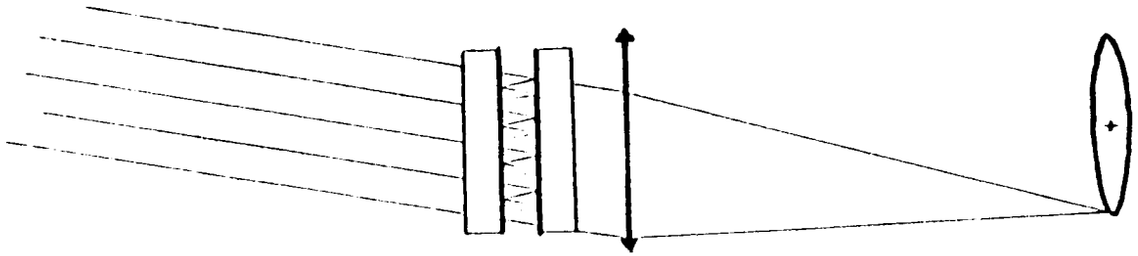

$$m\lambda = 2\mu t \cos\theta$$

$$I_T = I_0 \frac{(1-R)^2}{(1-R)^2 + 4R \sin^2(\delta/2)}$$

FIG. VI.2

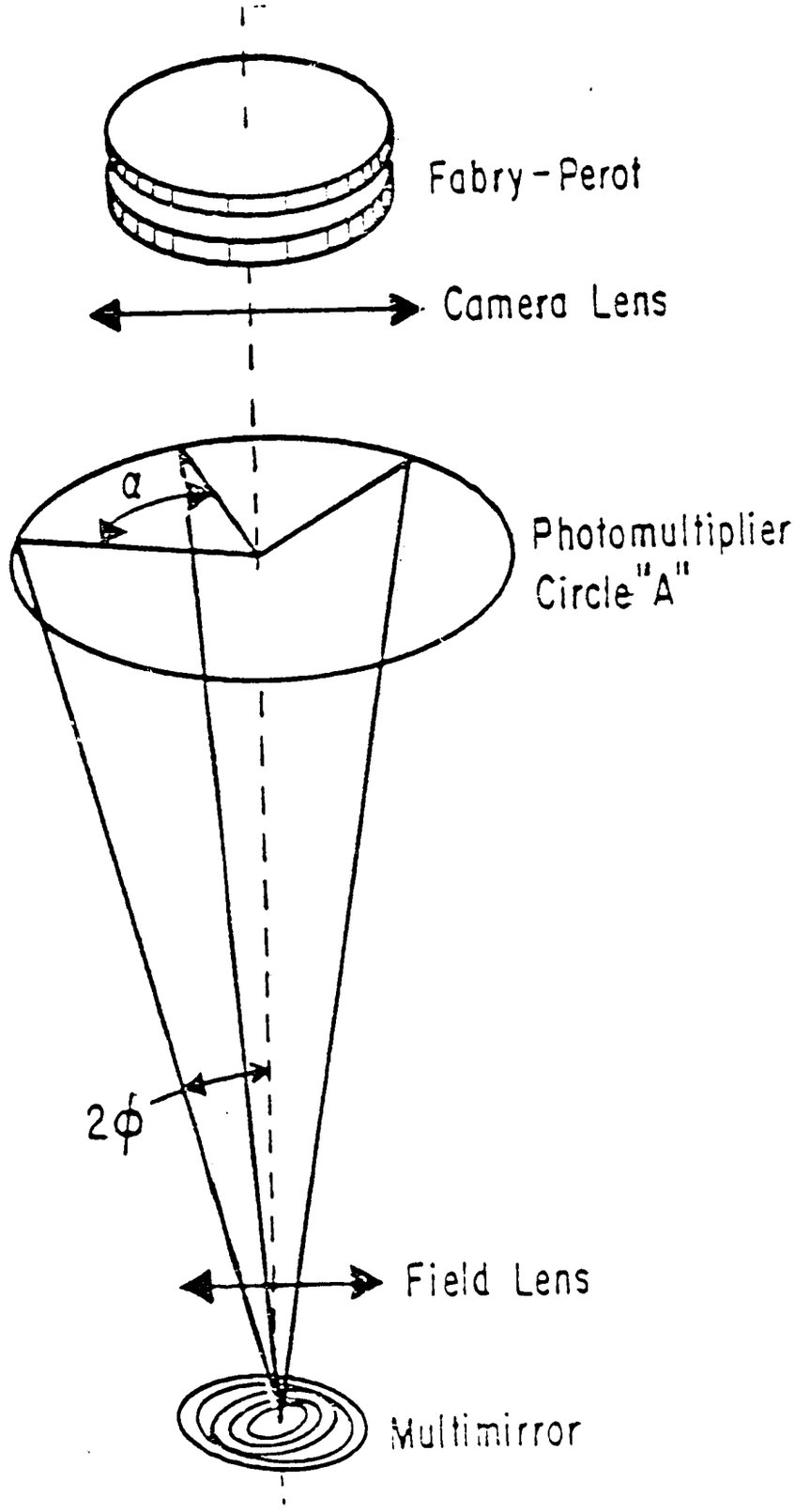
Fabry-Perot
Camera Lens
α
Photomultiplier
Circle "A"
2φ
Field Lens
Multimirror

FIGURE VI.3

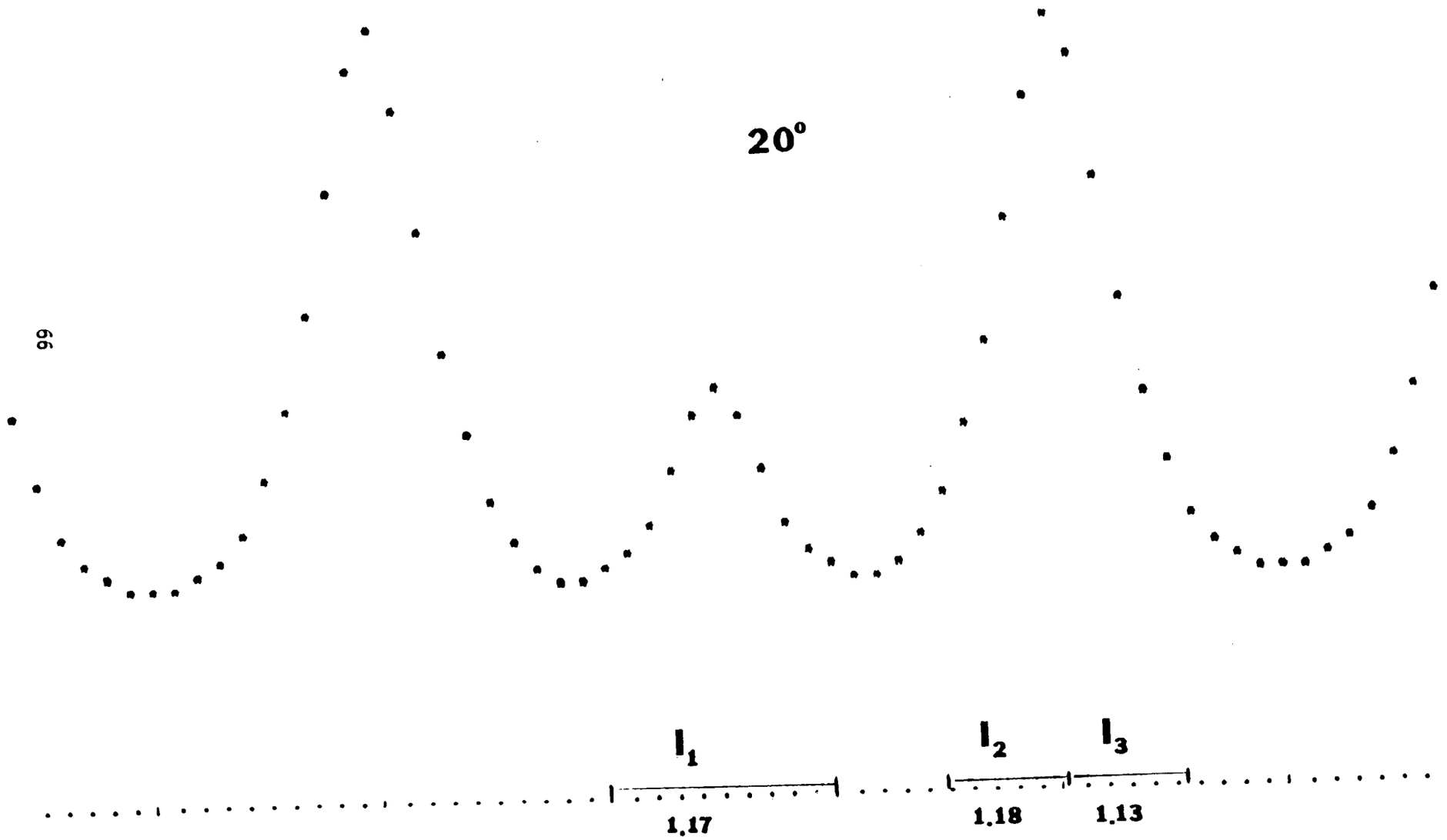

FIG. VI.4

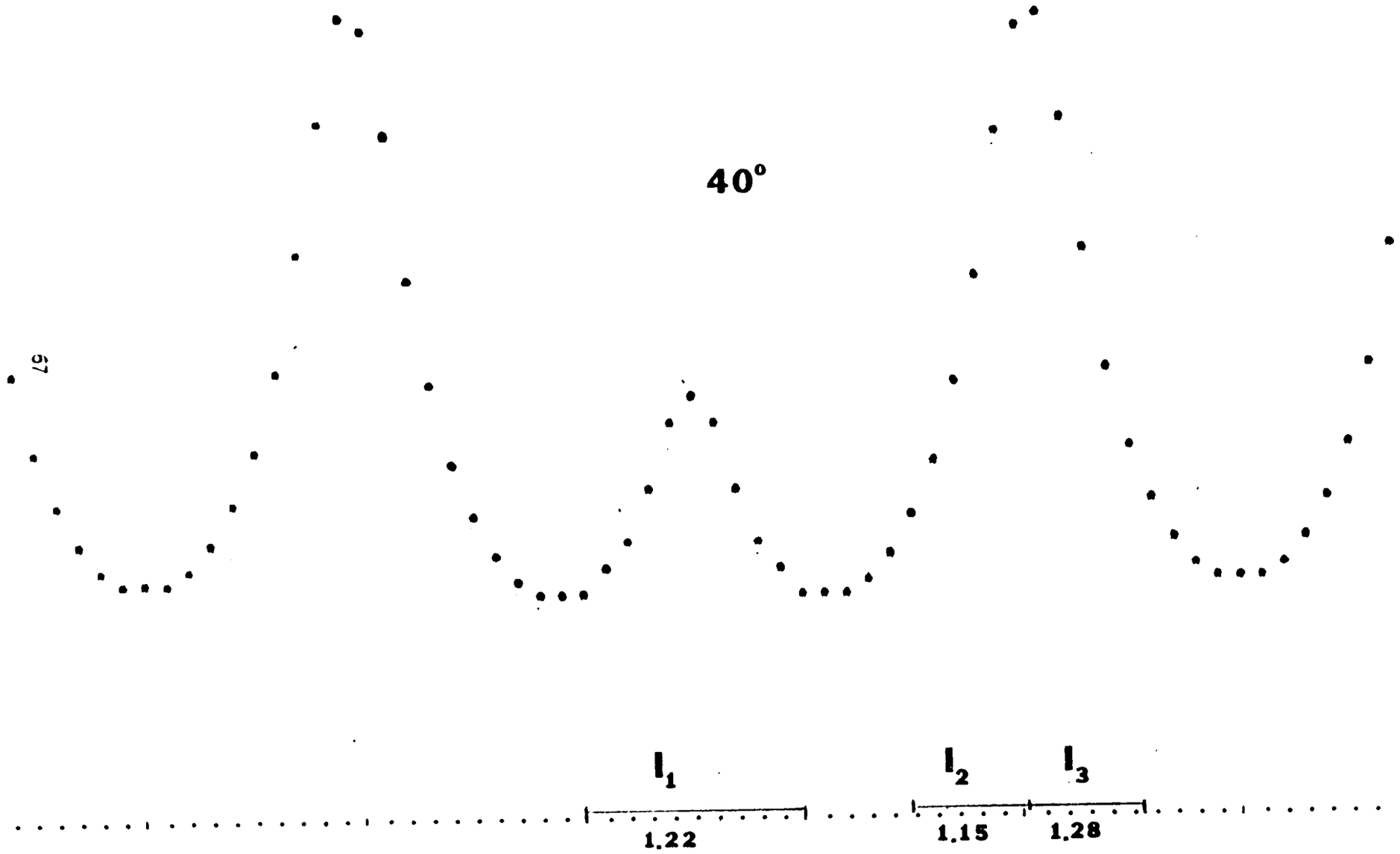

FIG. VI.5

Fabry-Perot

system

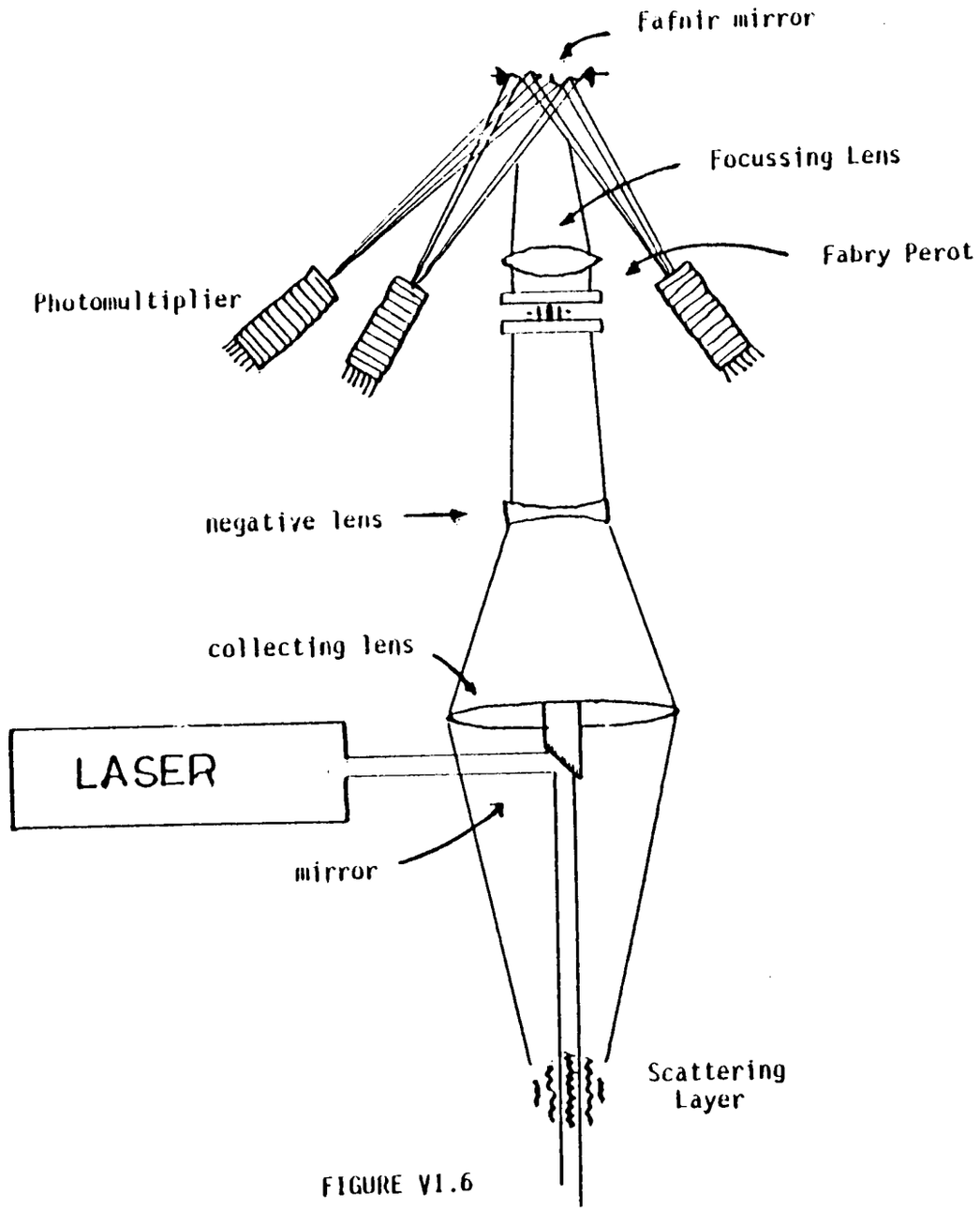

FIGURE VI.6

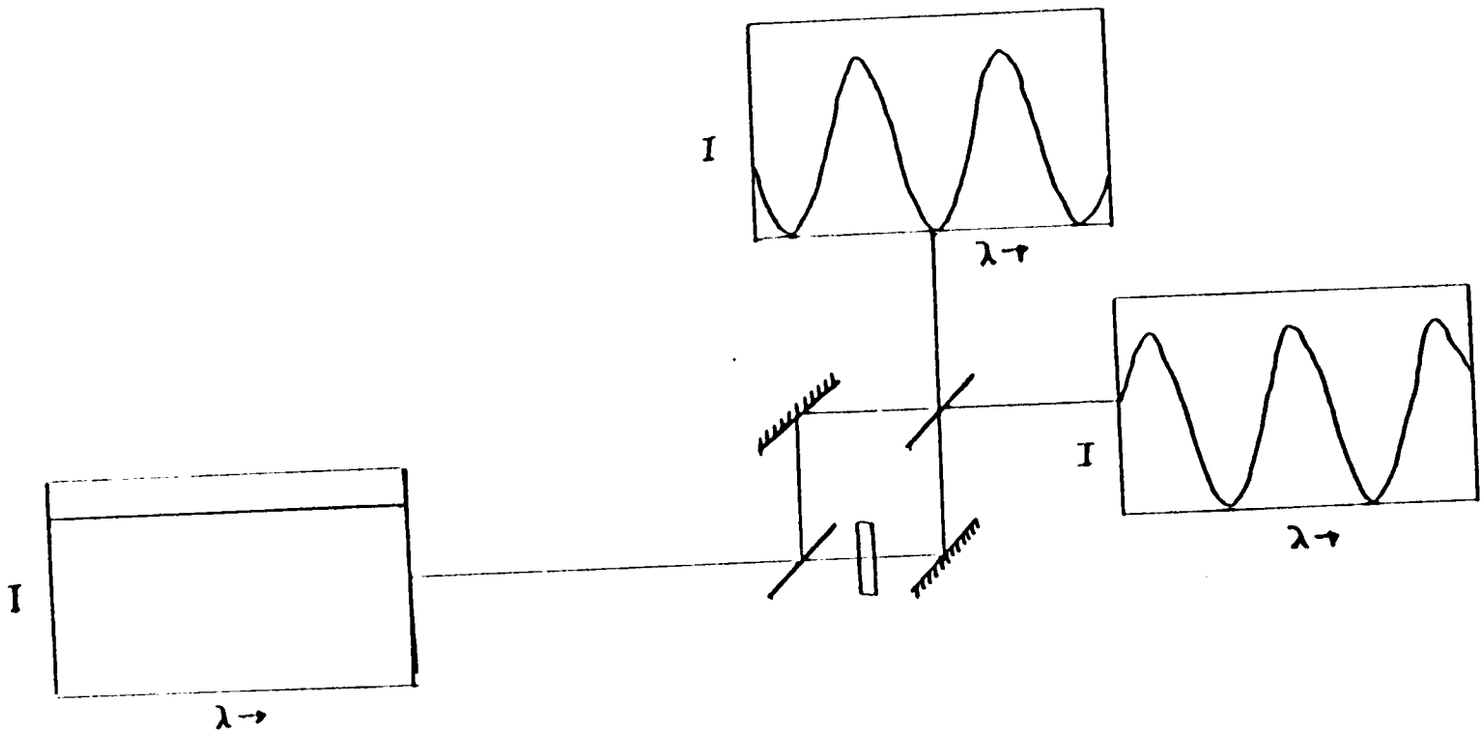

Mach-Zehnder

FIG. VI.7

The amount of light accepted by the interferometer is easily increased by field widening as in Fig. VI.8. To obtain the necessary three channels, two Mach-Zehnder interferometer are used in succession: A first one is used to separate the Tyndall peak, and the second one for analyzing the remaining light to get the Brillouin separation. The transmission in these channels will be of the form

$$T(\nu) = \alpha[1 - \beta\cos\Delta_1(\nu+\nu_0)][1 \pm \gamma\cos\Delta_2(\nu+\nu_0)] \ .$$

A schematic of the complete system is shown in Fig. VI.9, and the expected transmission of the Brillouin channels in Figs. VI.10 and VI.11.

Field Widened

Mach-Zehnder

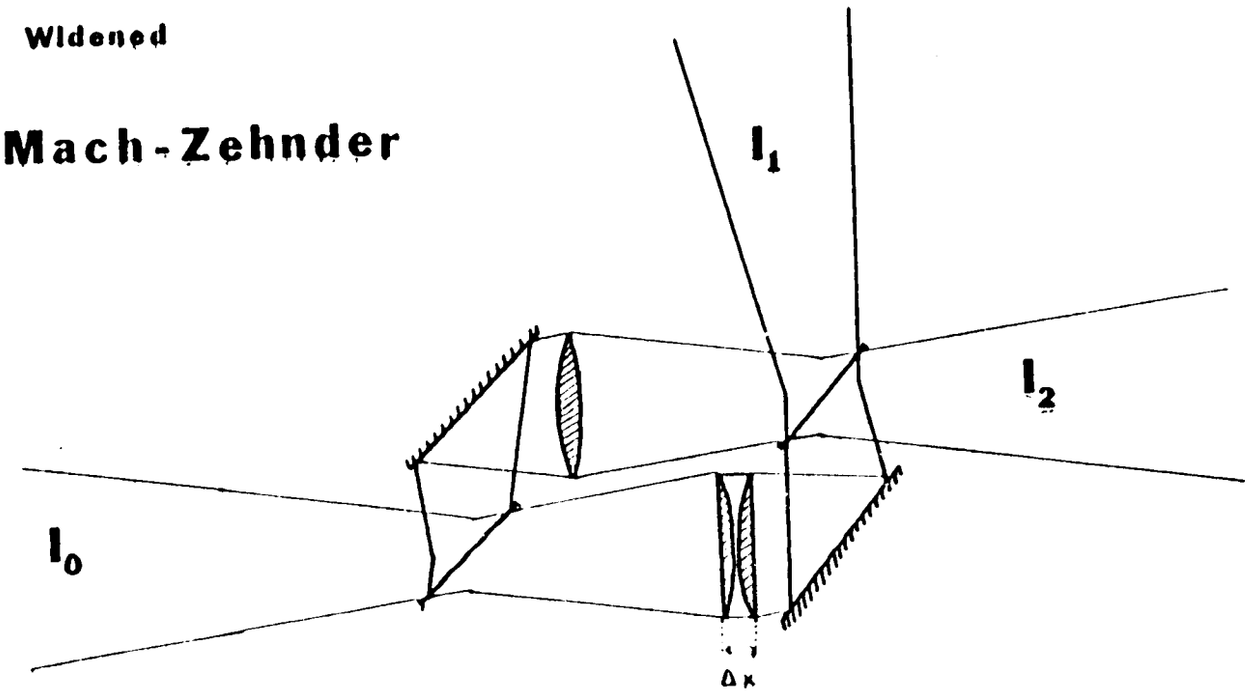

FIG. VI.8

Mach-Zehnder

system

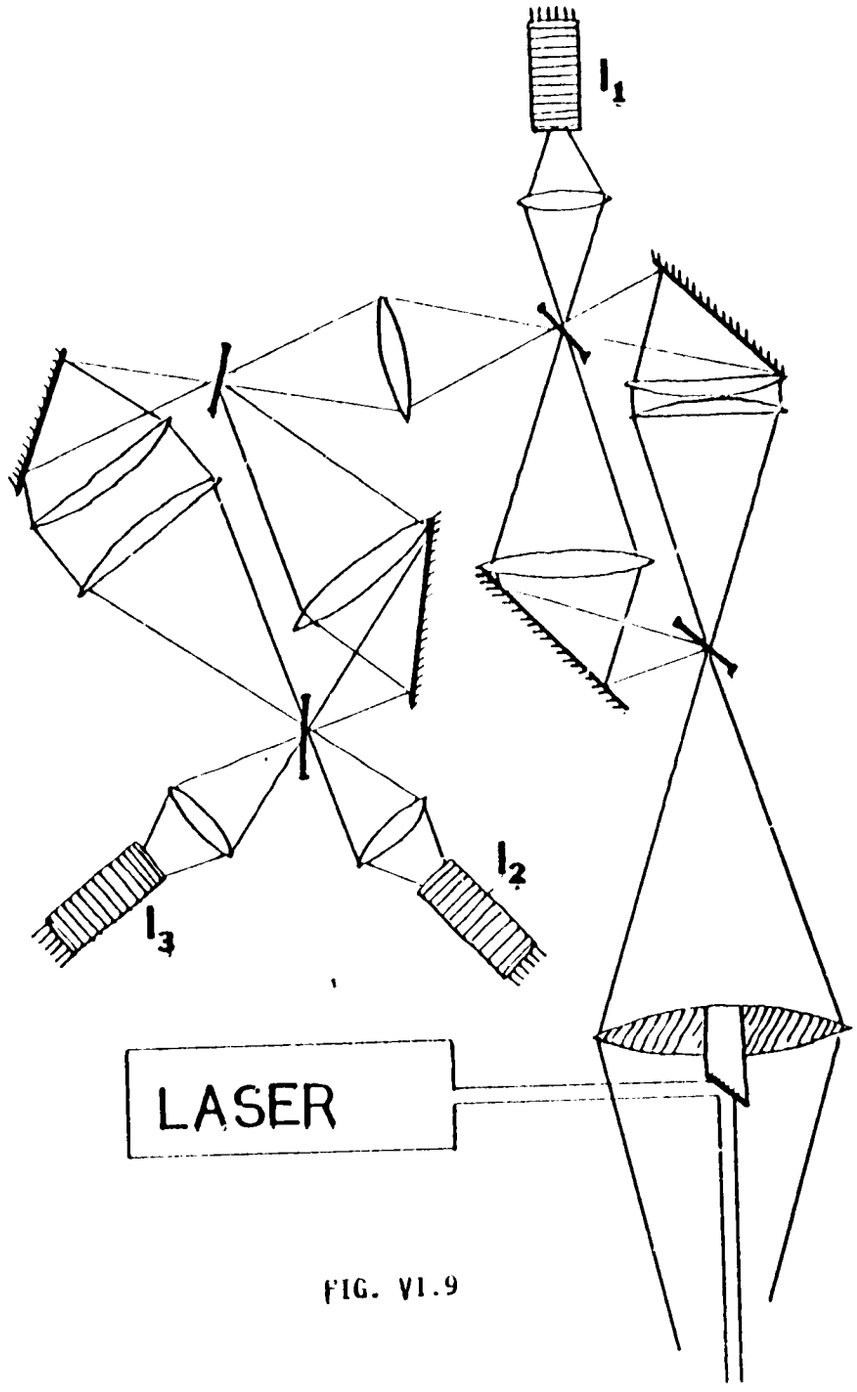

FIG. VI.9

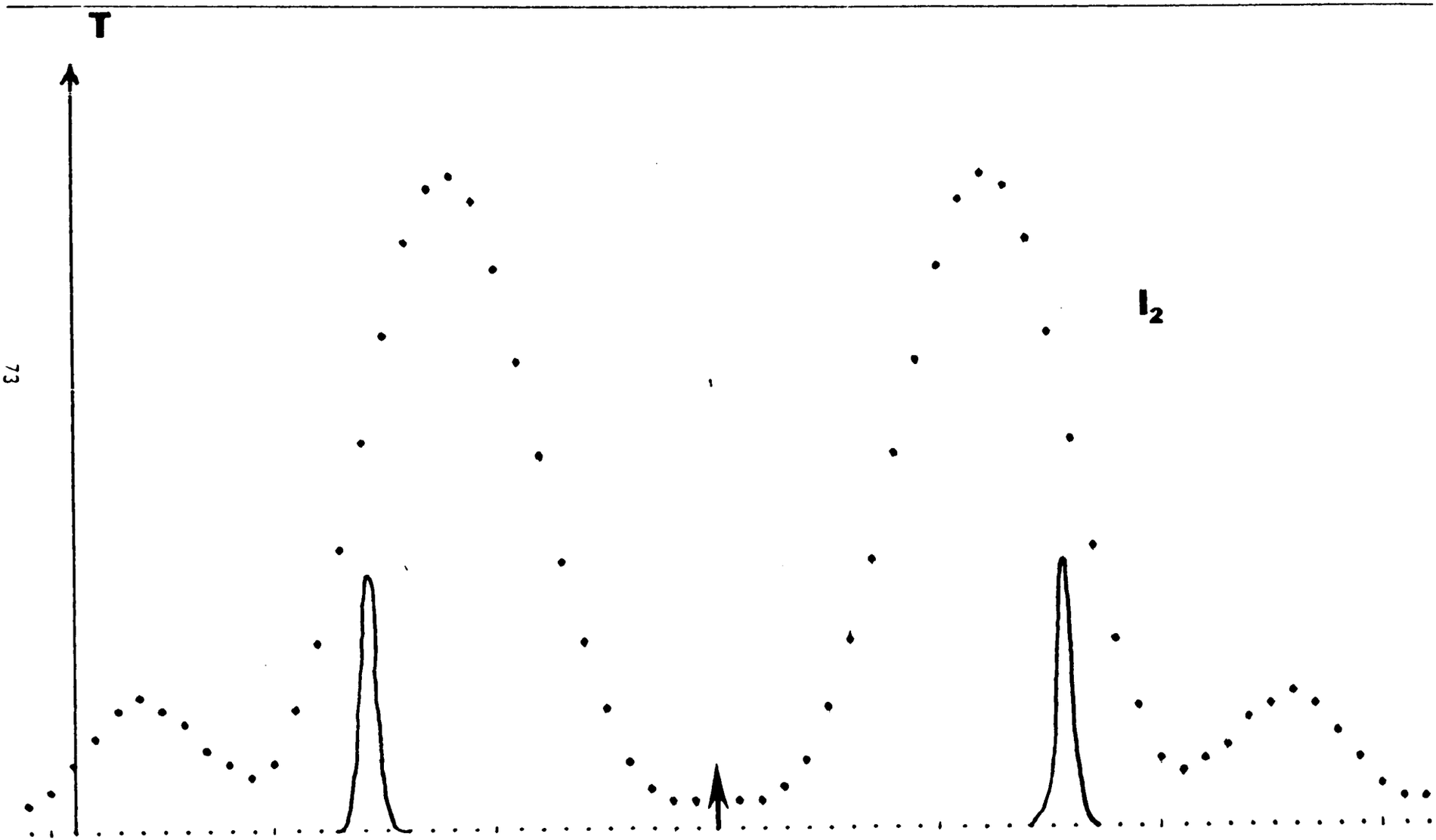

FIG. VI.10

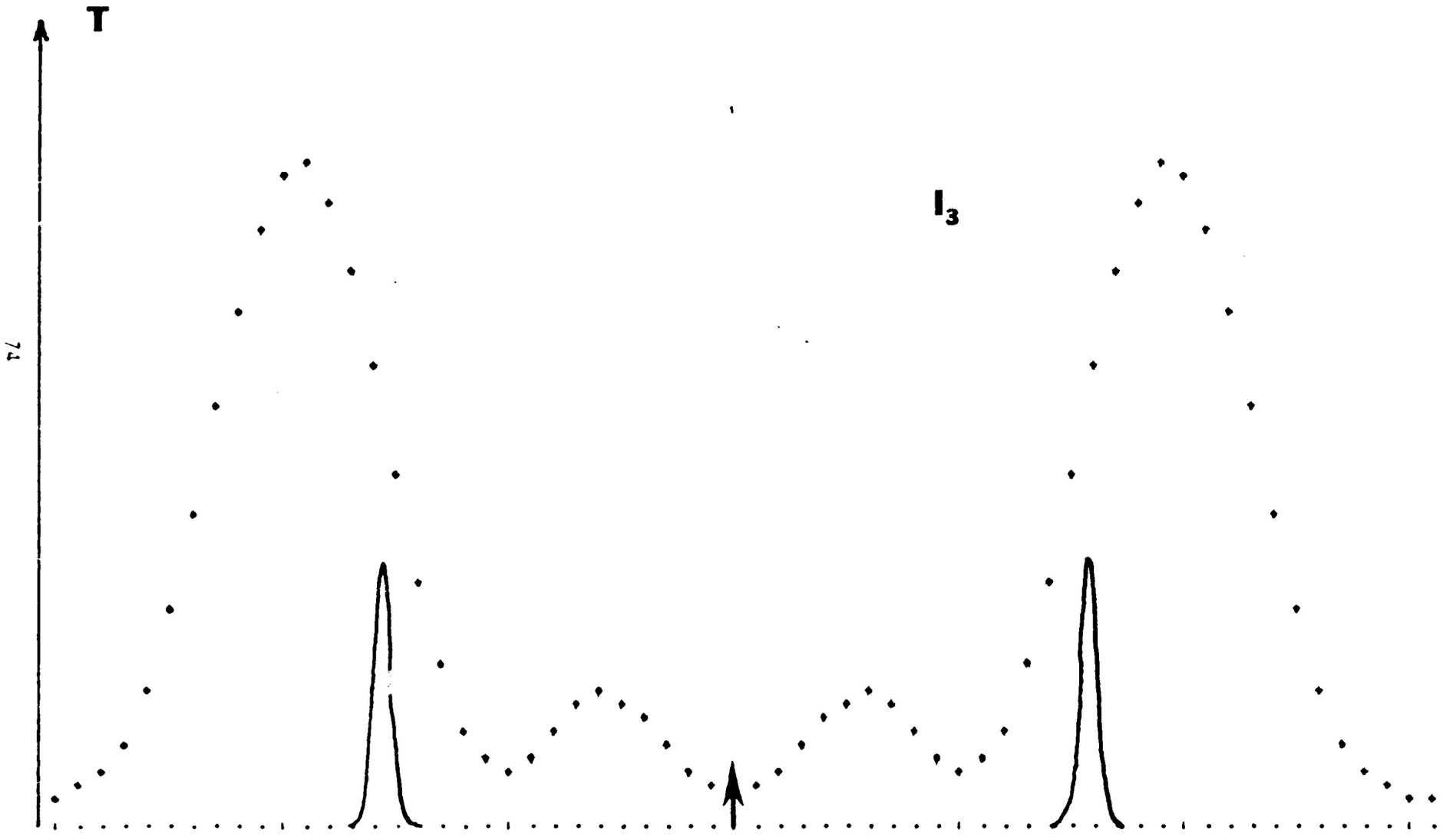

FIG. VI.11

D. Collection and Recording

The systems used to detect and record the photons in each channel have to be quite different in a bistatic, monostatic pulse, and monostatic modulated Brillouin remote sensor. The bistatic configuration is certainly the simplest because continuous or chopped light has to be detected: We will simply use good sensitive photomultipliers with quantum efficiency in the blue of about 20 to 30%. With these detectors we don't expect to have to use a photon counting mode even though this option is available if more sensitivity is desired. The voltage signal of the three channels will then be read sequentially by the NOVA 800 computer. The material for the analog data acquisition system is already on hand and we are working on the modifications to the computer. The data accumulated in the computer during a complete run will then be dumped on teletype or magnetic tape for future reference.

The detection system is a difficult and expensive part of the monostatic pulsed system. The extremely fast varying signal must be measured precisely with a time resolution of a few nanoseconds; just maintaining a pulse shape in the electronics at these speeds is a complex undertaking. The best solution is to reduce the electronics to a minimum and thus use fast photomultipliers with large gains (these may have long delay times but are designed to avoid the spread and jitter in this delay) and then, after minimum amplification, we digitize and slow down the pulse by the use of a Tektronic transient digitizer, which can digitize signals of mVolt range at nanosecond speed. This however represents a large expense (about $8,400 per transient digitizer), and we will need 3 digitizers (one per channel) and a special control computer. For testing purposes, a cheaper system without continuous depth information could probably be rigged up from short aperture samples and holds. This may be a method for measuring the quality of the photomultipliers without the expense of a full recording system.

E. Data Processing

For reasons of convenience, we will record the data in a minicomputer, which allows great flexibility in subsequent processing of the data. However, a relatively simple linear algorithm such as shown below will be sufficient for the prototype:

The intensity in the three channels described in Section C of this chapter are assigned the notation I_1, I_2, I_3 in the following way:

I_1 is the channel that increases most with an increase of Tyndall scattering (central channel),

I_2 and I_3 are the channels that respectively decrease and and increase with an increase in the separation of the Brillouin peaks.

Then in a large number of experiments, either simulated or real, the temperature T_o of equality of I_2 and I_3 is determined, and a regression on data at this temperature but at different turbidities gives the coefficients C_2 and C_4 of Tyndall rejection by requiring that the quantities

$$I_4 = I_2 + I_3 - C_2 I_1$$

$$I_5 = I_3 - I_2 + C_4 I_1$$

became independent in first order of the turbidity.

It then becomes easy, for this case of assumed salinity, to find the coefficients for the linear expressions for temperature and turbidity by further regressions:

$$t = C_1 \; I_1/I_4$$

$$T = T_o + C_3 \; I_5/I_4 \quad .$$

This linear processing was used in the simulations for the design of different configurations, so that the noise could be obtained by a method similar

to the square root of the signal. We also discovered at that time the remarkable precision of such a simple computation: no noticeable error with turbidity from .01 to 100 and drifts of less than 1°C for range of more than 20°C.

An easy method for avoiding the error due to even this drift is to make a table of the needed corrections as a function of the raw results; such a correction table may already be stored in the computer memory for the bistatic system so that the direct result of an experiment will be given immediately by the computer as correct temperature.

VII. Feasibility Criteria

A. Seaborne Bistatic System

The feasibility of the seaborne bistatic system is indicated in part by numerous laboratory experiments to measure the speed of sound from the Brillouin spectrum. Typically, a laser beam is directed into the liquid, and a Fabry Perot is used to analyze the spectrum. This corresponds almost exactly to the prooosed bistatic system except that we will encounter field conditions and impure water.

Since we demonstrated the overall feasibility of the Brillouin temperature remote sensing, we feel that the intensity of the return and freedom from noise will be quite sufficient in the bistatic system. Comparing with the detailed computation on the seaborne monostatic Fabry-Perot system discussed in this chapter, using a 1 second integration time with a 650 mW laser which corresponds to 650 mJ instead of only 100, and assuming that the bistatic system could easily look at the same scattering lengths (about 1 meter), we conclude that measurements up to a depth of 20 meters should be possible with the limited instrumentation we are contemplating. Our confidence results in good part from our previous experience with the Fabry-Perot interferometer and high sensitivity photomultipliers. We have developed techniques for modeling and assessing these systems. We know that if extreme sensitivity is needed we can use photon counting; and with the resulting data in a computer, many processings and time integration schemes may easily be tested.

Even without searching at this time for the exact capabilities of a working bistatic system, we will need the experience that such a simple system with flexible design only can bring. It not only is the simplest and most direct demonstration of the principle of the Brillouin temperature remote sensing, but also offer a similarly simple and direct method of checking the

whole of the theory we have developed. The verification can start with a situation very close to the normal laboratory Brillouin experiment, and then be varied continuously up to a practical remote sensing situation in biologically active water with normal turbidity at a depth around 10 meters.

B. Seaborne Monostatic System

This system was completely modeled in a computer program on the Nova 800. The expressions relevant to the simple system: laser, scattering, collection lens and Fabry-Perot were taken from chapter V and VI of this report and programmed in Basic. A printout of the program is given in Appendix B. The results appear as the typical computer run shown in Tables VII.1 and 2. After a series of questions and answers about the kind of instrument to be modeled, the computer determines the best coefficients of the processing on the data, and thereafter, for each temperature, salinity, turbidity and depth, the program computes the expected signal of each channel in number of photons. These channels responses are processed to obtain the temperature and turbidity, and their root mean square variance.

The most interesting results of this study are expressed in Fig. VII.1: Temperature precision in degree centigrade (1σ) compared to laser wavelength for different depth, and Fig. VII.2: Turbidity precision in per cents (1σ) compared to laser wavelengths for different depths. The program was also used to give numerical answers to two important questions on the system: The influence of the turbidity on the measurement, and the effect of an error in salinity. The most noticeable effect of turbidity was on the precision in temperature, and is shown in Fig. VII.3, as a function of the finesse of the Fabry-Perot. It is however a very encouraging sign that this effect begins to appear in relatively dirty water: A turbidity of 10 corresponds to half transmission length of only 62 cm. As seen in Fig. VII.4,

```
RUN
LASER:POWER,LAMBDA,WIDTH,PULSE LENGHT
? 100? 4500? .05? 4
OBSERVATION:HEIGHT,PUPIL AREA,SEA SURFACE FACTOR,EFFICIENCY,ANGLE
? 0? 300? 1? .1? 130
SINGLE F.P. INSTRUMENT.GIVE FSR,FINESSE,DAMPING TIME
? 1? 10? 5
ASSUME SALINITY OF WATER
? .035
SHIFT AT 25 C IS: .306068
GIVE THE CHANNEL LIMITS (6 WAVENUMBERS)
? -.1? .1? .2? .306? .306? .412
THE PROCESSING IS:
LST= .881466 I1/(I2+I3+ .115398 I1)- .256487
T= 20.0399 + 290.564 (I3-I2+ 2.80705E-2 I1)/(I2+I3- .115398 I1)


GIVE ACTUAL VALUES OF TEMP. SALINITY,TURBIDITY,DEPTH
? 30? .035? .1? 2

THE INSTRUMENT GIVES
CHANNEL'S SIGNALS OF          2.3276E+9      2.91051E+9     3.03953E+9
VIZ: TEMPERATURE OF           29.9802        INSTEAD OF     30
WITH A RMS BETWEEN            3.9479E-3 AND 4.08089E-3 C
AND A TURBIDITY OF            .104637        INSTEAD OF     .1
WITH A RMS BETWEEN            8.55814E-3 AND                1.16513E-2 %
AND AN IMPRECISION IN DEPTH OF 100.3 CM


GIVE ACTUAL VALUES OF TEMP. SALINITY,TURBIDITY,DEPTH
? 25? .035? .1? 20

THE INSTRUMENT GIVES
CHANNEL'S SIGNALS OF          1.27397E+7     1.64532E+7     1.66807E+7
VIZ: TEMPERATURE OF           25.4089        INSTEAD OF     25
WITH A RMS BETWEEN            5.28392E-2 AND                5.38087E-2 C
AND A TURBIDITY OF            9.81646E-2     INSTEAD OF     .1
WITH A RMS BETWEEN            .120753 AND    .167066 %
AND AN IMPRECISION IN DEPTH OF 100.257 CM


GIVE ACTUAL VALUES OF TEMP. SALINITY,TURBIDITY,DEPTH
? 25? .035? .1? 50

THE INSTRUMENT GIVES
CHANNEL'S SIGNALS OF          748859         974937         988891
VIZ: TEMPERATURE OF           25.453         INSTEAD OF     25
WITH A RMS BETWEEN            .216958 AND    .220971 C
AND A TURBIDITY OF            9.51112E-2     INSTEAD OF     .1
WITH A RMS BETWEEN            .508903 AND    .703618 %
AND AN IMPRECISION IN DEPTH OF 100.254 CM
```

TABLE VIII.1

```
GIVE ACTUAL VALUES OF TEMP. SALINITY,TURBIDITY,DEPTH
? 25? .035? .1? 100

THE INSTRUMENT GIVES
CHANNEL'S SIGNALS OF          32184.3          40225.6          40780
VIZ: TEMPERATURE OF           25.5205          INSTEAD OF       25
WITH A RMS BETWEEN            1.07032 AND      1.09036 C
AND A TURBIDITY OF            .110557          INSTEAD OF       .1
WITH A RMS BETWEEN            2.21972 AND      3.07634 %
AND AN IMPRECISION IN DEPTH OF 100.248 CM


GIVE ACTUAL VALUES OF TEMP. SALINITY,TURBIDITY,DEPTH
? 25? .034? .1? 20

THE INSTRUMENT GIVES
CHANNEL'S SIGNALS OF          1.2404E+7        1.56395E+7       1.57843E+7
VIZ: TEMPERATURE OF           24.816           INSTEAD OF       25
WITH A RMS BETWEEN            5.43234E-2 AND                    5.52111E-2 C
AND A TURBIDITY OF            .108063          INSTEAD OF       .1
WITH A RMS BETWEEN            .114766 AND      .159002 %
AND AN IMPRECISION IN DEPTH OF 100.275 CM


GIVE ACTUAL VALUES OF TEMP. SALINITY,TURBIDITY,DEPTH
? 25? .035? 1? 20

THE INSTRUMENT GIVES
CHANNEL'S SIGNALS OF          4.44642E+7       1.87872E+7       1.81013E+7
VIZ: TEMPERATURE OF           25.1843          INSTEAD OF       25
WITH A RMS BETWEEN            5.56054E-2 AND                    5.65883E-2 C
AND A TURBIDITY OF            .977669          INSTEAD OF       1
WITH A RMS BETWEEN            3.08316E-2 AND                    4.32662E-2 %
AND AN IMPRECISION IN DEPTH OF 100.257 CM


GIVE ACTUAL VALUES OF TEMP. SALINITY,TURBIDITY,DEPTH
? 28? .035? 10? 25

THE INSTRUMENT GIVES
CHANNEL'S SIGNALS OF          1.95056E+6       2.24236E+7       1.72842E+7
VIZ: TEMPERATURE OF           25.7131          INSTEAD OF       28
WITH A RMS BETWEEN            .106686 AND      .10681 C
AND A TURBIDITY OF            9.74046          INSTEAD OF       10
WITH A RMS BETWEEN            3.95035E-2 AND                    4.61626E-2 %
AND AN IMPRECISION IN DEPTH OF 100.23 CM
```

TABLE VII.2

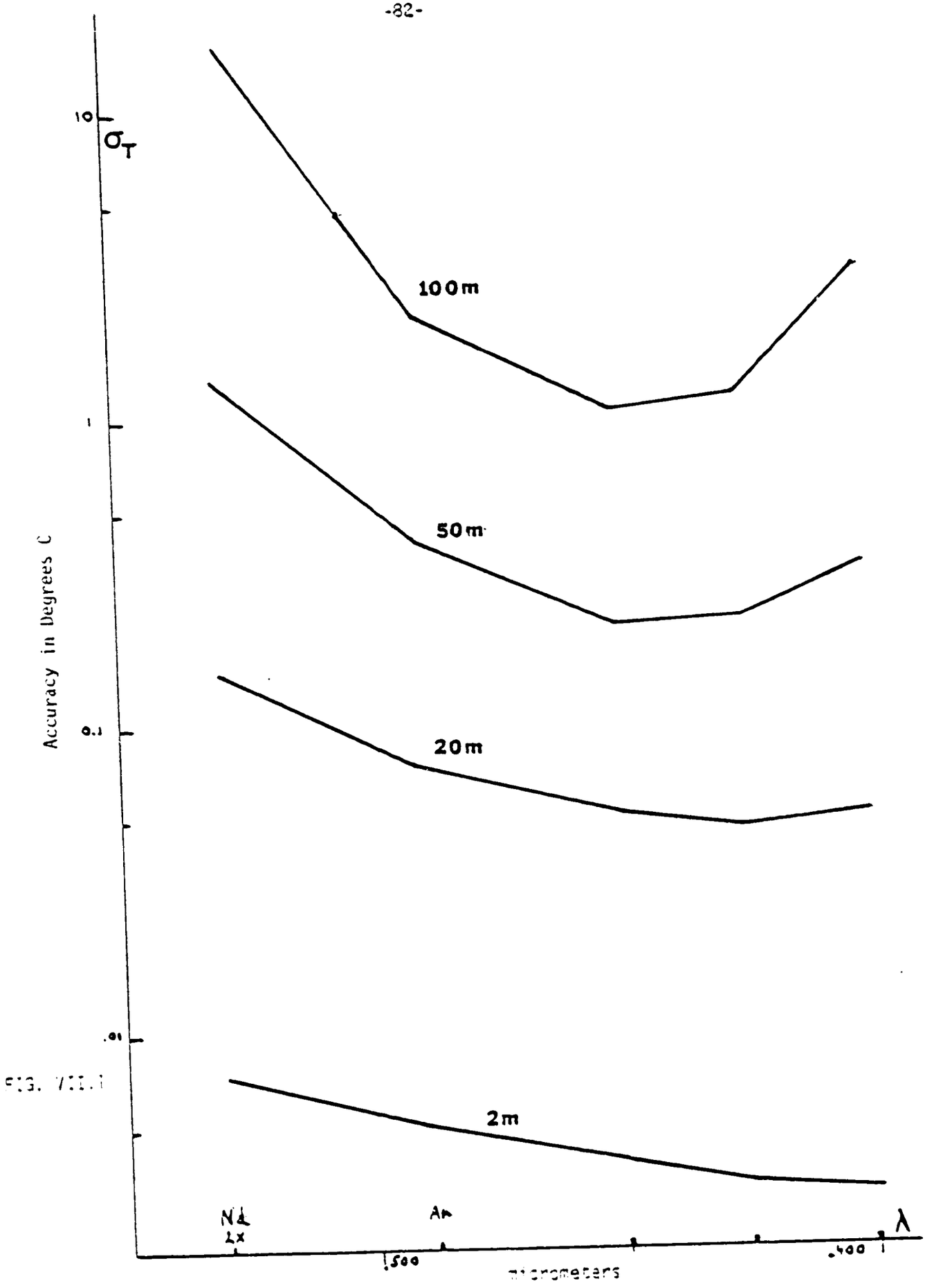
10
σ_T
1
0.1
.01
100m
50m
20m
2m
Accuracy in Degrees C
Nd
2x
Ar
λ
micrometers

FIG. VII.1

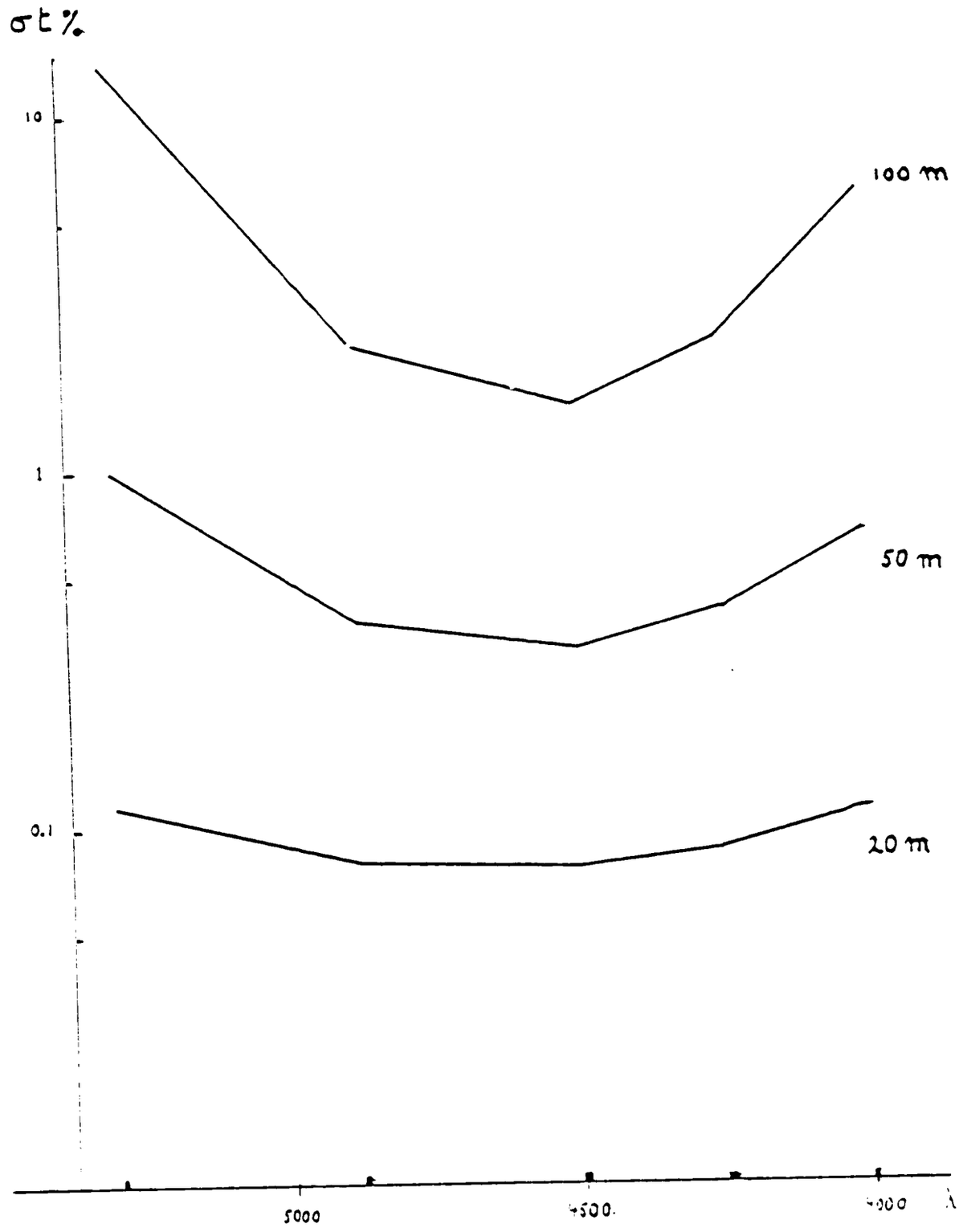

FIG. VII.2

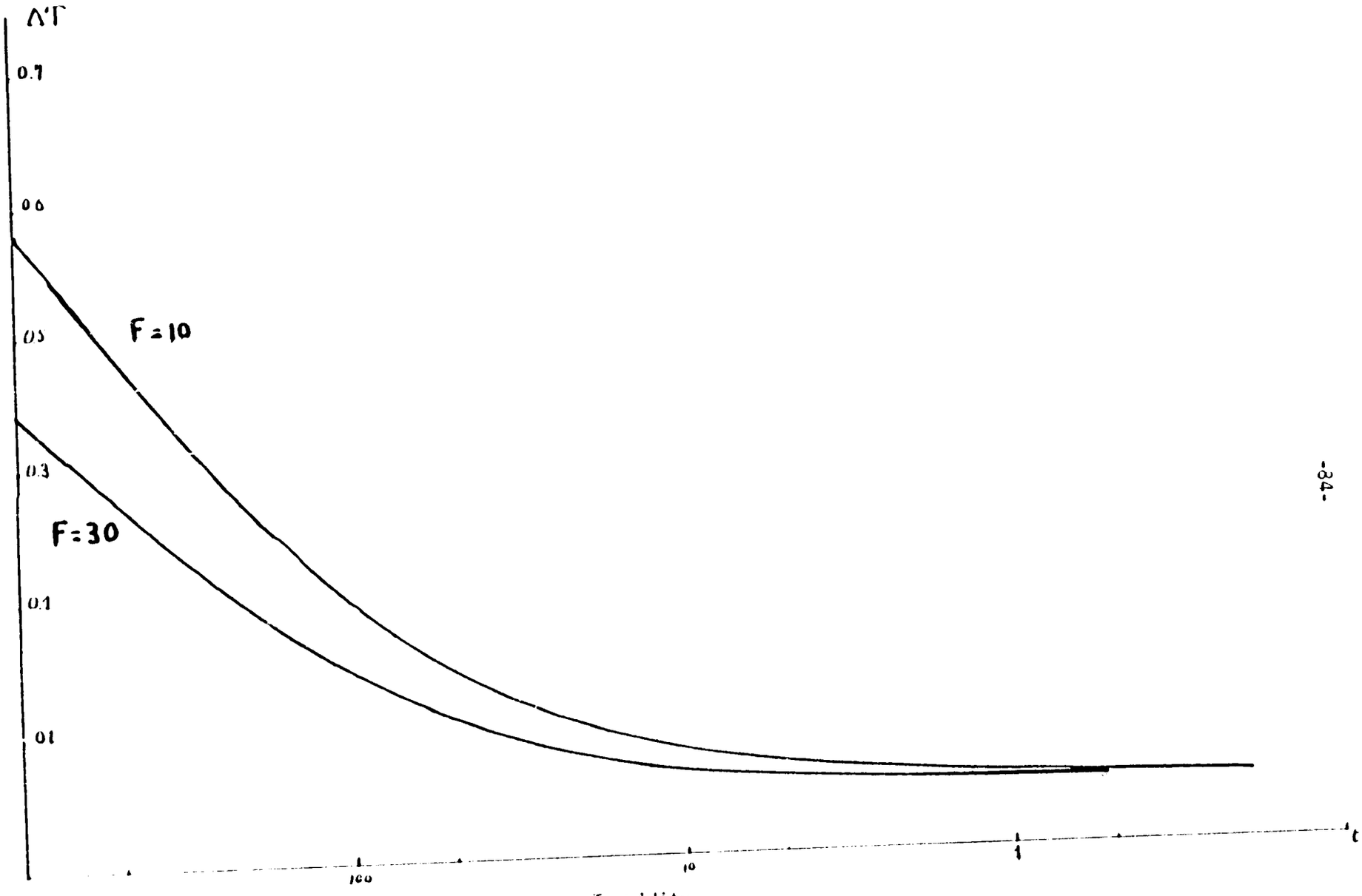

FIG. VII.3

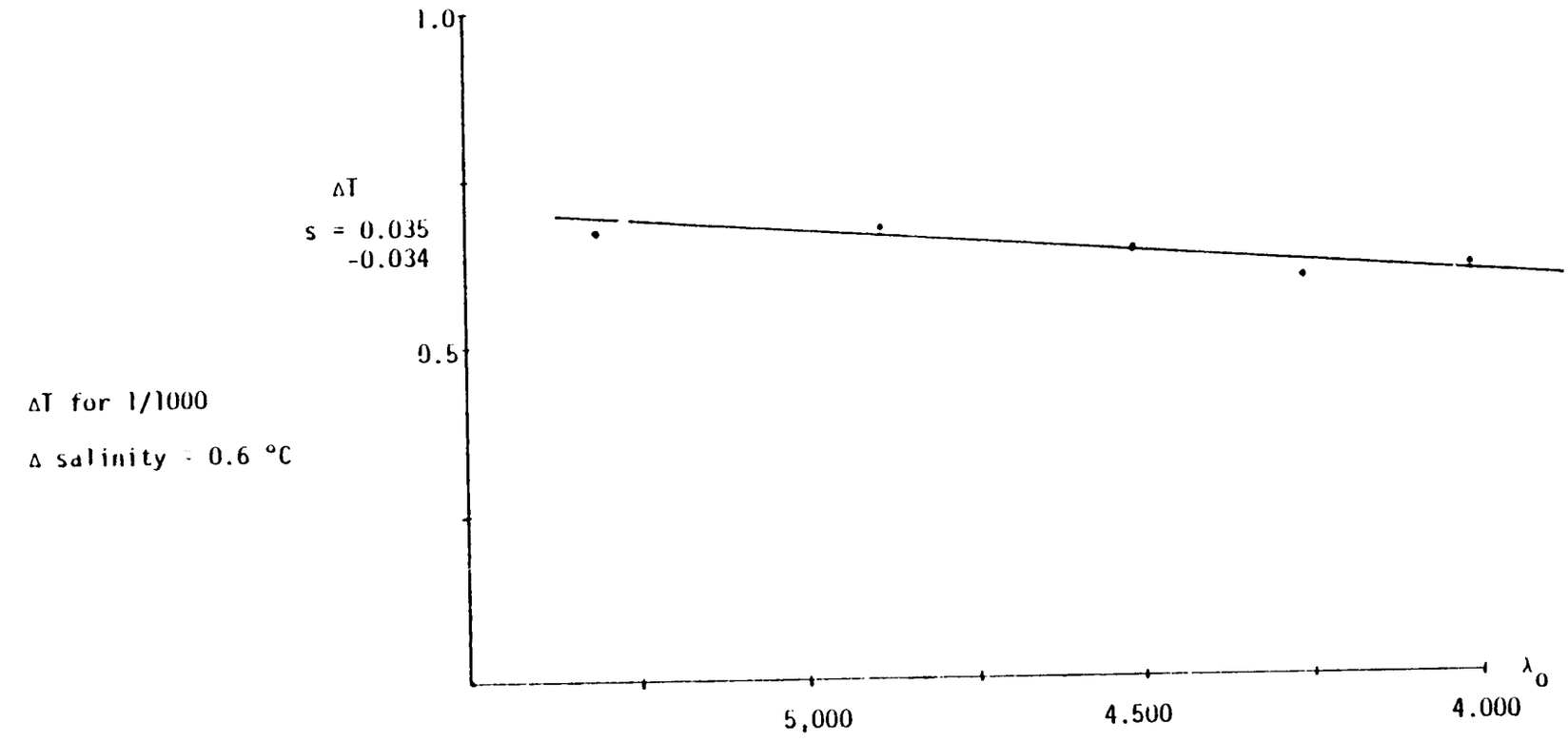
1.0
ΔT
s = 0.035
-0.034
0.5
ΔT for 1/1000
Δ salinity = 0.6 °C
λo
5,000
4.500
4.000

FIG. VII.4

the effect of an error of one part per thousand in salinity corresponds to a drift of 0.6 °C.

These computations give us full confidence in the practicability of a seaborne monostatic system, but there is no doubt that utmost care will have to be exercised in the design of the detection and recording system. Fortunately, fast light pulse detection has been the subject of many technological studies, and our requirements for a monostatic system are within commercial specifications.

C. The Airborne Monostatic

The feasibility of the airborne system was demonstrated in the NASA report[2] CR-139184, January 1975, and the computations made so far have only increased our confidence in those computations. Since then, we have improved the design of the airborne system by the proposed use of a double Mach-Zehnder interferometer, thereby increasing the luminosity by a factor of more than three and avoiding troublesome sea surface effects.

D. Extraneous Light Noise

In a chapter on feasibility, it is adequate to discuss the problem of the possibility of error arising from extraneous signals in the photomultiplier. All our computations indicate that with suitable interference filters, there is no extraneous light problem in a monostatic Brillouin temperature remote sensor because the scattered light is distributed in an extremely small spectral and temporal resolution. Actually, even assuming that the sea surface sends all the reflected sunlight possible into the instrument, a Fabry-Perot working at spectral resolution 0.02 A and temporal resolution of 5 ns, receives only extraneous light of 1,300 photons to be compared with the expected 10^7 photons of signal.

VIII. Bistatic System

The next phase will be to prove directly that the Brillouin scattering method can be used in a practical way to measure temperatures outside the laboratory. A laser will be mounted on a barge or dock and its beam will probe the water to a distance depending on the water clarity at the site available.

In detail the bistatic system will consist of a platform which will initially be a dock, and ultimately, if possible, a ship, upon which is mounted the technical equipment. The instrument is shown in Figure VIII.1 and consists of a laser system and a receiving system.

The laser system will consist of an RCA-LD 2101 Argon Ion Laser (or equal) complete with power supply. There will also be a mirror system with a flat under-water window to guide the laser beam into the water. Adjustments for aiming the laser beam will be provided.

The receiving system will include a second mirror system with lens and under-water window to collect the scattered light from the sea. We have available for comparison a 9"x24" plastic Fresnel lens, a 6" achromat, and a 10" apochromat). An optical train must be built to carry the light to the Fabry-Perot interferometer. The interferometer itself, which is already in the laboratory, must be adjusted and mounted. A triple mirror ("Fafnir" in Fig. VI.6) divides the spectrum into three E.M.I. model 95588 photomultipliers, as shown also in Fig. VI.6. These photomultipliers as well as their power supplies are already in our laboratory, but they must be mounted in place.

The signals from the phototubes will be amplified by three model 1025 Teledyne Philbrick FET operational amplifiers, and their output fed through

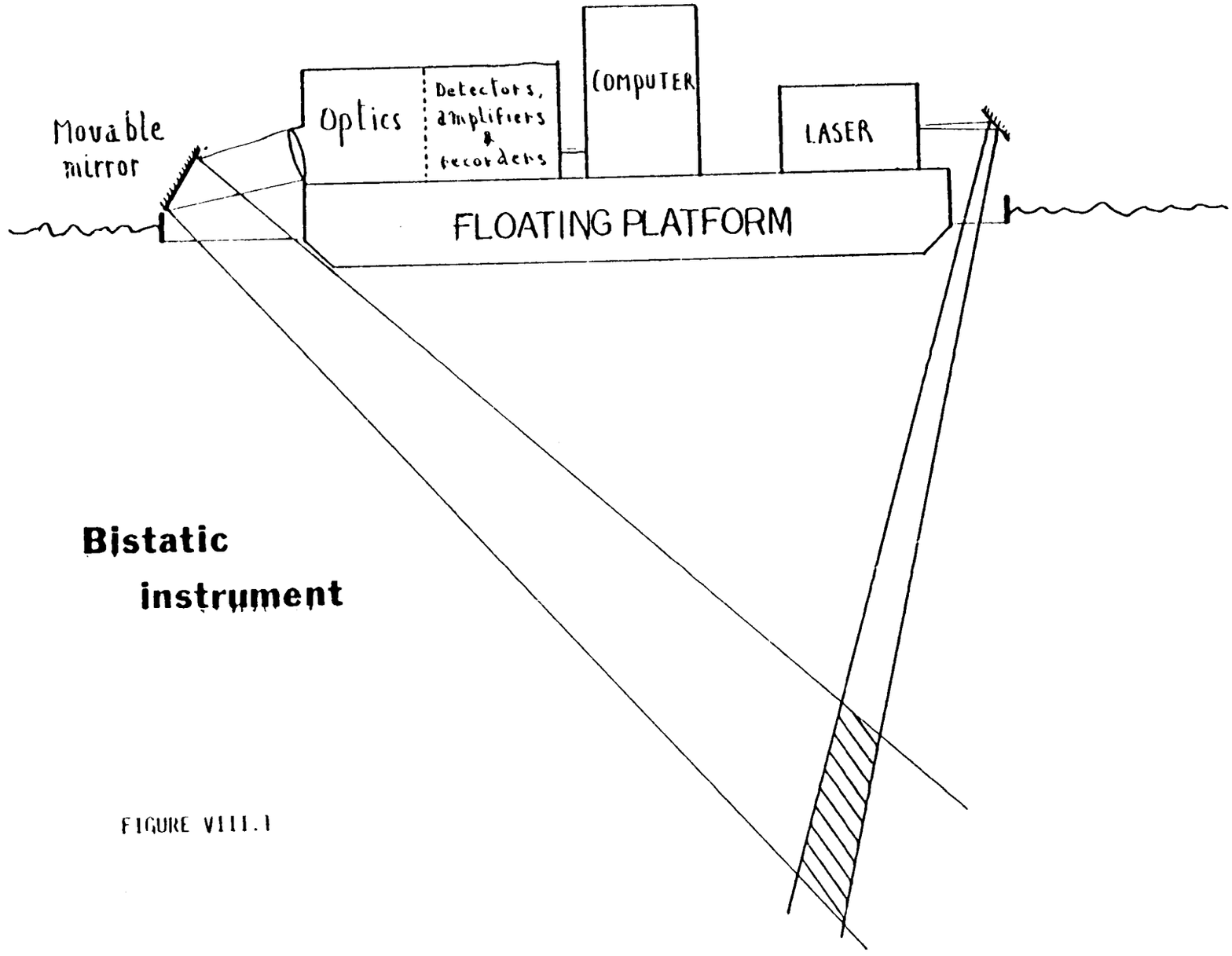

Bistatic instrument

FIGURE VIII.1

3 channels of an 8-channel data acquisition "Hybrid Systems model DAS400" into a Nova 800 computer. The amplifiers, 8 channel system, and computer are already in our laboratory.

The raw data will be available in a magnetic tape dump, but the 12 kiloword memory of the computer will allow quite complex processing in real time and the resulting temperatures and turbidities will be available on an ASR33 Teletype, also in our laboratory.

IX. Implementation Plan.

A. Bistatic Experiment.

Although the ultimate airborne system will be monostatic, with essentially parallel laser and scattered-light beams, the next phase of this work will be bistatic (see flow chart, Fig. IX.1), with separated sending and receiving locations. The reasons for using this intermediate step are twofold:

1) The budget for the period March 1, 1976 - February 28, 1977 was cut from the requested level of about $100,000 to $50,000. This meant that the amount to be spent had to be greatly reduced, and that the experiment will be based on materials already on hand or borrowed, or on surplus equipment. Accordingly, we plan to use a continuous argon-ion laser borrowed from the Navy, and electronics already in our Laboratory. This necessitates a bistatic system.

2) It is probable that even without the budget cut, we would have initially used a bistatic method. This is because it is simpler in execution than the monostatic system. Temperature and turbidity information at depth have never been obtained by laser beams in the open, and it is best to begin with the simplest possible configuration. The vital thing is the demonstration that practical laser beams in the sea can indeed generate the Brillouin, Raman, and Tyndall scattering in intensities sufficient to be useful.

This can be demonstrated as well with the bistatic experiment planned for the next phase as with the considerably more complicated monostatic method. The development of the systems through bistatic, seaborne monostatic, and airborne is shown schematically in Figure IX.2.

B. How the Monostatic Method Develops from the Bistatic.

For airborne measurements the effect of the sea surface can be minimized by utilizing the same optical path for downgoing and upcoming beams. This means that time of flight, rather than the angle, is used for depth information. Since

FLOW CHART

BISTATIC PHASE

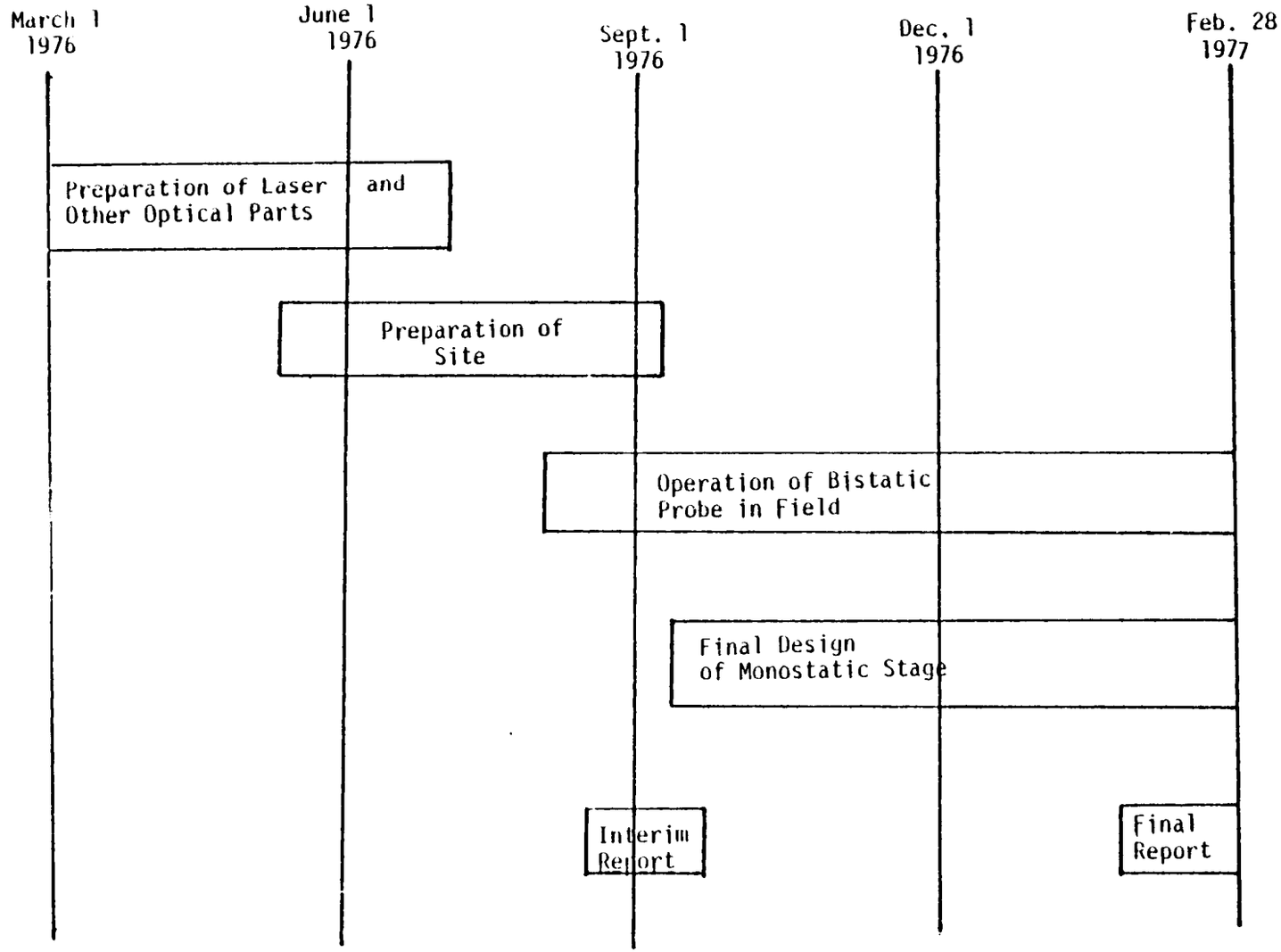

Figure IX.1

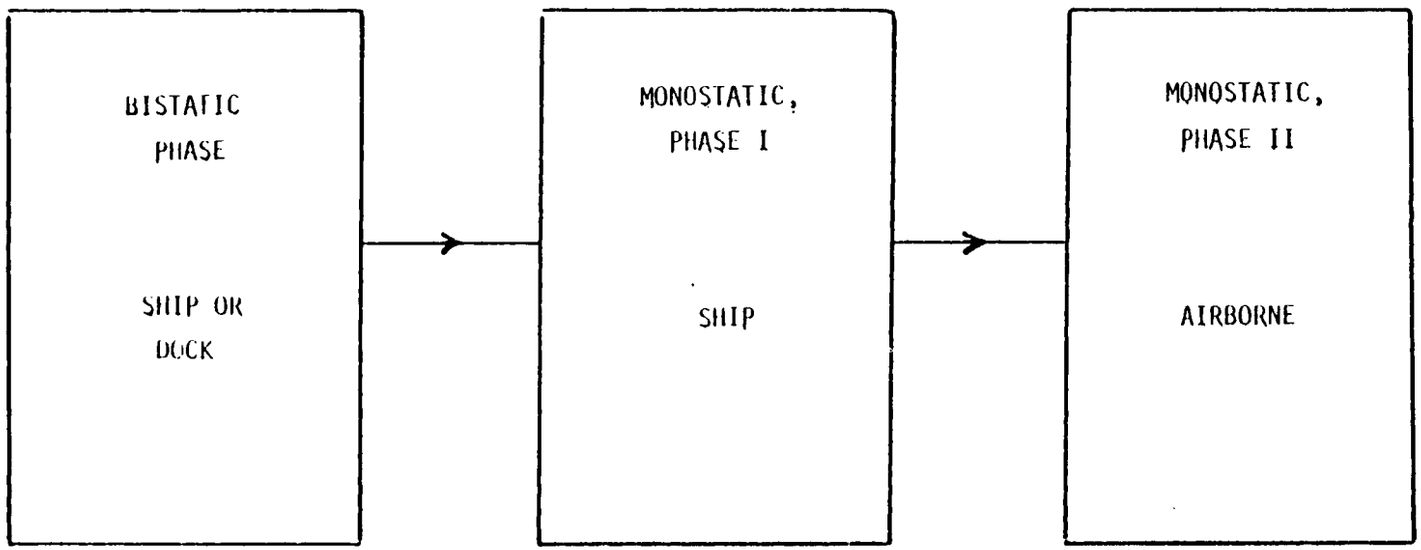
BISTATIC
PHASE
SHIP OR
DOCK
MONOSTATIC,
PHASE I
SHIP
MONOSTATIC,
PHASE II
AIRBORNE

FIGURE IX.2

one location is used for projecting the downgoing beam and receiving the upcoming beam, this is called a monostatic system.

The physical principle, however, with the exception of the depth measurement, is exactly the same with the monostatic as with the bistatic method. Brillouin scattering is used for obtaining the speed of sound in exactly the same way. A combination of Tyndall and Brillouin scattering is used to obtain the turbidity, and finally the Raman scattering is used in the same way to measure the salinity. Only the depth measurements differ, angles being used with the bistatic system and time gates being used with the monostatic method. Since the principle of the experiment is almost identical, the monostatic seaborne program follows logically from the bistatic program and prepares directly for the airborne work to follow.

There will, however, be equipment changes, as explained above. Since depth information is to be obtained by the time delay between the downgoing laser and returning scattered light, a pulsed laser or a modulator for the laser beam will be necessary. A fast electronic receiving and recording system will also be necessary. All these components are now available from commercial establishments. Pulsed lasers and modulators have long been in use, (in fact a pulsed ruby was the first operating laser made) and recently Tectronix Incorporated has brought out a suitable detector-recording system.

C. How the Airborne System Develops from the Monostatic Seaborne System.

The basic requirements of an airborne system are adequate power, compactness, lightness, and reliability. In principle, the system is identical with the seaborne monostatic system. Therefore, our experience with the seaborne system should provide crucial information on the choice of components for the airborne system. Because of the weight and compactness requirements in an aircraft, we probably will have to custom-design the power supply sections of the

apparatus. The laser itself, together with the receiving and recording electronics, will probably be identical with or only slightly modified from the sea-borne system.

D. Design Differences Between Stages

The design changes through each stage are shown in Figure IX.3, and the following discussion refers to that figure.

1) The basic method (except depth measurement) is the same throughout.

2) The dispersive element for the first and second stages is planned to be the Fabry-Perot. This is because a suitable Fabry-Perot interferometer is already in operation in our Laboratory and has been used successfully in preliminary experiments on the Brillouin effect itself. As explained elsewhere in this report, however, a tandem Mach-Zehnder is the ideal instrument for the monostatic airborne phase, and it will, therefore, be used at that point in the program.

3) The optical system will be somewhat different in each phase. In the bistatic configuration, the projecting and collecting optical systems are separated by the baseline distance. There must also be a means for changing the angle between the two beams. The two monostatic configurations will be almost identical with colinear beams, but because of the more stringent space and weight requirements in the airborne phase, there will probably be some redesign called for at that point.

4) The bistatic detector will be a standard high-sensitive photomultiplier, such as we have already in our Laboratory, since the bistatic signals will be low-frequency in nature. For the two monostatic phases of the work, a high speed photomultiplier and associated electronics will be used.

5) The power supply for the bistatic phase will be the unit already in our Laboratory, which was delivered with the RCA argon-ion laser. In the two later stages, power supplies for the pulsed laser will be necessary. Although the same laser is planned for both of the monostatic phases, the space and

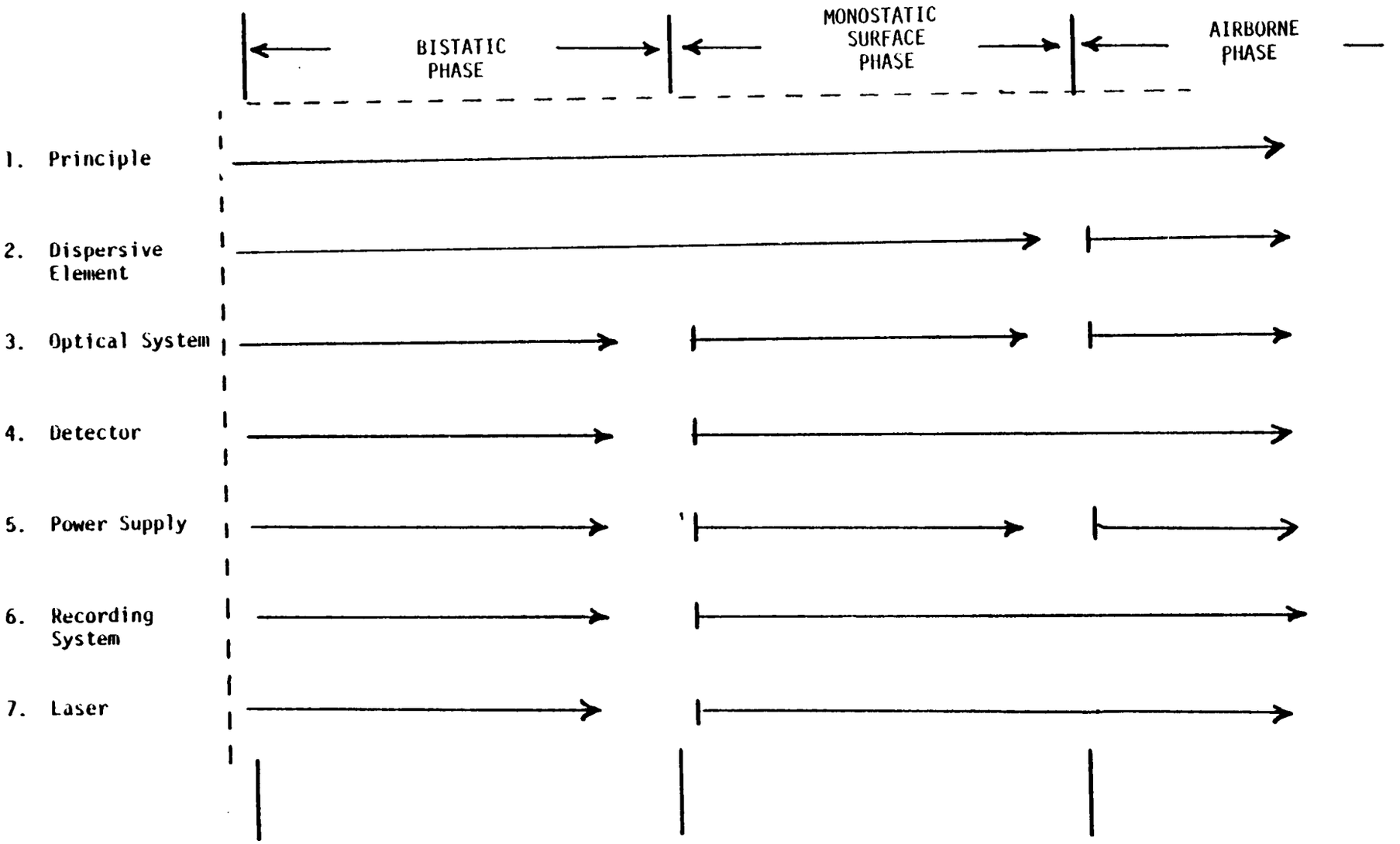
BISTATIC PHASE
MONOSTATIC SURFACE PHASE
AIRBORNE PHASE
1. Principle
2. Dispersive Element
3. Optical System
4. Detector
5. Power Supply
6. Recording System
7. Laser

FIGURE IX.3

weight requirements of the airplane will probably necessitate a special version of the pulsed laser power supply.

6) The recording system for the bistatic phase is already in the Laboratory. Since time resolution is not used to measure the depth, the system is essentially d.c., and the problem is easily solved. In the two monostatic cases, a very fast recording system is necessary. As mentioned above, at least one commercially available unit (Tectronix) is available and suitable, and it will operate both for the seaborne and airborne phases.

7) For the bistatic phase, our plan is to use the RCA two-watt argon ion laser already in our Laboratory. As discussed elsewhere, a pulsed or modulated laser will be necessary for the two monostatic phases. We plan to use the same laser for both the seaborne and airborne monostatic phases to cut down expense.

E. Cost and Time Estimate of Each Phase.

Because of the continuous development of the state of the art, especially in the areas of powerful pulsed laser and data handling equipment, our estimates for Experimental Phases II and III (monostatic, seaborne and airborne) are considerably less certain than for the first Experimental Stage. However, it is possible to make rough estimates of the cost of principal subsystems. These are listed in Table IX.1 and Table IX.2 below.

The time for each phase is now estimated to be one year. See Tables IX.3 and IX.4.

TABLE IX.1

TABLE OF VALUE OF COMPONENTS

BISTATIC SYSTEM

Item	Source	Approximate Value
Laser System	Loan from NASA	$16,000
Window and Lens System	To be purchased and constructed	1,000
Fabry Perot 100 mm	Laboratory	6,000
3 EMI 9558B Photomultipliers and Power Supplies	Laboratory	3,000
Operational Amplifier Teledyne Model 1025 and Power supplies	Laboratory	1,000
Data Acquisition System Hybrid DAS400	Laboratory	500
Nova 800 Minicomputer with 12 K Memory	Laboratory	8,000
Teletype ASR 33	Laboratory	2,000
Magnetic Tape Dump	Laboratory	2,000
Trailer for Site	To be converted from surplus	2,000
Power cables and connection for site	To be purchased and built	1,500
	Total	43,000
	of which is already on hand	38,500

TABLE IX.2

COST BREAKDOWN (APPROXIMATE) OF ENTIRE PROJECT.

I.	Experimental Phase I — March 1976-February 1977	
	Salaries, Benefits and Indirect Costs	36,000
	Supplies, Equipment, Reproduction, Computing and Related Items	7,800
	Travel and Site Expenses	6,200
	TOTAL	$50,000
II.	Experimental Phase II — May 1977-April 1978	
	Salaries, Benefits and Indirect Costs	60,000
	Supplies, Equipment, Reproduction, Computing and Related Items	30,000
	Travel and Site Expenses	10,000
	TOTAL	$ 100,000
III.	Experimental Phase III — May 1978-April 1979	
	Salaries, Benefits and Indirect Costs	80,000
	Supplies, Equipment, Reproduction, Computing and Related Items	60,000
	Travel and Site Expenses	10,000
	TOTAL	$ 150,000
	TOTAL FOR THE THREE PHASES	$300,000

Experimental Stage I

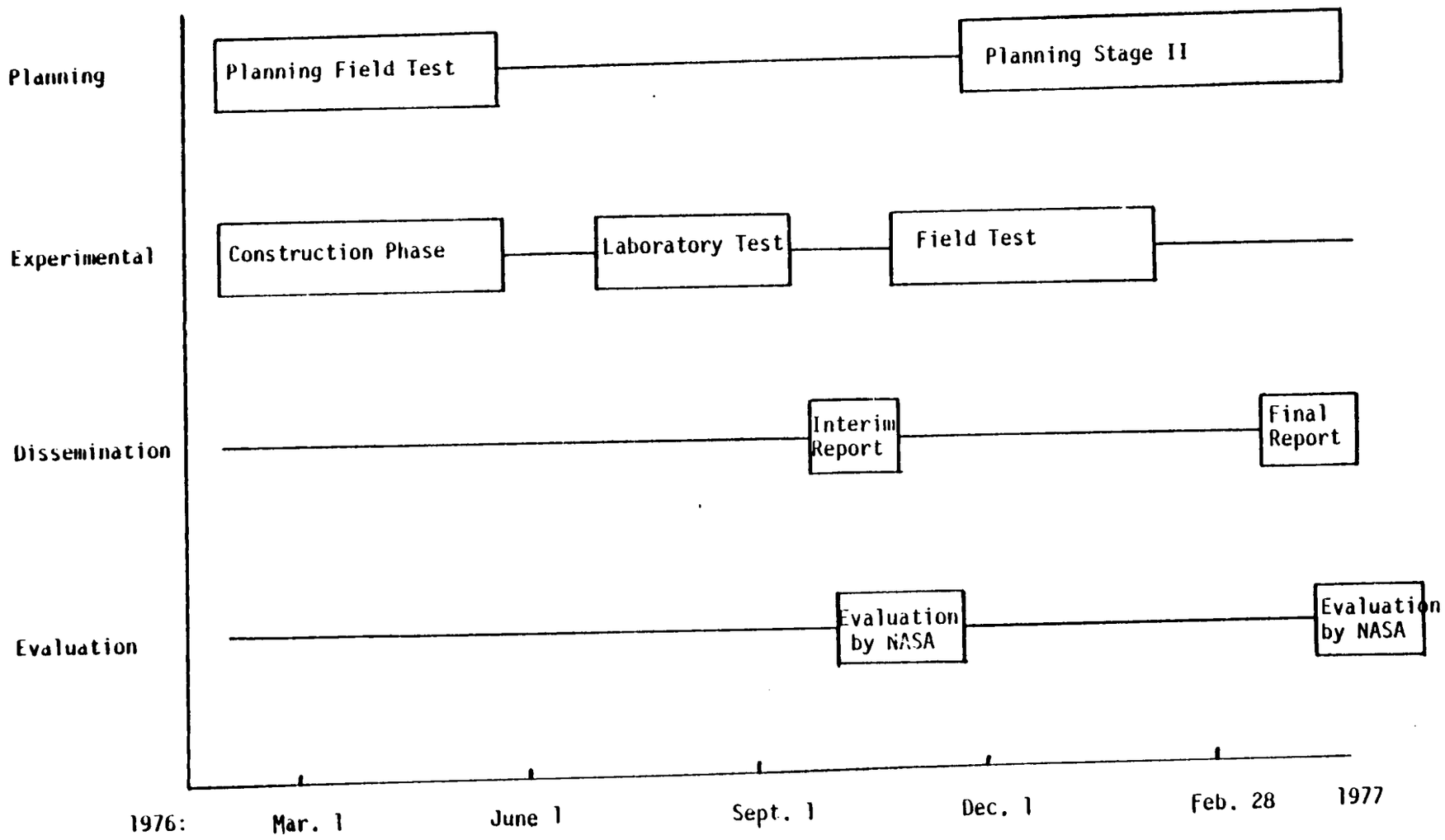

TABLE IX.3

Experimental Stage II

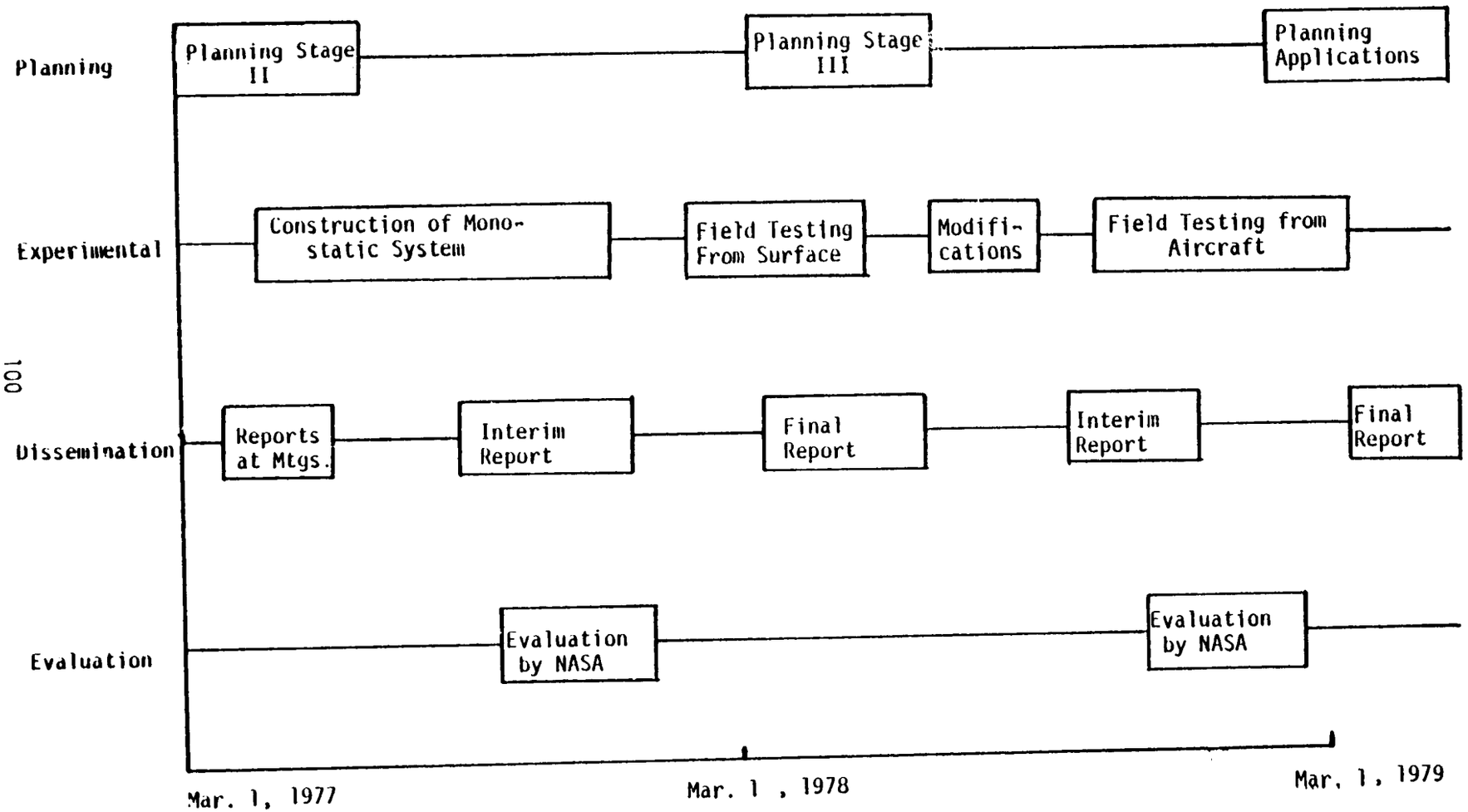

TABLE IX.4

X. Summary and Conclusion

A. How the Parameters Are to Be Measured.

As detailed in the Report above, the oceanographic parameters to be measured are sound, velocity, turbidity, temperature and salinity, all as a function of depth. The measurement principles are shown in Table X.1 for each phase of the Experimental Program. Note that as far as the principles are concerned, there is no difference between the phases except that the depth measurement in Experimental Phases II and III is by time of flight while in Phase I it is by trigonometry.

Of course as we move from bistatic to monostatic seaborne to airborne, the requirements on equipment that must be used become more and more stringent in weight, space, and reliability. This means that the components are continually increasing in sophistication as we proceed through the phases.

B. Criteria for Determining Feasibility and Acceptability.

In any program where something is to be measured, the accuracy of the resulting measurement is a primary goal. Accuracy of measurement of the various parameters in the program is therefore a criterion for feasibility. In the feasibility study, we found that according to our calculations,the accuracy expected from these methods depends on the length of time of the observations, the depth of the observations, and the clarity of the water. The accuracy also depends on the design of the equipment to be used, and we concluded that practicable equipment could be assembled which would give useful information.

In order to prove feasibility we should show that the laser probe method is superior to other methods for determining the parameters in shallow seas. This superiority is expected to show itself in the much greater speed with which the observations can be accomplished, as described in the Introduction to this Report. If temperature measurements at depth can be made by laser scattering from a ship or airplane, a very large improvement in information

Principle of Parameter Measurement \ Phase	Experimental I Bistatic Sea-Surface	Experimental II Monostatic Sea-Surface	Experimental III Airborne
Sound Velocity	Brillouin Scattering Frequency Shift	Same as Phase I	Same as Phases I and II
Turbidity	Ratio of Tyndall Scattering Intensity to Brillouin	Same as Phase I	Same as Phases I and II
Temperature	Sound Velocity Data Together with Salinity and Depth Information	Same as Phase I	Same as Phases I and II
Salinity	Raman Scattering Intensity and Depolarization	Same as Phase I	Same as Phases I and II
Depth	Angle Between Laser Beam and Scattered Light; Trigonometry	Time Difference Between Laser Pulse and Arrival of Scattered Light	Same as Phase II

Table X.1

gathering capability will have been provided. The accuracy at a single point cannot match the thermometer method, since thermometers can measure to a small fraction of a degree, but in the study of the ocean, it is the measurement of temperature gradients that is important, and here the laser method can disclose information that the point-by-point thermometric methods would not obtain, either by providing too coarse a grid or simply by taking too long for each observation. Therefore the criterion for acceptance is whether or not useful data can be gathered by our method that would not have been obtained by the classical methods.

C. Proof that Raman and Brillouin Scattering Can Be Measured Remotely.

Of course, the best proof is the actual carrying out of the program. This we hope and plan to do. In the meantime we must base our judgments on the best information available. These are listed below:

1. Theory

The Theory of Brillouin Scattering is one of the best examples of the application of the principles of physics. It is described in detail in Chapter II of the Detailed Technical Report of our Feasibility Study, NASA CR-139184 dated January 1975, and is developed in Chapter V of this report. This theory has been checked experimentally in many laboratories over a period of almost forty years and has been found correct within experimental error. We have made laboratory studies of our own described in the foregoing report which agree with the theory in every way. The theoretical material relating to the optical part of the plan is also beyond question. Our own experience with similar methods (see the publication lists in the Appendix to this Report) have provided very high confidence in our predictions.

As we have stated in the body of this report, the calculations we have made borne out by our experiments in the Laboratory, show that field measurements of the oceanic parameters can be made.

2. Experiments by Others

Many of the elements that make up our Program have been performed in the field by other groups, for various purposes, greatly adding to our confidence that all of these measurements can be accomplished together.

a) Depth measurements have been made routinely from aircraft by laser. Just as in our system, a low-flying airplane was used[7] as a platform for a pulsed laser firing vertically downward. Light scattered from the bottom was received back in the airplane and the time difference used to measure depths. Accuracies of at least .5 meter were considered routine, and most important, the state of the sea (providing that the conditions were reasonable) seemed to have minimal effect on the accuracy of the observations or the intensity of the back-scattered light.

b) Raman spectra have been used to measure impurities (oil spills) on the sea surface by a laser probe from an airplane.[7] Here again, the fact that Raman scattering, which is of the same order of intensity as the Brillouin spectrum we plan to use, can be observed from an aircraft is very encouraging indeed.

c) Brillouin scattering has been used routinely in the laboratory for the measurement of sound speed in liquids. Here again, the fact that it has been found desirable to use this method is an indication of its practicability that argues well for the success of the program.

3. Conclusion

Thus, our conclusion is based both on theory and experiment, and nothing we have learned has decreased our confidence in the program. In fact, as each new result has been obtained, our expectation of success has increased.

D. A Brief Description of the Following Phases of the Program.

1. The next phase will be to prove directly that the Brillouin scattering method can be used in a practical way to measure temperatures outside the

laboratory. A laser will be mounted on a barge or dock and its beam will probe the water to a distance depending on the water clarity at the site.

Because of fund limitations, this may be in the Miami area initially. Scattered light will be received at a nearby location and the Brillouin spectrum analyzed as function of distance. This is the bistatic experiment described in detail in the body of the Report. Success here will prove that the method is practicable in the field.

2. The following phase will employ the time of flight method of determining distance, which is the method that will be used in the final, airborne phase. The results of the preceding step will be used here, but now the laser is to be pulsed in order to provide time data. Recording instrumentation for this purpose must be added at this point.

3. The final stage is airborne, as described in the body of the Report (see Figure I.6). Here, the space and weight requirements of an aircraft will necessitate a certain amount of redesign. Also, the equipment will be partially automated, and special care will be concentrated on questions of reliability.

4. At each stage, reports and visits will be used to insure close cooperation between the Laboratory and NASA. A flow plan for the entire project is shown in Figure X.2.

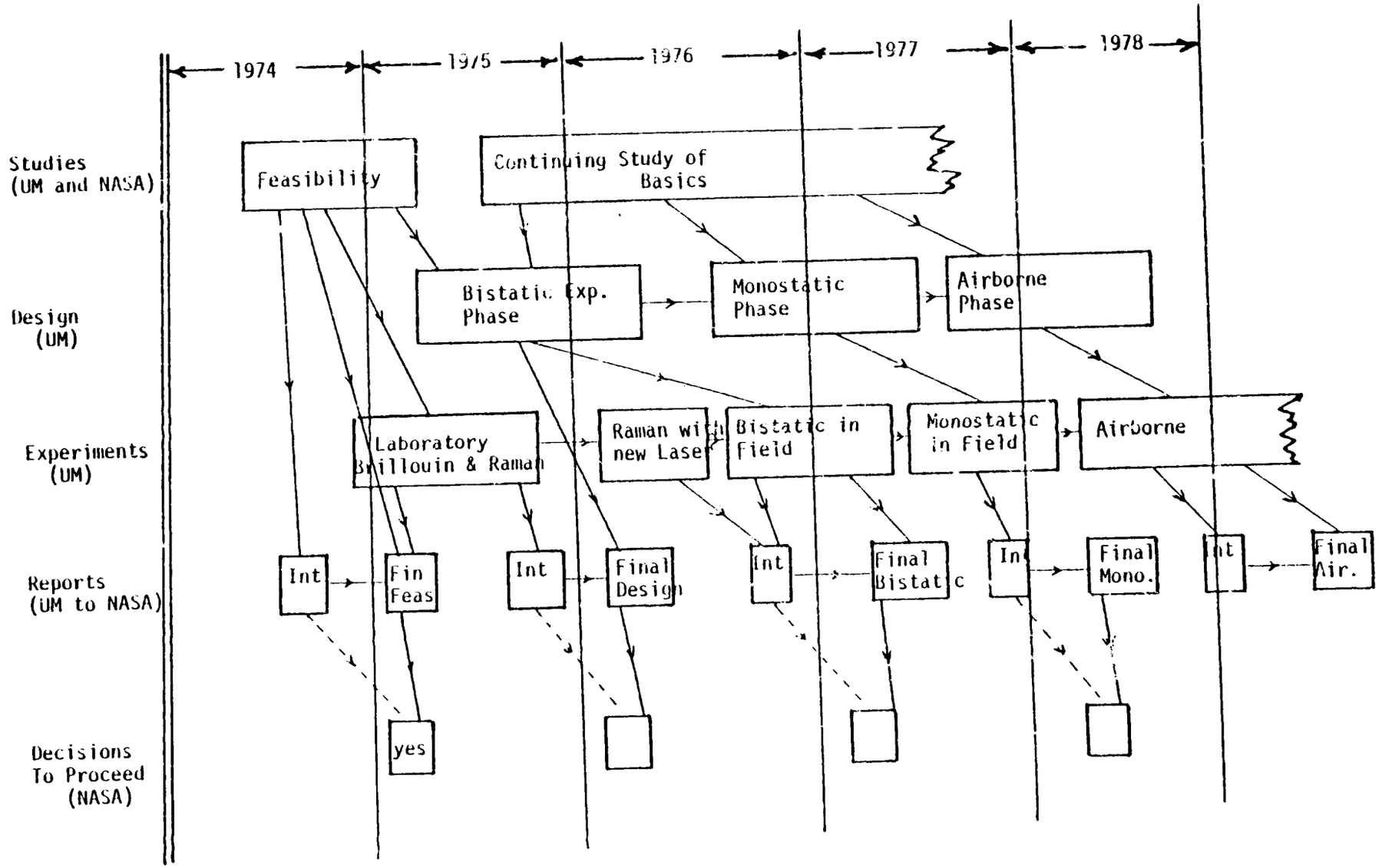

FIGURE X.2

FLOW CHART FOR ENTIRE PROJECT

REFERENCES

1. J. G. Hirschberg, Final Report for NAS10-8740, December 1975.

2. J.G. Hirschberg, A.W. Wouters, F.N. Cooke, Jr., K.M. Simon, and J.D. Byrne, "Laser Application to Measure Vertical Sea Temperature and Turbidity", NASA Report NASA CR-139184, January 1975.

3. See for example, Reeds Nautical Almanac, American East Coast Edition, 1976, Chesapeake Bay tidal currents, p. 400, et seq.

4. G. Benedek and T. Greytak, Proc. IEEE 53, 1623 (1965).

5. J.G. Hirschberg and P. Platz, Applied Optics 4, 1375 (1965).

6. C.H. Chang and L.A. Young. AVCO Everett Research Laboratory Research Note 960, Everett, Mass, 1974. Also C.H. Chang and Lee A. Young "Remote Measurement of Ocean Temperature from Depolarization in Raman Scattering", Symposium Proceedings: The Use of Lasers for Hydrographic Studies, Sept. 12, 1973, NASA, Wallops Island.

7. Private communication, P. Cervenska, Wallops Flight Center, Wallops Island, Va., 1975.

8. V.A. Del Grosso, J. Acoust. Soc. Am. 56, 1084 (1974).

9. Discussion (unpublished) in the Oceanographic and Hydrologic Measurement from Satellites Workshop of the Remote Sensing Applied to Energy Related Problems Symposium held in Miami, December 1974.

10. W.R. McCluney,"Radiometry of Water Turbidity Measurements", Jour. Water Pollution Control Federation 47, No. 2, 252-266 (Feb. 1975).

11. The overall shape of the scattering angular function was read from a number of figures in G. Kullenberg paper in Optical Aspects of Oceanography, edited by N.G. Jerlov and E. Steemann Nielsen, Academic Press, 1974.

12. These results were obtained by visual comparison with figures of R.S. Shifrin, et al., "Using the Light Scattering Function for Studying Suspended Matter in the Sea", NASA Technical Translation (NASA TT F-14, 781) from Optika okeana i atmosfery, "Navka" Press, 1972.

13. These results were obtained by visual comparison and scaling of Otis B. Brown, Jr., "A Study of Light Scattering by Ocean Borne Particulates", Ph.D. Dissertation, University of Miami, 1973.

14. F.G. Walton Smith, C.R.C. Handbook of Marine Science, 1974 ed.

15. K. Krishen, "Remote Sensing of Oceans Using Microwave Sensors", Remote Sensing Energy Related Studies, Hemisphere Publ. Co., 1975, p. 61 et seq.

16. G. Neumenn and W.J. Pierson, Jr. Principles of Physical Oceanography Prentice Hall, 1966, p. 39-40.

17. J.P. Riley and G. Skirrow. Chemical Oceanography, Vol. 1, 2nd Ed., Academic Press, 1975.

18. T. Hirschfeld, J. Galina, S. Kleiner, "The Applications of Remote Raman Spectrometry to Measurements in Natural Water Bodies", 3rd Northeast Regional Meeting, American Chemical Society, Buffalo, NY, October, 1971.

19. W.M. Houghton, "Measurement of Raman Spectrum of H_2O and SO_4 in Seawater", op cit. The Use of Lasers for Hydrographic Studies Symposium Proceedings.

20. C.L. O'Conner and J.P. Schlupf, J. Chem. Phys. 47, 31 (1967).

APPENDIX A

SELECTED REPORTS AND PUBLICATIONS
BY MEMBERS OF THE LABORATORY FOR OPTICS & ASTROPHYSICS

1. "Nine Channel Photoelectric Fabry-Perot Interferometer", J.G. Hirschberg, J. Opt. Soc. Am. 50, 514 (1960).

2. "Simple Duochromator for the Measurement of Mass Motion in a Plasma", J.G. Hirschberg, Applied Optics 4, 243 (1965).

3. "A Device for Accurately Bending a Light Beam Through Small Angles", J. G. Hirschberg, Applied Optics 4, 759 (1965).

4. "Etude de la Temperature Doppler dans une Decharge Toroidale a l'aide d'un Interferometre Fabry-Perot Multicanal", Peter Platz et Joseph G. Hirschberg, Comptes Rendus Acad. Sc. Paris, 261, 1207 (1965).

5. "A Multichannel Fabry-Perot Interferometer", J.G. Hirschberg and P. Platz, Applied Optics 4, 1375 (1965).

6. "Measurements of the Kinetic Temperature of Barium Atoms and Ions in a Schuler Hollow Cathode Discharge", J.G. Hirschberg, J. Opt. Soc. Am. 55, 1573A (1965).

7. "An Infrared Vacuum Grating - Prism Spectromer", T.K. McCubbin, Jr., J.A. Lowenthal and H.R. Gordon, Applied Optics, Vol. 4, 711 (1965).

8. "The 15-Micron Bands of $C^{12}O_2^{16}$", H.R. Gordon and T.K. McCubbin, Jr., Jour. of Molecular Spectroscopy, Vol. 18, 73-82 (1965).

9. "The 2.8 - Micron Bands of CO_2", H.R. Grodon and T.K. McCubbin, Jour. of Molecular Spectroscopy, Vol. 19, 137-154 (1966).

10. "Recent Measurements of the Infrared Spectrum of CO_2", H.R. Gordon and T.K. McCubbin, Jr., Bull. Am. Phys. Soc., Vol. 11, 526 (1966).

11. "A Fabry-Perot Duochromator for the Measurement of Small Wavelength Displacements of Spectral Lines", J.G. Hirschberg and W.I. Fried, Oak Ridge National Laboratory Report 4019, Physics (1966) and Proc. of 8th Annual Meeting of the Plasma Physics Division, Am. Phys. Soc. (1966).

12. "Anomalously High Ion Temperatures in a Full-Ionized Barium Plasma", N. Rynn, E. Hinnov and J.G. Hirschberg, Proc. of 8th Annual Meeting of Plasma Physics Division, Am. Phys. Soc. (1966).

13. "Recent Developments in the Application of the Multichannel Fabry-Perot to Plasma Spectroscopy", J.G. Hirschberg, Colloque CNRS, sur les Methodes Nouvelles de Spectroscopic Instrumentale, Orsay, France, 25-29 April, 1966. Colloque C-2, Suppl. No. 3-4, Jour. De Phys. 28, C2-226 (1967).

14. "Utilization of a Laser for Illumination of a Single Point Reference Interferometer", J. Silvestre and J.G. Hirschberg, J. Opt. Soc. Am. 57, p. 561 (1967)

15. "Ion Temperature in a Plasma Produced by Contact Ionization", J.F. Hesser, E. Hinnov, R. Rynn and J.G. Hirschberg, Phys. Fluids 10, pp. 1114-1116, May (1967).

16. "Single Field Polarizing Spectrophotometer for Measuring Mass Motion in A Plasma", U.S. Patent, 3,316,412, April (1967).

17. "A Method for Accurately Measuring Repetitive Rapidly Varying Spectral Line Shapes with a Grating Monochromator", J.G. Hirschberg and E.L. Wilson, Princeton Plasma Physics Laboratory Report MATT-564 (1967).

18. "Limitations in Resolution of Image Transmission Through Turbulent Media", Dept. of Physics, University of Miami Report, D. Duke and E.E.H. Shin, MIAPH-67.3-OP, November (1967).

19. "Radiometry and Photometry", Ross McCluney, University of Miami Physics Dept. Report MIAPH-OP-67.9 (Nov. 1967).

20. "Diffraction and Interference", J.G. Hirschberg, J.E. Mack and F.L. Roesler, Chapter 5, Part 6, Optics, Handbook of Physics, McGraw Hill, 2nd Edition (1967).

21. "Ion Temperatures with the Multichannel Fabry-Perot", J.G. Hirschberg, Proc. 9th Annual Meeting of Plasma Physics Division, Am. Phys. Soc. (Nov. 1967).

22. "An Automatically Swept Photoelectric Fabry-Perot Spectrometer", J.G. Hirschberg and E.L. Wilson, Princeton Plasma Physics Laboratory Report, MATT-562 (1968).

23. "Fabry-Perot Measurements on High Atmospheric Barium Clouds", J.G. Hirschberg and A. Wouters, Bull. Am. Physics Soc. 13, 1494 (1968).

24. "Fresnel-Lens Multichannel Fabry-Perot Interferometer as Applied to a Rapidly Changing Plasma", J.G. Hirschberg and F.N. Cooke, Jr., Bull. Am. PHys. Soc. 13, 1511 (1968).

25. "Density Measurements of a Rapidly Changing Plasma Using a Point Reference Interferometer", J.G. Hirschberg and L. Hazelton, Bull. Am. Phys. Soc. 13, 1511 (1968).

26. "A New Code for the Wang Calculator Programmer", L. Hazelton, University of Miami Department of Physics Report MIAPH-OP-68.2 (April 1968).

27. "Coherence Degradation in Random Media", E.E.H. Shin and D. Duke, Jour. Opt. Soc. Am. 58, 1419-1420 (1968).

28. "Measurement of Very Small Drifts in a Schüler Hollow Cathode Plasma", J.G. Hirschberg and W. Fried, Bull. Am. Phys. Soc. 13, 1512 (1968).

29. "Fabry-Perot Interferometer Measurements of Temperature and Optical Density of Barium Clouds", J.G. Hirschberg and A. Wouters, U. of Miami Dept. of Physics Report MIAPH-OP-68.10 (Dec. 1968).

30. "Light Field Fluctuations In the Photic Zone", J. Dera and H.R. Gordon, Limnology and Oceanography, Vol. 13, 4, 697-699 (1968).

31. "Irradiance Attenuation Measurements in Sea Water off Southeast Florida", H.R. Gordon and J. Dera, Bull. of Marine Science, Vol. 19, 2, 279-294 (1969).

32. "A Polarization Fabry-Perot Duochromator", J.G. HIrschberg and W. Fried, Applied Optics, 9, 1137-39 (1970).

33. "A Novel Means of Thermal Imaging", J.G. Hirschberg, U. of Miami Dept. of Physics Report MIAPH-OP-69.12 (1969), Applied Optics 9, 761 (1970).

34. "Holographic Multiple-Pass Interferometer for Plasma Diagnostics", J.G. Hirschberg, W.R. McCluney, L. Hazelton and A. Aggarwal, Jour. Opt. Soc. Am. 59, 1541 (1969). Also published as U. of Miami Dept. of Physics MIAPH-OP-69.16.

35. "Doppler Temperature of the Solar Corona", J.G. Hirschberg, A. Wouters, W.I. Fried, F.N. Cooke, Jr., D. Duke, and M. Read, Nature 226, 1142 (1970).

36. "The HOMIN, A Holographic Multipass Interferometer", J.G. Hirschberg, W.R. McCluney, L.R. Hazelton, Jr. and A. K. Aggarwal, Nouv. Rev. d'Optique Appliquee, 1, Suppl. 2, p. 7 (1970).

37. "The Fresnel Annular Zone Objective: A New Optical Element", J.G. Hirschberg and F.N. Cooke, Jr. (Accepted by Applied Optics) (1970).

38. "Fabry-Perot STudies of the Solar Corona", J.G. Hirschberg and A. Wouters, Bull. "F" National Science Foundation Series on Total Solar Eclipse of March 7, 1970.

39. "The Optical Physics Laboratory of the University of Miami", an address delivered as an invited paper at the Symposium on Education in Optics, Hollywood, Fla. (1970).

40. "Ion and Neutral Drifts in a Hollow Cathod Discharge Tube", W.I. Fried, read at Annual Meeting of the OSA, Hollywood, Fla., Sept. 30, 1970.

41. "Noise Limitation in the PHotographic Fabry-Perot Spectrograph", A. Wouters, read at the Annual Meeting of the OSA, Hollywood, Fla., (1970).

42. "Fifty-Channel Multiplex Fabry-Perot Interferometer", J.G. Hirschberg, W.I. Fried, and L. Hazelton, Jr., Jour. Opt. Soc. Am., 11, 1576 (1970).

43. "Line Profile Measurements of a Pulsed Holow-Cathode Discharge Using the 16-Channel Fresnel-Lens Fabry-Perot Interferometer", F.N. Cooke, Jr. and J.G.Hirschberg, Jour. Opt. Soc. Am., 11, 1576 (1970).

44. "Multiplex Fabry-Perot Interferometer",.J.G. Hirschberg, W.I. Fried, L. Hazelton and A. Wouters, Appl. Optics 10, 1979-80 (1971).

45. "Interferometric Studies of Spectral Lines in the Solar Corona", J.G. Hirschberg, A. Wouters, and L. Hazelton, Solar Physics 19, 164-167 (1971).

46. "Ion and Neutral Drifts in the Hollow Cathode Discharge", W.I. Fried, U. of Miami Physics Dept. Report MIAPH-OP-71.2 (March 1971). Also Dissertation for Ph.D. degree, Feb. 1971.

47. "Spectra of Underwater Lightfield Fluctuations in the Photic Zone",

48. "Small Angle Mie-Scattering Calculations for Low-Index Hydrosals", H.R. Gordon and O.B. Brown, presented at Fall Meeting of OSA, Ottawa, Canada (1971).

49. "Theoretical Modeling of Light Scattering by Hydrosols", H.R. Gordon and O.B. Brown, Transactions, Amer. Geophys. Un. 52, 245 (1971).

50. "Tables of Mie Scattering Functions for Low-Index Particles Suspended in Water", O.B. Brown and H.R. Gordon, U. of Miami Physics Dept. Report MIAPH-OP-71.5 (1971).

51. "Theory of Coincidence Counts and Simple Practical Methods of Coincidence Count Correction for Optical and Resistive-Pulse Particle Counters", H. Bader, H.R. Gordon and O.B. Brown, accepted for publication in Rev. Sci. Inst. (1972).

52. "On the Shape of the Point-Source Response Function", M. Read and S. Amtey, U. of Miami Physics Dept. Report MIAPH-OP-72.1 (1972).

53. "Consideration of Certain Advantages of the Multiplex Fabry-Perot Interferometer", Hirschberg, Fried, Hazelton and Wouters, J. Opt. Soc. Am. 61, 1560 (1971).

54. Signal to Noise Ratio and Information in a Spectrometer, A. Wouters and J.G. Hirschberg. Paper read by Wouters at Dec. 11, 1971 meeting of Optical Society of America, Florida Section, Coral Gables, Fla.

55. Image Recording Device. Patent 3,644,014, J.G. Hirschberg, Feb. 22, 1972. Assigned to Research Corporation and University of Miami.

56. Study of Methods of Non-Scanning Infrared Photography, K. Simon and J.G. Hirschberg. Paper read by Simon at Annual Meeting of Optical Society of America, Florida Section, April 8, 1972.

57. Spectroscopy of Laser-Induced Plasmas, L.G. Phadke and J.G. Hirschberg. Paper read by Phadke at Annual Meeting of Optical Society of America, Florida Section, April 8, 1972.

58. Fraunhofer Diffraction at Infinite Distance and Finite Distance As a Special Case of Fresnel Transforms, J. Hallak, J.G. Hirschberg and J. Nearing, University of Miami Department of Physics Report MIAPH-OP-73.1 (1973).

59. A Directly Decodable Multiple Pinhole Camera, A. Wouters, K.M. Simon, and J.G. Hirschberg, University of Miami Department of Physics Report MIAPH-OP-73.2 (1973).

60. Preliminary Report of Interferometric Measurement of the Solar Corona at the Eclipse of July 10, 1972, J.G. Hirschberg, F.N. Cooke, Jr., K. Finello, L. Phadke, K.M. Simon, and A. Wouters, University of Miami Department of Physics Report MIAPH-OP-73.3 (1973).

61. Eclipse: Rare Show, Museum 5, 42 (1973) Published monthly by the Museum of Science, Miami, Florida.

62. Direct Method of Decoding Multiple Images, A. Wouters, K.M. Simon, and J.G. Hirschberg, Applied Optics 12, 1871 (1973).

63. Solar Corona Studies at the Eclipse of 10 July 1972. J.G. Hirschberg, F.N. Cooke, Jr., K. Finello, L.G. Phadke, K.M. Simon, and A. Wouters. Solar Eclipse 1973 Bulletin No. 4, NSF, Washington, D.C., p. 87-8 (1973).

64. Field-widened Michelson Spectrometer with No Moving Parts. J.G. Hirschberg. Applied Optics 13, 233 (1974).

65. Solar Energy from the Sea. J.G. Hirschberg. Proceedings of the Ocean Energy Systems Workshop, University of Miami, 1974.

66. Hydrogen, The Ultimate Energy Source. J.G. Hirschberg. Proceedings of The Hydrogen Economy Miami Energy Conference, Miami Beach, 1974.

67. Investigation of the Working Principles of Tomographic Devices and their Imaging Quality. M.E. Read, Ph.D. Dissertation, University of Miami, 1973.

68. The 16 Channel Fresnel Lens Fabry-Perot Interferometer. F.N. Cooke, Jr., Ph.D. Dissertation, Univ. of Miami, 1974.

69. Information Theory Applied to the Measurement of Line Shapes with the Fabry-Perot Interferometer. A.W. Wouters, Ph.D. Dissertation, Univ. of Miami, 1974.

70. Adiabatic Compression of Plasma Vortex Structures. D.R. Wells, E. Nolting, F. Cooke, Jr., J. Tunstall, P. Jindra, and J. Hirschberg. Phys. Rev. Letters 33, 1203 (1974).

71. Laser Application to Measure Vertical Sea Temperature and Turbidity. J.G. Hirschberg, A.W. Wouters, K.M. Simon, F.N. Cooke, and J.D. Byrne. Detailed Technical Report CR-139184 for NASA Contract NAS10-8600, January 1975.

72. Multisite Fluorometry and Microspectrofluorometry of Biochemical Reactions in Single Living Cells. J.G. Hirschberg, E. Kohen and J.M. Salmon. Paper accepted by Fed. Eur. Biochem. Soc. Journ. 1975.

73. The Use of Sound for Guiding a Laser Beam. Paper presented to Colloquium on the Optics of Guided Waves, Paris, France, April 1975.

74. Microspectrofluorometry for Rapid Optional Analysis of Metabolic Topography or Fluorescence Spectra in Single Living Cells. J.G. Hirschberg, E. Kohen, and C. Kohen. Paper presented to the American Society of Biological Chemists by E. Kohen.

75. Biomedical Transducers in the Study of Metabolic Interactions in Single Living Cells and Intra or Intercellular Transport, J.G. Hirschberg, E. Kohen, C. Kohen, and J.M. Salmon, to be published in Proceedings of Colloque International Sur les Capteurs Biomedicaux.

76. Multichannel microspectrofluorometry for topographic and spectral analysis of NAD(P)H fluorescence in single living cells. J.G. Hirschberg, E. Kohen, C. Kohen, A. Wouters, A. Pearson, J.M. Salmon, and B. Thorell. Accepted for publication in Biochemica et Biophysica Act.

77. A Floating Island Solar Energy Collector for Hydrogen Production. J.G. Hirschberg. Presented to 1st World Hydrogen Energy Conference, March 1-3, 1976, Miami Beach, Florida.

78. Computer Simulation and Decoding Techniques for MCA. K.M. Simon, J.G. Hirschberg, and A.W. Wouters. University of Miami Report MIAPM-CP-76.1, March, 1976.

APPENDIX B

PROGRAM FOR SEABORNE MONOSTATIC SYSTEM

```
10  PRINT "LASER:POWER,LAMBDA,WIDTH,PULSE LENGHT"
15  INPUT P1,L,W7,N1
17  PRINT
20  PRINT "OBSERVATION:HEIGHT,PUPIL AREA,SEA SURFACE FACTOR,";
21  PRINT "EFFICIENCY,ANGLE"
25  INPUT H,A,K1,K2,T2
26  LET H=100*H
27  PRINT
30  PRINT "SINGLE F.P. INSTRUMENT.GIVE FSR,FINESSE,DAMPING TIME"
32  GOSUB 7500
33  LET B1=1
35  INPUT F1,F2,N2
36  PRINT
37  PRINT "ASSUME SALINITY OF WATER"
38  INPUT S
39  PRINT
40  LET T=25
41  GOSUB  8400
42  GOSUB  8600
43  GOSUB  8700
44  GOSUB  8000
45  PRINT "SHIFT AT 25 C IS:"H1
46  DIM B[5]
50  PRINT "GIVE THE CHANNEL LIMITS (6 WAVENUMBERS)"
55  INPUT B[0],B[1],B[2],B[3],B[4],B[5]
57  PRINT
60  DIM X[6],Y[6]
61  LET K3=6E+11*L*P1*K1*K2*A*N2/F2
62  LET A3= COS (1.74533E-2*T2)
63  LET A4=3*(1+A3*A3)/4
64  LET A3=3*(13+A3*A3)/40
65  LET W8=W7+F1/F2
67  LET A5=100*10↑(-.25*T2)+.3*10↑(-.025*T2)+.0003*10↑(T2/130)
68  GOSUB  7900
69  LET K3=K3*F1/B[5]
70  LET P2=1
71  LET A5=A5/100
72  LET T6= 0
75  FOR T= 0 TO 60
80    GOSUB  4000
85    IF (I2-I3)<= 0 GOTO  100
90  NEXT T
95  PRINT "ERROR: T0 LARGER THAN 60 C"
97  GOTO  40
98  PRINT "ERROR: T0 SMALLER THAN 3C"
99  GOTO  40
100  LET I4=I2+I3
101  IF T<3 GOTO  96
105  LET I5=I3-I2
110  LET T6=I3
115  GOSUB  4000
```

```
120  LET C2=(I2+I3-I4)/I1
125  LET C4=(I5+I2-I3)/I1
130  LET C1=(T6*I4)/I1
135  LET T6=0
140  FOR T=T TO  0 STEP -.1
145    GOSUB  4000
150    IF (I3-I2+C4*I1)<=0 GOTO  155
152  NEXT T
155  FOR T=T TO 60 STEP .01
156    GOSUB  4000
157    IF (I3-I2+C4*I1)>=0 GOTO  159
158  NEXT T
159  LET T0=T
160  LET C5=C1*I1/(I2+I3-C2*I1)
165  LET T=T0+10
170  GOSUB  4000
175  LET C3=10*(I3+I2-C2*I1)/(I3-I2+C4*I1)
180  PRINT "THE PROCESSING IS:"
185  PRINT "LBT=";C1;"I1/(I2+I3+";C2;"I1)-";C5
190  PRINT "T=";T0;"+";C3;"(I3-I2+";C4;"I1)/(I2+I3-";C2;"I1)"
191  PRINT
192  PRINT
300  PRINT "GIVE ACTUAL VALUES OF TEMP. SALINITY,TURBIDITY,DEPTH"
305  INPUT T,S,T6,P2
306  LET P2=100*P2
307  PRINT
308  PRINT
310  GOSUB  4000
315  LET I4=I2+I3-C2*I1
317  LET I5=I3-I2+C4*I1
320  LET N4= SQR (I2+I3+C2*C2*I1)
322  LET N5= SQR (I2+I3+C4*C4*I1)
325  LET T7=C1*I1/I4-C5
327  LET T5=C1* SQR (I1)/I4
330  LET T9=C1*N4*I1/(I4*I4)
331  LET T8=100* SQR (T5*T5+T9*T9)/T7
332  LET T9=100*(T5+T9)/T7
333  LET T4=C3*N5/I4
334  LET T5=C3*I5*N4/(I4*I4)
336  LET T3= SQR (T4*T4+T5*T5)
337  LET T5=T4+T5
338  LET T4=T3
339  LET T3=T0+C3*I5/I4
340  LET P3=14.9896*(N1+N2)/N
345  PRINT "THE INSTRUMENT GIVES"
347  PRINT "CHANNEL'S SIGNALS OF",I1,I2,I3
350  PRINT "I.E: TEMPERATURE OF";T3,"INSTEAD OF",T
355  PRINT "WITH A RMS BETWEEN";T4;"AND",T5;"C"
360  PRINT "AND A TURBIDITY OF ",T7;"INSTEAD OF",T6
365  PRINT "WITH A RMS BETWEEN";T8;"AND",T9;"%"
366  PRINT "AND AN IMPRECISION IN DEPTH OF";P3;"CM"
367  PRINT
```

```
368  PRINT
369  PRINT
370  GOTO  300
4000  LET K4=K3* EXP (A7*P2)/((P2+1.33*H)*(P2+1.33*H))
4005  LET P=980.665*P2+1.01325E+6
4010  GOSUB  8400
4015  GOSUB  8600
4020  GOSUB  8700
4025  GOSUB  8900
4030  GOSUB  9000
4035  GOSUB  9100
4040  GOSUB  9200
4045  GOSUB  9300
4050  GOSUB  8000
4055  FOR Q= 0 TO 2
4060    LET X[Q]= 0
4065    FOR U2=B[2*Q] TO B[2*Q+1] STEP .001
4070      GOSUB  9500
4075      LET X[Q]=X[Q]+.001*U1
4080    NEXT U2
4085  NEXT Q
4090  LET I1=K4*X[ 0]
4095  LET I2=K4*X[1]
4100  LET I3=K4*X[2]
4102  PRINT "";
4105  RETURN
7500  LET C9=4.18E+7
7505  LET F9=1
7510  LET U=.08
7515  LET K=59200
7520  LET G=.02
7522  LET D=.000015
7525  RETURN
7900  LET A7=-.00034-8.6E-10*(L-4550)*(L-4550)
7910  RETURN
8000  LET T1=T+273.16
8005  LET R6=N*T1*D1/(L*L)
8010  LET R6=R6*R6*4.56564E+18/(R0*C9)
8015  LET B6=(R0*C9*D2-D1*A1*T1)*N/(L*L)
8020  LET B6=B6*B6*4.56564E+18*T1/((C9*R0*B1-A1*A1*T1)*R0*C9)
8025  LET S6=N*D3/(L*L)
8030  LET S6=S6*S6*5.49E+10*S/F9
8035  LET A6=10*U*(R6+B6+S6)/(6-7*U)
8040  LET A2=4094.7*N* SIN (8.7266E-3*T2)/L
8045  LET W0=W8+K*A2*A2/(R0*C9)
8050  LET W1=W8+G*A2*A2/(2*R0)
8055  LET W2=W8+D*A2*A2
8060  LET W3=W8+.01832*T1
8065  LET H1=1.62924E-6*V*A2
8070  RETURN
8400  REM              SPEED OF SOUND(V) IN SEAWATER AS V(S,T,P)
8420  LET V4=1402.39
```

```
8425  LET V5=(5.01109)*T
8430  LET V5=V5-(5.50947E-2)*T*T
8435  LET V5=V5+(2.21536E-4)*T*T*T
8440  LET V6=(1.32952)*S*(1000)
8445  LET V6=V6+((1.28956E-4)*S*S*(1E+6))
8450  LET V7=(.156059)*P/(9.81E+6)
8455  LET V7=V7+((2.44999E-5)*P*P/(9.81E+6↑2))
8460  LET V7=V7-((8.83392E-9)*P*P*P/(9.81E+6↑3))
8465  LET V8=-(1.27563E-2)*T*S*(1000)
8470  LET V8=V8+((6.35192E-3)*T*P/(9.81E+6))
8475  LET V8=V8+((2.65485E-8)*T*T*P*P/(9.81E+6↑2))
8480  LET V8=V8-((1.59349E-6)*T*P*P/(9.81E+6↑2))
8485  LET V8=V8+((5.22116E-10)*T*P*P*P/(9.81E+6↑3))
8490  LET V8=V8-((4.38031E-7)*T*T*T*P/(9.81E+6))
8495  LET V8=V8-((1.61674E-9)*S*S*P*P/(9810↑2))
8500  LET V8=V8+((9.68403E-8)*T*T*S*(1000))
8505  LET V8=V8+((4.8564E-6)*T*S*S*P/(9.81))
8510  LET V8=V8-((3.40597E-4)*T*S*P/(9810))
8515  LET V=V4+V5+V6+V7+V8
8517  LET V=V*(100)
8520  RETURN
8600  REM                DENSITY(S,T,P)--R0(S,T,P)
8620  LET R0=((2.996E+9+P)/(2.996E+9+1.8136E+6))↑.1368
8625  LET R0=R0*.998492* EXP (S*.697363)
8630  LET R0=R0*.999973*.999875
8635  LET R0=R0/(1-(6.427E-5)*T+(8.5053E-6)*T*T-(6.79E-8)*T*T*T)
8640  RETURN
8700  REM                INDEX(S,T,P,L)--N(S,T,P,L)
8720  LET N=L*L*.32427/(L*L-(952.68↑2))
8725  LET N=N+(.000001)*(20-.06*T)*S
8730  LET N=N*(R0↑.972)* EXP ((-7.09E-5)*T)
8732  LET N=N+1
8735  RETURN
8800  REM                DERIVATIVE SUBROUTINE
8801  REM                NEEDS X(1-5) AND Y(1-5)
8802  REM                SLOPE RETURNED AS Q9
8805  LET Q3= 0
8810  LET Q4= 0
8815  LET Q5= 0
8820  LET Q6= 0
8825  FOR Q=1 TO 5
8830    LET Q3=Q3+X[Q]
8835    LET Q4=Q4+Y[Q]
8840    LET Q5=Q5+X[Q]*Y[Q]
8845    LET Q6=Q6+X[Q]*X[Q]
8850  NEXT Q
8855  LET Q9=(5*Q5-Q3*Q4)/(5*Q6-Q3*Q3)
8860  RETURN
8900  REM                EVALUATES D3=(DN/DS) AT CONSTANT T,P
8905  LET Y[ 0]=N
8910  LET X[ 0]=S
8912  LET X[6]=R0
```

```
8915  FOR Q=1 TO 5
8920    LET S=X[ 0]+(Q-3)*(.002)
8922    GOSUB  8600
8925    GOSUB  8700
8930    LET X[Q]=S
8935    LET Y[Q]=N
8940  NEXT Q
8945  GOSUB  8800
8950  LET D3=Q9
8955  LET N=Y[ 0]
8960  LET S=X[ 0]
8965  LET R0=X[6]
8990  RETURN
9000  REM              EVALUATES D2=(DN/DP) AT CONSTANT T,S
9005  LET Y[ 0]=N
9010  LET X[ 0]=P
9012  LET X[6]=R0
9015  FOR Q=1 TO 5
9020    LET P=X[ 0]+(Q-3)*(1E+6)
9022    GOSUB  8600
9025    GOSUB  8700
9030    LET X[Q]=P
9035    LET Y[Q]=N
9040  NEXT Q
9045  GOSUB  8800
9050  LET D2=Q9
9055  LET N=Y[ 0]
9060  LET P=X[ 0]
9065  LET R0=X[6]
9090  RETURN
9100  REM              EVALUATES D1=(DN/DT) AT CONSTANT P,S
9105  LET Y[ 0]=N
9110  LET X[ 0]=T
9112  LET X[6]=R0
9115  FOR Q=1 TO 5
9120    LET T=X[ 0]+(Q-3)*(1)
9122    GOSUB  8600
9125    GOSUB  8700
9130    LET X[Q]=T
9135    LET Y[Q]=N
9140  NEXT Q
9145  GOSUB  8800
9150  LET D1=Q9
9155  LET N=Y[ 0]
9160  LET T=X[ 0]
9165  LET R0=X[6]
9190  RETURN
9200  REM          EVALUATES A1=-(DR0/DT)/R0
9205  LET Y[ 0]=R0
9210  LET X[ 0]=T
9215  FOR Q=1 TO 5
9220    LET T=X[ 0]+(Q-3)*(1)
```

```
9225     GOSUB  8600
9230     LET X[Q]=T
9235     LET Y[Q]=R0
9240   NEXT Q
9245   GOSUB  8800
9250   LET A1=-Q9/R0
9255   LET R0=Y[ 0]
9260   LET T=X[ 0]
9290   RETURN
9300   REM            EVALUATES B1=(DR0/DP)/R0
9305   LET Y[ 0]=R0
9310   LET X[ 0]=P
9315   FOR Q=1 TO 5
9320     LET P=X[ 0]+(Q-3)*(1E+6)
9325     GOSUB  8600
9330     LET X[Q]=P
9335     LET Y[Q]=R0
9340   NEXT Q
9345   GOSUB  8800
9350   LET B1=Q9/R0
9355   LET R0=Y[ 0]
9360   LET P=X[ 0]
9390   RETURN
9400   REM              CALCULATES INTENSITY(V1)
9405   LET V1=(W1*W1)+(4*(V2-H1)*(V2-H1))
9410   LET V3=(W1*W1)+(4*(V2+H1)*(V2+H1))
9415   LET V1=B6*W1*((1/V1)+(1/V3))/2
9420   LET V1=V1+(S6*W2/(W2*W2+4*V2*V2))+(R6*W0/(W0*W0+4*V2*V2))
9430   LET V3=A6*W3/(W3*W3-4*V2*V2)
9440   LET V1=V1*A4+V3*A3+T6*W8*A5/(W8*W8+4*V2*V2)
9450   RETURN
9500   LET U1= 0
9505   FOR Q3=1 TO 3
9510     LET V2=U2+(Q3-2)*F1
9515     GOSUB  9400
9520     LET U1=U1+V1
9525   NEXT Q3
9530   RETURN
9999   END
```

END

DATE

FILMED

FEB 3 1977